

-1-

CANADA

DEPARTMENT OF MINES AND TECHNICAL SURVEYS
MINES BRANCH

OTTAWA

Fuels Division
Technical Memorandum - 83/58-RBS

A NEW METHOD OF HYDROCARBON STRUCTURAL GROUP ANALYSIS

by

D.S. Montgomery and M. L. Boyd

This paper is published with the permission of the Director,
Mines Branch, Department of Mines and Technical Surveys,
Ottawa, Canada.

Paper Prepared for Presentation Before the Division of Gas
and Fuel Chemistry. American Chemical Society
Chicago, Illinois Meeting, September 7 - 12, 1958.

(Copy No. ___)

June 1, 1958.

A NEW METHOD OF HYDROCARBON
STRUCTURAL GROUP ANALYSIS

by

D.S. Montgomery and M.L. Boyd

Fuels Division, Mines Branch,
Department of Mines and Technical Surveys.

ABSTRACT

A method of hydrocarbon structural group analysis has been developed for application to pure compounds in which three chemical and two physical properties have been expressed in terms of five structural groups in a form which may be simultaneously solved by modern high speed computing equipment. The chemical properties include the carbon and hydrogen content as well as the number of aromatic carbon atoms present per molecule. The physical properties required for the analysis are the molar volume and molar refraction. This method has been tested on a selected group of 114 hydrocarbons whose properties have been determined by A. P. I. Project 42. The results of the application of this structural analysis system are described in detail and the accuracies attained have been tabulated.

PRESENTED BEFORE THE DIVISION OF GAS AND FUEL CHEMISTRY
AMERICAN CHEMICAL SOCIETY
Chicago, Illinois, Meeting, September 7-12, 1958.

by

D. S. Montgomery and M. L. Boyd
Department of Mines and Technical Surveys, Ottawa, Ontario.

INTRODUCTION

The synthesis and systematic study of the physical properties of pure hydrocarbons has been in progress for a number of years to facilitate the determination of the molecular structure of hydrocarbons directly or by analogy, that is by comparing certain properties of compounds of unknown structure with those of compounds whose structures are known.

The value of studying physical properties of a series of compounds, as a means of predicting the properties of unknown compounds and affording a means of checking the accuracy of the physical constants of compounds, has also been repeatedly demonstrated. In general, the study of the physical properties of hydrocarbons has been undertaken by a number of independent investigators and usually has been confined to hydrocarbons containing a limited number of types of structural groups, or, alternatively, only one physical property of a large variety of compounds has been examined.

This paper describes a method of simultaneously analyzing certain physical and chemical properties of liquid hydrocarbons to secure structural information. Although the system described is confined to specific classes of hydrocarbons, it is more general than any system so far proposed and involves the simultaneous consideration of three chemical and two physical properties to yield quantitative information concerning five structural groups. The investigation was promoted by a desire to improve existing structural analysis systems for pure hydrocarbons and to facilitate the study of naturally occurring hydrocarbons. The new possibilities offered by modern high speed computing equipment provided an additional incentive to re-examine and extend the earlier work in the field of structural analysis.

The most extensively used structural analysis system applied to hydrocarbon mixtures has been developed by Waterman and his school (13) beginning with the classical Waterman Ring Analysis of 1932 (19, 20) and extending to the n-d-M method of 1947 (14). van Krevelen employed some of the concepts of the Waterman Ring Analysis to develop a system that was particularly suited to the study of highly condensed aromatic structures which were assumed to be the major constituents of coal (7, 8). The chief criticism of the various methods of struc-

tural group analysis (15) of oil and coal is that when applied to pure compounds poor results are obtained. These considerations made it desirable to attempt to formulate a structural analysis system based on the physical properties of known compounds, but of such a form that it could be used with reasonable confidence to analyze the structure of high molecular weight material.

The method presented here was evolved from a method of carbon type analysis published by van Krevelen (4) in 1952. In this method, van Krevelen divided the carbon atoms in a structure into four main types:-

$$C_1 = \frac{CH}{C}; C_2 = \frac{CH_2}{C}; C_3 = \frac{CH_{aromatic}}{C}; C_4 = \frac{C}{C} \text{ aromatic};$$

where C in the denominator of each fraction represented the total number of carbon atoms per molecule. He then set up the following four quantitative relationships:

- (a) $C_1 + C_2 + C_3 + C_4 = 1$ (carbon balance)
- (b) $2C_1 + C_2 + C_3 = H/C$ (hydrogen balance)
- (c) $C_2 + C_4 = 2R/C$ (ring balance)
- (d) $C_3 + C_4 = fa$ (aromatic carbon balance)

These equations were not independent, and hence could not be solved simultaneously. van Krevelen solved these equations by giving an equation for C_1 as a function of H/C which represented the statistical probability of the occurrence of a CH_2 group in the molecule. The use of this equation was open to considerable question and consequently the method was never widely applied. Equations (a), (b) and (d), above, are true by definition; however, equation (c), the ring balance equation, is only valid for high molecular weight hydrocarbons where the factor $2/C$ can be neglected and where two junctions are associated with the formation of every ring. There are structures where this relation is not valid, such as in spiro compounds, and in three-dimensional structures where three rings possess a common side. van Krevelen's system was devised to elucidate the structure of coal and coal-like products where the proportion of saturated carbon atoms was small or negligible. While this choice of carbon types was suitable for the study of coal, it was undesirable for the study of petroleum since it failed to differentiate between chain and cyclic CH_2 groups. Hence, a five-type carbon classification was chosen which differed from that of van Krevelen by dividing his C_1 into two types. The carbon linkages have therefore been divided into the following five types.

C_1 = number per molecule of CH_3 , CH_2 , CH , and C groups in linear and branched chains.

- C_2 = number per molecule of CH_2 groups in saturated rings, including the case where the hydrogen atoms may be replaced by branched or linear chains.
- C_3 = number per molecule of CH groups which are junctions in fused saturated rings, as well as similarly situated groups where the hydrogen is replaced by linear or branched chains.
- C_4 = number per molecule of CH groups in aromatic rings, including the case where the hydrogen may be replaced by branched or linear chains.
- C_5 = number per molecule C groups which are junctions in fused aromatic rings, as well as junctions between saturated and aromatic rings.

It is possible to rewrite the carbon balance, the hydrogen balance and the aromatic carbon balance equations in terms of this new classification of structural groups. It should be especially noted that in the van Krevelen system the molecular weight was unknown and hence the structure was described in terms of fractions of the total number of carbon atoms. However, the present system was designed for the case where the molecular weight (as well as % carbon, % hydrogen, density, refractive index, and aromatic carbon content) was either known or could be determined. The carbon classification was therefore expressed in terms of the actual numbers of the different carbon types $C_1 - C_5$ present in the molecule. The Ring Balance Equation could not be used when analyzing an unknown hydrocarbon, as there was no accurate method of estimating the number of rings in the molecule. The fundamental basis of this structural analysis system, therefore, consisted in finding two additional physical properties which could be accurately expressed in terms of the above structural groups to give five independent equations which could then be solved simultaneously.

Theoretically, any two physical properties would be suitable, provided it were possible to express them as independent equations in terms of the structural types already defined. The two physical properties chosen were the molar volume and the molar refraction (the Lorentz-Lorenz expression). Both of these physical properties of liquids can be approximately described in terms of a linear combination of the atomic contributions, and both quantities have been extensively used for the purposes of elucidating structure (7, 18, 5, 10). It was assumed that the same functional form of the equation would apply to both physical properties, and that both properties could be expressed in terms of the same groups of chemical types. Owing to the intimate relation between these two quantities, it was felt that the loss in accuracy associated with grouping together so many different chemical linkages might easily yield two expressions which were merely linear combinations of each other. It remained for this investigation to demonstrate that the differences between the expression derived for the molar volume and that for the molar refraction were of such a magnitude that reliable structural information could be secured by the simultaneous solution of these expressions.

DEVELOPMENT OF THE FIVE EQUATIONS

It should be emphasized at the outset that this method as presently constituted is applicable only to certain specific classes of compounds. In the division of the carbon groups into the various types, care was taken that the hydrogen balance equation should always be satisfied. It was recognized that this equation was not strictly true as defined for the normal and branched paraffins. This case will subsequently be discussed. The present system will deal with monocyclic compounds and fused ring compounds, both saturated aromatic, but will not include polycyclic non-fused structures. Spiro compounds and three-dimensional ring systems are also excluded. It can be shown that the contributions to the molar volume and molar refraction of junction atoms in polycyclic non-fused compounds are not identical with any of the five types dealt with here, but in fact, represent a 6th (saturated) and a 7th (aromatic) type of linkage. Another class of compounds excluded are those containing olefinic or acetylenic bonds. In this work only double bonds existing in aromatic rings have been considered.

The method depends upon the ability to measure the density and refractive index of hydrocarbons in the liquid state at 20° C. at one atmosphere pressure, or on the capacity to correct to this standard state measurements made under other conditions. Except where otherwise specified, the coefficients of the molar volume and molar refraction equations have been determined from the properties of the hydrocarbons prepared by A. P. I. Project 42 (16).

The Carbon, Hydrogen and Aromatic Carbon Balance Equations The carbon balance, hydrogen balance, and aromatic carbon balance can be written as follows, by definition:

$$C_1 + C_2 + C_3 + C_4 + C_5 = \epsilon C \quad (1)$$

$$2C_1 + 2C_2 + C_3 + C_4 = \epsilon H \quad (2)$$

$$C_4 + C_5 = \epsilon C_a \quad (3)$$

The total number of carbon atoms per molecule ϵC was calculated from the carbon analysis and the molecular weight. The total number of hydrogen atoms per molecule ϵH , was similarly calculated from the hydrogen analysis and the molecular weight. The total number of aromatic carbon atoms in the molecule, ϵC_a , was not quite so readily available, although it could be determined by spectroscopic means (1). For the purposes of the present investigation (testing the method on known compounds), direct measurement of this quantity was not required.

The Molar Volume Equation The following molar volume equation was developed for the purpose of this structural analysis system:

$$\begin{aligned} \text{M. V.} &= C_1(16.38 + \frac{30.61}{\xi C}) + C_2(13.20 + \frac{28.48}{\xi C}) + & (4) \\ \text{at} & & \\ 20^\circ\text{C.} & & \\ 1 \text{ atm.} & C_3(10.981 + \frac{20.679}{\xi C}) + C_4(12.406 + \frac{14.042}{\xi C} - 1.96 \frac{C_1}{\xi C} + 10.13 \frac{C_2}{\xi C}) \\ \text{press.} & + C_5(5.124 - \frac{5.238}{\xi C}) \end{aligned}$$

A detailed account of this equation is in preparation. However to clarify the basis of this method of structural analysis, a brief description of the manner in which this equation was developed will now be given.

Initially, on the basis of Kurtz and Sankin's (9) work, the following general form of the molar volume equation was assumed:

$$\text{M. V.} = v_1 C_1 + v_2 C_2 + v_3 C_3 + v_4 C_4 + v_5 C_5 + K \quad (5)$$

A preliminary investigation to evaluate the coefficients in this expression indicated several difficulties with this functional form. No system of constant coefficients v_1 to v_5 could be found for the five structural types covered by the present classification. This work also revealed that k was not constant.

To overcome these difficulties, the following approach was adopted. From the definition of ξC , in Equation 1, the following expression was derived by multiplication by k :

$$\frac{C_1 K}{\xi C} + \frac{C_2 K}{\xi C} + \frac{C_3 K}{\xi C} + \frac{C_4 K}{\xi C} + \frac{C_5 K}{\xi C} = K \quad (6)$$

When K in equation 5 was replaced by the value in equation 6, the following equation was obtained:

$$\begin{aligned} \text{M. V.} &= C_1(v_1 + \frac{K}{\xi C}) + C_2(v_2 + \frac{K}{\xi C}) + C_3(v_3 + \frac{K}{\xi C}) & (7) \\ &+ C_4(v_4 + \frac{K}{\xi C}) + C_5(v_5 + \frac{K}{\xi C}) \end{aligned}$$

To determine the coefficients of C_1 to C_5 , use was made of the fact that for a molecule containing only one species of carbon atom (C_i), Equation 7, assumed the following form, as C_i was equal to ξC :

$$\text{M. V.} = v_i C_i + K_i \quad (8)$$

When the molar volume was plotted against C_i , the resultant straight line had a slope of v_i and an intercept of k_i . Consequently, v_i represented the contribution to the molar volume of a C_i group in the presence of an infinite number of C_i groups.

It will subsequently be shown that the K's in each bracket are not identical, these have hence been designated k_1 to k_5 respectively. The quantity K in the above equation expresses the increase in the molar volume that takes place on reducing the molecular weight of a particular species.

Determination of v_1 and k_1

The molar volume for the 13 normal paraffins on the list of A. P. I. Project 42 (16) was plotted against the number of carbon atoms in the molecule. The equation of the resulting straight line was determined by the method of least squares and found to be as follows:

$$M. V. = 16.38C_1 + 30.61 \quad (9)$$

Determination of v_2 and k_2

These quantities were calculated in a manner similar to that used for the calculation of v_1 and k_1 , using the physical properties given by Ward and Kurtz (21) for cyclopentane, cyclohexane, cycloheptane and cyclooctane. The molar volume of these compounds could be expressed by the following equation:

$$M. V. = 13.20C_2 + 28.48 \quad (10)$$

Determination of v_4 and k_4

Some difficulties were encountered in obtaining suitable data for compounds containing only C_4 's. The following compounds were used: benzene (properties taken from Egloff (3), cyclooctatetraene (properties by Eccleston (2) et al), and cyclopentadiene (Ward and Kurtz (21). A word of explanation about the use of the cyclopentadiene is required. Since it contained one C_2 group its use here is, strictly speaking, not justified in view of the presence of two different types of groups, C_2 and C_4 . Due to the scarcity of data, the observed molar volume of the cyclopentadiene was taken and the contribution of one CH_2 group was deducted. This amounted to considering a hypothetical compound C_4H_4 having four C_4 groups and a molar volume of $\frac{M. V. (\text{cyclopentadiene}) - 1(13.20 + \frac{28.48}{5})}{5}$. The resulting least squares equation of the straight line through these three compounds was found to be:

$$M. V. = 12.406C_4 + 14.042 \quad (11)$$

Determination of v_3 and k_3

A slightly different method had to be used to determine v_3 and k_3 , since no compounds existed containing C_3 groups only. Compounds containing C_2 and C_3 groups had to be used, and for this reason the following procedure was

adopted. $\left[(M.V. \text{ observed} - C_2(13.20 + \frac{28.48}{\xi C})) / C_3 \right]$ was plotted against $1/\xi C$. The result of this plot was a straight line whose slope was k_3 and intercept v_3 . Using the following compounds from the A.P.I. List (16): bicyclooctane 543, decahydronaphthalene 569 and 570, perhydrofluorene 561, perhydropyrene 578 and perhydrochrysene 575, v_3 was determined to be 10.981 and k_3 to be 20.679. The coefficient of C_3 was undoubtedly a function of the ring size, but the values found for five- and six-membered rings were almost identical.

Determination of v_5 and k_5

These quantities were determined in exactly the same manner as that used for the determination of v_3 and k_3 . Some difficulties were experienced in obtaining suitable liquid state molar volume data at 20°C for fused ring aromatic compounds that contained only C_4 and C_5 . Liquid molar volume data at 20°C have been determined by Ubbelohde (11, 12) for several fused ring aromatic compounds. This author also determined the molar volume for the solid state at 20°C. By plotting $(M.V._l - M.V._s)$ versus C_5/C_4 , it was possible to express this shrinkage in volume as a function of the degree of condensation. By means of this relationship, the solid state molar volume data of van Krevelen (17) for fused ring aromatic compounds was "converted" to the liquid state at 20°C. Using the data obtained in this manner for anthracene, chrysene, phenanthrene (Ubbelohde), and for dibenzanthracene, chrysene, pyrene and coronene (van Krevelen's data converted to the liquid state) v_5 was determined to be 5.124 and k_5 to be -5.238.

The molar volume equation thus obtained was used to calculate the molar volume for the appropriate classes of compounds on the A.P.I. List (16) and to compare the results with the experimental values. The results of this comparison showed that a study of the interactions between various types of structural groups had to be made. The most significant interactions were found when C_1 and C_4 occurred in the same molecule and when C_2 and C_4 occurred together. In the former case, data from Ward and Kurtz (21) were used to evaluate the magnitude of the interaction, and in the latter case A.P.I. data (16) were employed. In brief, the method of determining the functional form and magnitude of the interaction terms consisted of obtaining the difference between observed and calculated molar volume per C_4 group and plotting this difference against $C_1/\xi C$ in the first case and $C_2/\xi C$ in the second. Two straight lines were obtained, from which were derived the two terms in $C_1/\xi C$ and $C_2/\xi C$ which were added to the C_4 term in Equation 4. The accuracy with which this "corrected" equation predicted the molar volume of the A.P.I. (16) hydrocarbons is given in Table I.

Table I - Accuracy of the Authors' Molar Volume Equation Applied to A. P. I. 42 Hydrocarbons

Class of Compound	No. in Class	Average Value of $\frac{MV_{calc} - MV_{obs}}{MV_{obs}} \times 100$	Standard Deviation
n-paraffins	13	-0.02	0.07
br. -paraffins	38	+0.31	0.80
Monocyclic saturates	27	+0.10	0.33
Fused ring saturates	18	+0.66	0.80
Monocyclic aromatics	21	+0.03	0.19
Fused ring aromatics	13	- .46	0.89

The Molar Refraction Equation The following molar refraction equation was developed for the purpose of this analysis:

$$\begin{aligned}
 \text{M. R. at } 20^{\circ}\text{C. 1 atm. press.} &= C_1 \left(4.63 + \frac{2.314}{\epsilon C} \right) + C_2 \left(4.468 + \frac{0.868}{\epsilon C} - \frac{0.245C}{\epsilon C^2} \right) + \\
 &C_3 \left(3.693 + \frac{0.3395}{\epsilon C} \right) + \\
 &C_4 \left(4.5445 - \frac{1.021}{\epsilon C} - 0.396 \frac{C}{\epsilon C^2} - 5.701 \frac{C^2}{\epsilon C^3} \right) + \\
 &C_5 \left(5.734 - \frac{14.333}{\epsilon C} \right) \dots \dots \dots (12)
 \end{aligned}$$

In this equation, M. R. referred to the Lorentz-Lorenz expression for the molar refraction $\left(\frac{n^2 - 1}{n^2 + 2} \frac{M}{d} \right)$, where n was the refractive index for the sodium D line at 20°C. The coefficients in this equation were determined in exactly the same manner, and using the same compounds as in the molar volume equation. Attention is drawn to the fact that, in the determination of the C₅ term, the molar refraction data for the fused ring aromatic compounds of van Krevelen (17) refer to measurements made of the compounds in benzene solution and have been referred to by van Krevelen (6) as "hypothetical liquid state data". The accuracy with which this equation predicts the molar refraction of the A. P. I. 42 (16) hydrocarbons is indicated in Table II.

METHODS OF SOLUTION OF THE SET OF FIVE EQUATIONS

Equations 1, 2, 3, 4 and 12 constitute the three chemical and two physical property equations that, when solved simultaneously for C_1 , C_2 , C_3 , C_4 and C_5 , form the proposed system of analysis. The first three of these equations are linear but equations 4 and 12 are quadratic in C_1 and C_2 . This set of linear and quadratic equations was initially solved in the following manner. The solution was obtained by reducing the system to a linear form by substituting an initial value $C_1 = C_2 = 0$ in the non-linear terms. The resultant set of linear equations was then solved by the standard methods of matrix algebra.

Table II - Accuracy of the Authors' Molar Refraction Equation, Applied to A. P. I. 42 Hydrocarbons

Class of Compound	No. in Class	Average Value of $\frac{MR_{calc} - MR_{obs}}{MR_{obs}} \times 100$	Standard Deviation
n-paraffins	9	+0.012	0.056
br. -paraffins	37	+0.19	0.26
Monocyclic saturates	26	-0.01	0.20
Fused ring saturates	19	-0.008	0.26
Monocyclic aromatics	19	+0.16	0.51
Fused ring aromatics	8	+0.17	0.64

The new values of C_1 and C_2 from this solution were then substituted in the non-linear terms and another solution was obtained. This iterative procedure was repeated until two consecutive solutions were equal. The critical aspect of the solution was whether or not the iterative procedure would converge. From the practical point of view the rate of convergence was important. The number of iterations varied from three for the paraffins to thirty for some of the fused ring aromatic compounds.

Since the molar volume and the molar refraction equations were quadratic in C_1 and C_2 , in general there would be four roots. Since it was clear that the iterative procedure yielded only one root, it was desirable to obtain a method of solution which would give all the roots. For this reason the set of five equations was solved by a second method. It was possible, by simple algebraic re-arrangement of the three linear equations, to express C_3 , C_4 and C_5 in terms of C_1 and C_2 . These values for C_3 , C_4 and C_5 were then substituted

in the molar volume and molar refraction equations and the following two quadratic equations in C_1 and C_2 resulted:

$$\frac{1.96}{\xi C} C_1^2 + \frac{(0.077 \xi C - 1.96 \xi C_a - 8.17 C_2 - 1.96 \xi H - 9.349)}{\xi C} C_1 + (13) \\ (-15.193 C_2 - 11.479 \frac{C_2}{\xi C} + 10.13 \frac{C_2 \xi C_a}{\xi C} + 10.13 \frac{C_2 \xi H}{\xi C} - 10.13 \frac{C_2^2}{\xi C^2} + \\ 3.699 \xi C + 1.425 \xi C_a + 7.282 \xi H - 6.637 \frac{\xi C_a}{\xi C} + 19.280 \frac{\xi H}{\xi C} + \\ 1.399 - M.V.) = 0$$

and

$$\frac{0.396}{\xi C} C_1^2 + \frac{(2.516 \xi C + 5.852 C_2 - 0.396 \xi C_a - 0.396 \xi H - 11.338)}{\xi C} C_1 + (14) \\ + (7.666 C_2 - 12.784 \frac{C_2}{\xi C} - 5.70 \frac{C_2 \xi C_a}{\xi C} - 5.701 \frac{C_2 \xi H}{\xi C} + 5.701 \frac{C_2^2}{\xi C^2} \\ + 0.852 \xi C_a - 1.360 \frac{\xi C_a}{\xi C} - 1.190 \xi H + 13.312 \frac{\xi H}{\xi C} + 4.883 \xi C \\ - 12.973 - M.R.) = 0$$

These two quadratics were solved graphically by taking arbitrary values of C_2 and solving each equation for C_1 . These values of C_1 were plotted against C_2 and the intersection of the molar volume and molar refraction curves represented the roots of the system.

RESULTS

The iterative method of solution has been tested by application to 121 known compounds, of which 114 are from the list of properties of A. P. I. Project 42 (16) and seven are fused ring aromatic compounds whose properties were determined by van Krevelen (17). All calculations were made by the International Business Machines Company on a Type 650 Magnetic Drum Processing Machine. The results are shown in Table III. In this table, D_1 to D_5 refer to the differences between calculated and observed values of C_1 to C_5 (i. e. $[C_1(\text{calc.} - C_1(\text{observed})]$).

Some explanation is required concerning the application of this method to the paraffins. For this class of compounds, Equation 2, the hydrogen balance, is not strictly true as given but should be:

$$2C_1 + 2C_2 + C_3 + C_4 = \xi H - 2 \quad (15)$$

TABLE III. ANALYSIS OF PURE HYDROCARBONS TO SHOW THE ACCURACY OF THE FIVE STRUCTURAL GROUP ANALYSIS SYSTEM

API Compd. No.	C ₁		D ₁		C ₂		D ₂		C ₃		D ₃		C ₄		D ₄		C ₅		D ₅		
	Observed	Calc.	Observed	Calc.	Observed	Calc.	Observed	Calc.	Observed	Calc.	Observed	Calc.	Observed	Calc.	Observed	Calc.	Observed	Calc.	Observed	Calc.	
Group I - n-paraffins																					
528	12	12.07	+0.07	0	-0.094	-0.094	0	0	0.025	+0.025	0	0	0.025	+0.025	0	0	-0.025	-0.025	0	0	
529	13	13.04	+0.04	0	-0.070	-0.070	0	0	0.030	+0.030	0	0	0.030	+0.030	0	0	-0.030	-0.030	0	0	
531	14	13.99	-0.01	0	-0.016	-0.016	0	0	0.026	+0.026	0	0	0.026	+0.026	0	0	-0.026	-0.026	0	0	
532	15	15.04	+0.04	0	-0.030	-0.030	0	0	-0.015	-0.015	0	0	-0.015	-0.015	0	0	0.015	+0.015	0	0	
534	16	15.99	-0.02	0	0.024	+0.024	0	0	-0.016	-0.016	0	0	-0.016	-0.016	0	0	0.016	+0.016	0	0	
535	17	17.00	0.0	0	-0.0084	-0.0084	0	0	0.0049	+0.0049	0	0	0.0049	+0.0049	0	0	-0.0049	-0.0049	0	0	
537	18	17.91	-0.09	0	0.10	+0.10	0	0	-0.012	-0.012	0	0	-0.012	-0.012	0	0	0.012	+0.012	0	0	
540	20	19.59	-0.01	0	0.031	+0.031	0	0	-0.021	-0.021	0	0	-0.021	-0.021	0	0	0.021	+0.021	0	0	
106	26	25.90	-0.10	0	0.12	+0.12	0	0	-0.020	-0.020	0	0	-0.020	-0.020	0	0	0.020	+0.020	0	0	
Group II - branched paraffins																					
1	26	25.68	-0.32	0	0.22	+0.22	0	0	0.099	+0.099	0	0	0.099	+0.099	0	0	-0.099	-0.099	0	0	
107	34	33.97	-0.03	0	0.039	+0.039	0	0	-0.0098	-0.0098	0	0	-0.0098	-0.0098	0	0	0.0098	+0.0098	0	0	
109	26	25.40	-0.60	0	0.69	+0.69	0	0	-0.088	-0.088	0	0	-0.089	-0.089	0	0	0.089	+0.089	0	0	
133	36	36.22	+0.22	0	-0.13	-0.13	0	0	-0.092	-0.092	0	0	-0.092	-0.092	0	0	0.092	+0.092	0	0	
163	23	22.90	-0.10	0	0.11	+0.11	0	0	-0.0030	-0.0030	0	0	-0.0030	-0.0030	0	0	0.0030	+0.0030	0	0	
164	34	34.19	+0.19	0	-0.12	-0.12	0	0	-0.070	-0.070	0	0	-0.070	-0.070	0	0	0.070	+0.070	0	0	
184	28	28.34	+0.34	0	-0.47	-0.47	0	0	0.14	+0.14	0	0	0.14	+0.14	0	0	-0.14	-0.14	0	0	
191	32	32.10	+0.10	0	-0.044	-0.044	0	0	-0.061	-0.061	0	0	-0.061	-0.061	0	0	0.061	+0.061	0	0	
2	26	25.78	-0.22	0	0.16	+0.16	0	0	0.067	+0.067	0	0	0.067	+0.067	0	0	-0.067	-0.067	0	0	
22	26	25.27	-0.73	0	0.63	+0.63	0	0	0.10	+0.10	0	0	0.10	+0.10	0	0	-0.10	-0.10	0	0	
23	26	24.62	-1.38	0	1.33	+1.33	0	0	0.053	+0.053	0	0	0.053	+0.053	0	0	-0.052	-0.052	0	0	
25	25	24.85	-0.15	0	0.072	+0.072	0	0	0.075	+0.075	0	0	0.075	+0.075	0	0	-0.075	-0.075	0	0	
27	26	25.82	-0.18	0	0.097	+0.097	0	0	0.080	+0.080	0	0	0.080	+0.080	0	0	-0.080	-0.080	0	0	
3	26	25.80	-0.20	0	0.13	+0.13	0	0	0.073	+0.073	0	0	0.073	+0.073	0	0	-0.073	-0.073	0	0	
4	26	25.46	-0.54	0	0.44	+0.44	0	0	0.098	+0.098	0	0	0.098	+0.098	0	0	-0.098	-0.098	0	0	
5	28	27.72	-0.28	0	0.21	+0.21	0	0	0.077	+0.077	0	0	0.077	+0.077	0	0	-0.077	-0.077	0	0	
500	19	18.68	-0.32	0	0.31	+0.31	0	0	0.0016	+0.0016	0	0	0.0016	+0.0016	0	0	-0.0016	-0.0016	0	0	
51	26	25.22	-0.18	0	0.097	+0.097	0	0	0.080	+0.080	0	0	0.080	+0.080	0	0	-0.080	-0.080	0	0	
510	20	19.34	-0.66	0	0.62	+0.62	0	0	0.040	+0.040	0	0	0.040	+0.040	0	0	-0.040	-0.040	0	0	
511	20	19.75	-0.25	0	0.27	+0.27	0	0	-0.027	-0.027	0	0	-0.027	-0.027	0	0	0.027	+0.027	0	0	
512	14	13.97	-0.03	0	0.012	+0.012	0	0	0.018	+0.018	0	0	0.018	+0.018	0	0	-0.018	-0.018	0	0	
53	26	24.91	-1.09	0	1.02	+1.02	0	0	0.068	+0.068	0	0	0.068	+0.068	0	0	-0.068	-0.068	0	0	
545	16	15.68	-0.32	0	0.30	+0.30	0	0	0.018	+0.018	0	0	0.018	+0.018	0	0	-0.018	-0.018	0	0	
546	13	12.66	-0.34	0	0.34	+0.34	0	0	-0.0030	-0.0030	0	0	-0.0030	-0.0030	0	0	0.0030	+0.0030	0	0	
549	10	9.66	-0.34	0	0.29	+0.29	0	0	0.052	+0.052	0	0	0.052	+0.052	0	0	-0.052	-0.052	0	0	
55	26	25.17	-0.83	0	0.75	+0.75	0	0	0.079	+0.079	0	0	0.079	+0.079	0	0	-0.079	-0.079	0	0	
554	21	20.86	-0.14	0	0.15	+0.15	0	0	-0.011	-0.011	0	0	-0.011	-0.011	0	0	0.011	+0.011	0	0	
556	14	10.79	-3.21	0	3.40	+3.40	0	0	-0.20	-0.20	0	0	-0.20	-0.20	0	0	0.20	+0.20	0	0	
557	18	17.29	-0.71	0	0.74	+0.74	0	0	-0.023	-0.023	0	0	-0.023	-0.023	0	0	0.023	+0.023	0	0	
6	30	29.70	-0.30	0	0.25	+0.25	0	0	0.042	+0.042	0	0	0.042	+0.042	0	0	-0.042	-0.042	0	0	
63	28	27.79	-0.21	0	0.12	+0.12	0	0	0.096	+0.096	0	0	0.096	+0.096	0	0	-0.096	-0.096	0	0	
69	26	25.94	-0.06	0	-0.055	-0.055	0	0	0.12	+0.12	0	0	0.12	+0.12	0	0	-0.12	-0.12	0	0	
7	32	31.74	-0.26	0	0.18	+0.18	0	0	0.077	+0.077	0	0	0.077	+0.077	0	0	-0.077	-0.077	0	0	
8	11	10.92	-0.08	0	0.032	+0.032	0	0	0.052	+0.052	0	0	0.052	+0.052	0	0	-0.052	-0.052	0	0	

API Compd. No.	C ₁		D ₁		C ₂		D ₂		C ₃		D ₃		C ₄		D ₄		C ₅		D ₅		
	Observed	Calc.	Observed	Calc.	Observed	Calc.	Observed	Calc.	Observed	Calc.	Observed	Calc.	Observed	Calc.	Observed	Calc.	Observed	Calc.	Observed	Calc.	
Group III - monocyclic naphthenes																					
539	8	8.52	+0.52	6	5.52	-0.49	0	-0.029	-0.029	0	-0.029	-0.029	0	-0.029	-0.029	0	0.029	+0.029	0	+0.029	
528	8	7.68	-0.32	6	6.36	+0.36	0	-0.039	-0.039	0	-0.039	-0.039	0	-0.039	-0.039	0	0.039	+0.039	0	+0.039	
573	10	9.93	-0.07	5	5.07	-0.07	0	0.0039	+0.0039	0	0.0039	+0.0039	0	0.0039	+0.0039	0	-0.0039	-0.0039	0	-0.0039	
572	10	10.50	+0.50	6	5.54	-0.46	0	-0.032	-0.032	0	-0.032	-0.032	0	-0.032	-0.032	0	0.032	+0.032	0	+0.032	
582	16	13.53	-0.47	5	5.46	+0.46	0	0.011	+0.011	0	0.011	+0.011	0	0.011	+0.011	0	-0.011	-0.011	0	-0.011	
506	13	12.55	-0.45	6	6.48	+0.48	0	-0.025	-0.025	0	-0.025	-0.025	0	-0.025	-0.025	0	0.025	+0.025	0	+0.025	
509	17	16.80	-0.20	6	6.24	+0.24	0	-0.038	-0.038	0	-0.038	-0.038	0	-0.038	-0.038	0	0.038	+0.038	0	+0.038	
110	20	19.73	-0.27	5	5.26	+0.26	0	0.017	+0.017	0	0.017	+0.017	0	0.017	+0.017	0	-0.017	-0.017	0	-0.017	
88	19	19.15	+0.15	6	5.94	-0.16	0	0.016	+0.016	0	0.016	+0.016	0	0.016	+0.016	0	-0.016	-0.016	0	-0.016	
117	21	21.00	0.0	5	5.05	+0.05	0	-0.048	-0.048	0	-0.048	-0.048	0	-0.048	-0.048	0	0.048	+0.048	0	+0.048	
64	21	20.18	-0.82	5	5.76	+0.76	0	0.063	+0.063	0	0.063	+0.063	0	0.063	+0.063	0	-0.063	-0.063	0	-0.063	
100	20	20.60	+0.60	6	5.49	-0.51	0	-0.097	-0.097	0	-0.097	-0.097	0	-0.097	-0.097	0	0.097	+0.097	0	+0.097	
102	20	19.77	-0.23	6	6.29	+0.29	0	-0.055	-0.055	0	-0.055	-0.055	0	-0.055	-0.055	0	0.055	+0.055	0	+0.055	
75	20	19.40	-0.60	6	6.59	+0.59	0	0.052	+0.052	0	0.052	+0.052	0	0.052	+0.052	0	-0.052	-0.052	0	-0.052	
106	20	19.56	-0.44	6	6.48	+0.48	0	-0.044	-0.044	0	-0.044	-0.044	0	-0.044	-0.044	0	0.044	+0.044	0	+0.044	
76	20	19.58	-0.42	6	6.40	+0.40	0	0.025	+0.025	0	0.025	+0.025	0	0.025	+0.025	0	-0.025	-0.025	0	-0.025	
77	20	19.63	-0.37	6	6.34	+0.34	0	0.031	+0.031	0	0.031	+0.031	0	0.031	+0.031	0	-0.031	-0.031	0	-0.031	
78	20	19.60	-0.40	6	6.37	+0.37	0	0.028	+0.028	0	0.028	+0.028	0	0.028	+0.028	0	-0.028	-0.028	0	-0.028	
162	20	19.94	-0.06	6	6.10	+0.10	0	-0.035	-0.035	0	-0.035	-0.035	0	-0.035	-0.035	0	0.035	+0.035	0	+0.035	
74	22	21.73	-0.27	5	5.27	+0.27	0	-0.0008	-0.0008	0	-0.0008	-0.0008	0	-0.0008	-0.0008	0	0.0008	+0.0008	0	+0.0008	
60	21	20.62	-0.38	6	6.35	+0.35	0	0.037	+0.037	0	0.037	+0.037	0	0.037	+0.037	0	-0.037	-0.037	0	-0.037	
91	22	22.38	+0.38	6	5.70	-0.30	0	-0.074	-0.074	0	-0.074	-0.074	0	-0.074	-0.074	0	0.074	+0.074	0	+0.074	
160	24	24.81	+0.81	5	4.10	-0.90	0	0.099	+0.099	0	0.099	+0.099	0	0.099	+0.099	0	-0.099	-0.099	0	-0.099	
69	25	24.76	-0.24	6	6.23	+0.23	0	0.016	+0.016	0	0.016	+0.016	0	0.016	+0.016	0	-0.016	-0.016	0	-0.016	
136	29	29.02	+0.02	6	6.07	+0.07	0	-0.099	-0.099	0	-0.099	-0.099	0	-0.099	-0.099	0	0.099	+0.099	0	+0.099	
138	33	33.04	+0.04	6	6.07	+0.07	0	-0.10	-0.10	0	-0.10	-0.10	0	-0.10	-0.10	0	0.10	+0.10	0	+0.10	
Group IV - noncyclic aromatics																					
538	8	8.00	0	0	0.11	+0.11	0	-0.12	-0.12	6	5.88	-0.12	0	0.12	+0.12	0	0.12	+0.12	0	0.12	
513	8	8.06	+0.06	0	0.22	+0.22	0	-0.27	-0.27	6	5.73	-0.27	0	0.27	+0.27	0	0.27	+0.27	0	0.27	
571	10	9.96	-0.04	0	0.084	+0.084	0	-0.042	-0.042	6	5.96	-0.04	0	0.042	+0.042	0	0.042	+0.042	0	0.042	
521	13	12.86	-0.14	0	-0.061	-0.061	0	0.20	+0.20	6	6.20	+0.20	0	-0.20	-0.20	0	-0.20	-0.20	0	-0.20	
87	19	18.64	-0.36	0	0.64	+0.64	0	-0.28	-0.28	6	5.72	-0.28	0	0.28	+0.28	0	0.28	+0.28	0	0.28	
10	19	20.28	+1.28	0	-0.69	-0.69	0	-0.59	-0.59	6	5.61	-0.59	0	0.59	+0.59	0	0.59	+0.59	0	0.59	
99	20	19.92	-0.08	0	0.045	+0.045	0	0.037	+0.037	6	6.04	+0.04	0	-0.037	-0.037	0	-0.037	-0.037	0	-0.037	
101	20	19.71	-0.29	0	0.37	+0.37	0	-0.076	-0.076	6	5.92	-0.08	0	0.076	+0.076	0	0.076	+0.076	0	0.076	
79	20	19.66	-0.34	0	0.35	+0.35	0	-0.0093	-0.0093	6	5.99	+0.01	0	0.0093	+0.0093	0	0.0093	+0.0093	0	0.0093	
103	20	19.72	-0.28	0	0.30	+0.30	0	-0.025	-0.025	6	5.98	-0.02	0	0.025	+0.025	0	0.025	+0.025	0	0.025	
80	20	19.65	-0.35	0	0.41	+0.41	0	-0.061	-0.061	6	5.94	-0.06	0	0.061	+0.061	0	0.061	+0.061	0	0.061	
81	20	19.78	-0.22	0	-0.099	-0.099	0	0.32	+0.32	6	6.32	+0.32	0	-0.32	-0.32	0	-0.32	-0.32	0	-0.32	
82	20	19.79	-0.21	0	-0.25	-0.25	0	0.46	+0.46	6	6.46	+0.46	0	-0.46	-0.46	0	-0.46	-0.46	0	-0.46	
152	20	20.31	+0.31	0	-0.65	-0.65	0	0.35	+0.35	6	6.34	+0.34	0	-0.35	-0.35	0	-0.35	-0.35	0	-0.35	
161	20	20.13	+0.13	0	-0.52	-0.52	0	0.39	+0.39	6	6.39	+0.39	0	-0.39	-0.39	0	-0.39	-0.39	0	-0.39	
9	21	20.79	-0.21	0	-0.30	-0.30	0	0.51	+0.51	6	6.51	+0.51	0	-0.51	-0.51	0	-0.51	-0.51	0	-0.51	
54	22	21.54	+0.44	0	1.45	+1.45	0	-0.99	-0.99	6	5.00	-1.00	0	0.99	+0.99	0	0.99	+0.99	0	0.99	
148	23	22.79	-0.21	0	0.94	+0.94	0	-0.73	-0.73	6	5.27	-0.73	0	0.73	+0.73	0	0.73	+0.73	0	0.73	
68	25	24.73	-0.27	0	0.095	+0.095	0	0.37	+0.37	6	6.37	+0.37	0	-0.37	-0.37	0	-0.37	-0.37	0	-0.37	

At the outset, the effect of this comparatively small change was not known and the original hydrogen balance equation was used. The results on the n-paraffins are shown in Table IV. An examination of these results indicated that, although in error, they followed a very recognizable pattern. Since results for all the normal and branched paraffins on the A.P.I. 42 (16) list gave this same pattern, it was found possible to have the program for the Type 650 computer written in such a way that when this pattern occurred the revised hydrogen balance equation 15, would be substituted in place of the original.

Table IV - Analysis of n-paraffins to Illustrate the Use of Uncorrected Hydrogen Balance Equation

A. P. I. 42 Compd. #	C ₁		C ₂		C ₃		C ₄		C ₅	
	obs.	calc.								
528	12	10.14	0	3.75	0	-1.89	0	0.11	0	-0.11
529	13	11.13	0	3.75	0	-1.88	0	0.12	0	-0.12
531	14	12.09	0	3.78	0	-1.87	0	0.12	0	-0.12
532	15	13.15	0	3.73	0	-1.89	0	0.11	0	-0.11
534	16	14.12	0	3.77	0	-1.89	0	0.11	0	-0.11
535	17	15.15	0	3.72	0	-1.87	0	0.13	0	-0.13
537	18	16.05	0	3.82	0	-1.88	0	0.12	0	-0.12
540	20	18.17	0	3.71	0	-1.88	0	0.12	0	-0.12
106	26	24.12	0	3.74	0	-1.86	0	0.13	0	-0.13

For simplicity and also to illustrate that the use of the revised hydrogen balance equation led to accurate results, the revised hydrogen balance (equation 15) was used in analyzing groups I and II (Paraffins) and the original hydrogen balance (equation 2) for the remainder. A summary of the accuracy of this analysis is given in Table V.

The graphical method of solution which has been described was applied to 17 representative compounds taken from the five major classes. The relatively small number of compounds examined by this method was due to the fact that this method was much more time-consuming than the iterative procedure. The nature of the roots was essentially the same in all cases, they all possessed only one real root less than $\sum C$. There was one exception to this rule, A.P.I. compound #133 possessed two real roots but one of these lay in the second quadrant, which has no physical meaning. One representative example of the graphical method of solution showing the intersection between the molar volume and molar refraction curves which yields the single root less than $\sum C$ is given in Figure 1.

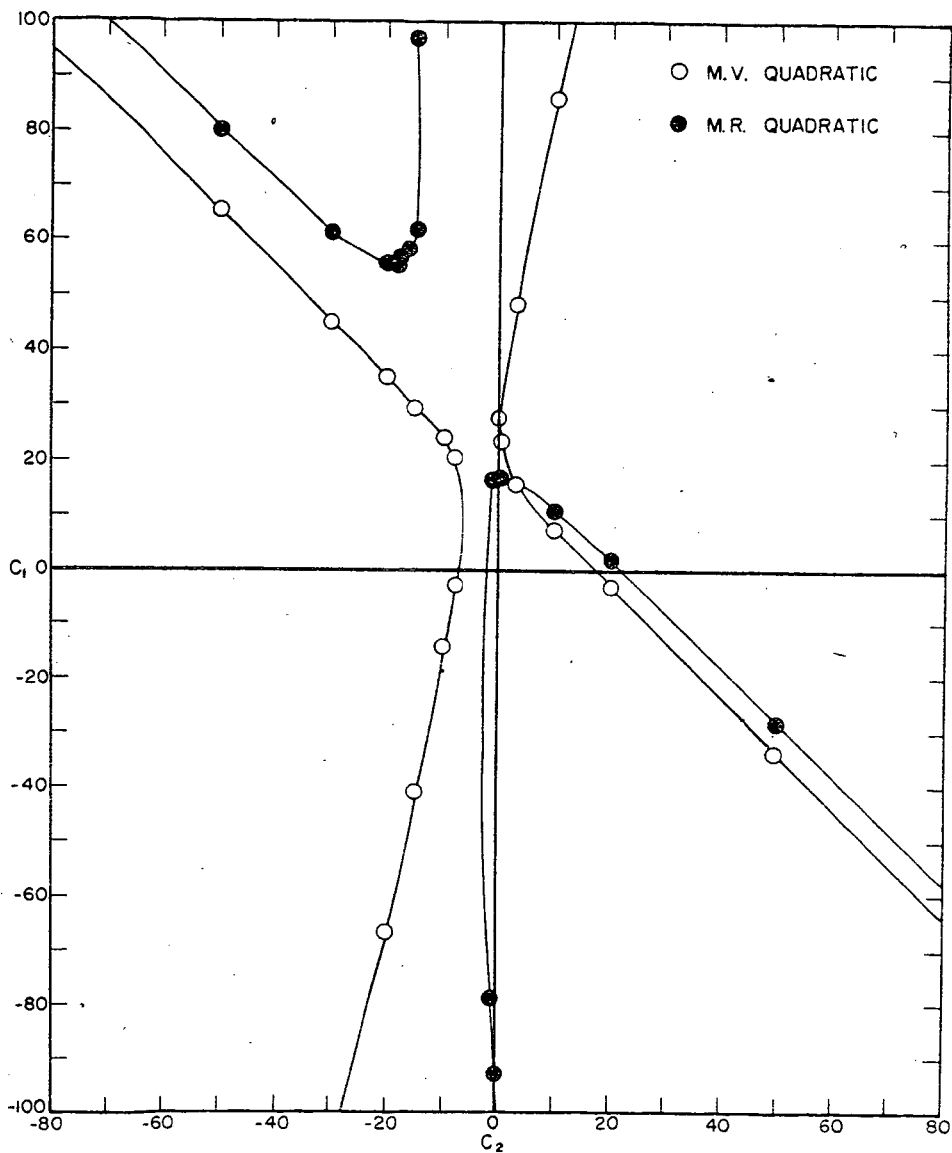


Figure I - Graphical Solution for A.P.I. Compound #16 to Illustrate the Existence of Only One Real Root.

DISCUSSION

Some additional information about the structure can be obtained by a detailed examination of the "pattern" of the results in Table III, within each of the seven groups of compounds into which this table is divided. This information can be used as a valuable aid when applying the method to unknown compounds. Before discussing the significance of the errors, it should be pointed out that for a given composition in terms of the five characteristic groups, there is a fixed relationship between the errors. If the error in C_1 is taken as x and the error in C_3 as y , then the error in C_2 will be $-(x + y)$, that in C_4 will be y and that in C_5 will be $-y$.

Considering, first of all, the branched paraffins, Group II, it will be noted that whereas C_2 should be zero, it is in fact positive and sometimes as high as +3. There appeared to be a direct relationship between the number of branches and the magnitude of the error. On the average, the error in C_2 per branch was +0.42 C_2 group. If, in the analysis of an unknown, C_2 , C_3 , C_4 and C_5 were less than 0.1, the compound could be predicted to be a normal paraffin with a high degree of certainty. However, if C_2 were between +0.1 and +0.4, then the compound would probably have one branch. On the other hand, if C_2 were greater than +0.4, the compound would probably have more than one branch.

The accuracy of the analysis of Group III, monocyclic naphthenes, was unusually high, due, no doubt, to the uniformity of the structures within the group. Little difficulty should be experienced in identifying this group in the analysis of unknown structures, since C_2 here must be greater than 3 (minimum ring size). A few structural effects were noted in the errors in C_1 and C_2 . The size of the ring and the number of branches on the ring would appear to be the effects having the most influence, whereas branching on a single side chain did not appreciably influence the results.

The accuracy of the results for Group IV, the monocyclic aromatics, was practically the same as for Group III, and for essentially the same reasons. The accuracy for compounds with a normal side chain was very high, as would be expected, since this was the type of compound upon which the interaction effect of C_1 and C_4 was based. Where one branched side chain was attached to the ring, the error in C_1 was about -0.3 and in C_2 about +0.3. The largest error for the entire group occurred for cases where there were more than one side chain attached to the ring. As with Group III, there should be no difficulty in recognizing this class of compound when analyzing unknown compounds, since C_4 should always be six in this class. At this level the errors were sufficiently small that no doubt should exist as to the structure.

Group V, the fused ring naphthenes, presented a much more difficult case to interpret. Since there appeared to be many more structural factors which could influence the analysis, and the examples available were very limited, no regular pattern between structure and the errors in the analysis could be determined. However, several important aspects of the errors associated with this

Table V - Summary of the Accuracy of the Hydrocarbon Analysis

Class of Comps.	No. in Class	\bar{D}_1	C_1	\bar{D}_2	C_2	\bar{D}_3	C_3	\bar{D}_4	C_4	\bar{D}_5	C_5
n-paraffins	9	-0.008	0.05	+0.006	0.07	+0.0002	0.02	+0.0002	0.02	-0.0002	0.02
br. -paraffins	34	-0.39	0.60	+0.36	0.63	+0.03	0.07	+0.03	0.07	-0.03	0.07
Monocyclic saturates	26	-0.11	0.40	+0.13	0.38	-0.01	0.04	-0.01	0.04	+0.01	0.04
Monocyclic aromatics	19	-0.09	0.37	+0.13	0.51	-0.03	0.40	-0.03	0.40	+0.03	0.40
Fused ring saturates	17	-0.49	0.56	+0.49	0.61	-0.006	0.21	-0.06	0.06	+0.06	0.06
A.P.I. fused ring aromatics	9	+0.09	1.20	-0.54	0.95	+0.45	0.82	+0.45	0.82	-0.45	0.82
Fused ring aromatics (van Krevelen)	7	-1.53	2.49	+2.72	2.25	-1.19	1.43	-1.19	1.43	+1.19	1.43

\bar{D} = arithmetic mean of C_i (calc) - C_i (obs)

σ = standard deviation of errors from the mean

$$\sigma = \sqrt{\frac{\sum (D_i - \bar{D}_i)^2}{N}}$$

group should be mentioned. The mean error and standard deviation were very small for C_3 , so that there should be no difficulty in detecting the presence of a relatively small number of C_3 groups in a saturated compound. An examination of the analysis of compounds 543, 561, 577 and 578 indicated that in cases where C_1 was actually zero the analysis yielded small negative values for C_1 ; when this occurred, if the value of C_1 was added to the value obtained for C_2 , the true value of C_2 was obtained. This suggested that in the analyses of unknown compounds, if a negative value of C_1 occurred, it should be replaced by zero and the negative value of C_1 should be added to C_2 to give the correct amount of C_2 present (#575 was an exception to this rule). Side chains and carbon atoms common to three rings appeared to have some influence on the accuracy of the analysis.

Group VI consisted of the A.P.I. fused ring aromatics. The error here was, of course, higher than for the preceding groups, but still small enough to enable the structural analysis system to be used. In this class, where the largest number of structural groups was present in a single compound, the largest number of interaction effects could be expected. The total number of compounds available in this group was so small that it was not possible to make any generalizations about the relationship between the errors in the predicted analysis and the structure. Attention is drawn to the analysis of compound #179, which exhibited the highest error in C_1 and C_2 . This result was not unexpected, as during the evaluation of the interaction effect of C_2 on C_4 it was observed that #179 did not fit the straightline relation on which this interaction factor was based.

Group VII consisted of fused ring aromatic compounds whose properties had been determined by van Krevelen (17). The errors in the predicted values of the structural groups in this class are considerably greater than in the other classes. It should be noted that the results for coronene and dodecahydrotriphenylene were not unexpected. When the original coefficients for C_5 were calculated, the data for coronene were not consistent with the other compounds and were therefore omitted. Consequently, it was expected that the accuracy of the analysis of this compound would not be very high. Dodecahydrotriphenylene represented a type of structure which the present system was not designed to treat. The unusual characteristic of this structure was the presence of C_2 and C_5 in the absence of C_4 . It will be recalled that fused ring aromatics containing C_2 groups were not successfully dealt with by determining the interaction effect of C_2 on C_4 . Clearly, this method of structural analysis was not applicable to the case where $C_4 = 0$ and C_2 and $C_5 = 0$. As in Group V, use could be made of the fact that negative values of C_1 usually indicated a true value for C_1 of zero, and that if this negative value of C_1 were added to the value obtained for C_2 , the resulting revised C_2 would be considerably closer to the true value. The rather high error for this group as a whole was considered to be due to the general unreliability of the physical property data, which has already been discussed. The accuracy of the molar volume and the molar refraction equations for this group was not as great as for all other classes. However, it was considered necessary to include this group, because of the scarcity of data for fused ring aromatic compounds.

The average accuracy for all A. P. I. hydrocarbons analyzed was considerably less than one carbon group for each type. This was considered adequate for determining the average number of the various structural groups.

It was realized, initially, that the molar volume and the molar refraction were very intimately related properties and that the equations developed in terms of the five structural groups might not be independent. However, this investigation revealed that these two equations were in fact independent, and that the differences between them were of such a magnitude that the solutions obtained were in substantial agreement with the known values of the groups present. Consequently, it was established that it was possible to deduce a considerable amount of structural information from these two closely related properties.

The results of the application of this method indicated the merits and some of the deficiencies of this type of structural analysis. As physical properties become available on "new" types of structures, the scope of this method may be extended. This approach could be applied to types of structures not already covered, by developing analogous equations for other physical properties and also by considering additional interaction effects. One of the merits of this system lay in the manner in which the coefficients in the molar volume and molar refraction equations were determined. This gave confidence in extrapolating beyond the molecular weight range of the known compounds that were used to establish the system.

- (1) Burdett, R. A., Taylor, L. W., Jones, L. C. Jr., "Molecular Spectroscopy". Report of a Conference Organized by the Spectroscopic Panel of the Hydrocarbon Research Group of the Institute of Petroleum, London, Oct. 28-29, 1954, p. 36.
- (2) Eccleston, B. H., Coleman, H. J., Adams, N. G.; J. Am. Chem. Soc. 72. 3866-70 (1950).
- (3) Egloff, G., Physical Constants of Hydrocarbons, Vol. III, 25, A. C. S. Monograph, Reinhold, New York, 1946.
- (4) Krevelen, D. W. van, Brennstoff-Chemie, 33, 260-8 (1952).
- (5) Ibid., 34, 167-82 (1953).
- (6) Krevelen, D. W. van, Blom, L., and Cherrmin, H. A. G., Nature 171. 1075-6 (1953).
- (7) Krevelen, D. W. van, and Cherrmin, H. A. G., Fuel, 33, 79-87 (1954).
- (8) Krevelen, D. W. van, and Schuyer, J., "Coal Science, Aspects of Coal Constitution", Chapters VI and VII, Elsevier, Amsterdam, 1957.
- (9) Kurtz, S. S. Jr., and Sankin, A., Ind. Eng. Chem. 46, 2186-91 (1954).
- (10) Lorentz, H. A., Ann Physik. 9. 641 (1880).
- (11) Mahdi, A. A. K. Al., and Ubbelohde, A. R., Proc. Roy. Soc. (London), 220A. 143-56 (1953).
- (12) Mahdi, A. A. K. Al., and Ubbelohde, A. R. Changements de Phases, Comptes-rendus de la deuxieme Reunion Annuelle, Soc. Chim. Phys., Paris, June 1952, pp. 360-65.
- (13) Nes, K. van, and Westen, H. A. van, "Aspects of the Constitution of Mineral Oils", pp. 299-314, Elsevier, Amsterdam, 1951.
- (14) Ibid., pp. 318-49 and pp. 445-53.
- (15) Ibid., Chapter IV.
- (16) Schiessler, R. W., and Whitmore, F. C., Ind. Eng. Chem. 47, 1660-5 (1956); Am. Doc. Inst., Doc. 4597.
- (17) Schuyer, J., Blom, L., and Krevelen, D. W. van. Trans. Far. Soc. 49, 1391-1401 (1953).

- (18) Schuyer, J., and Krevelen, D.W. van, *Fuel*, 33, 176-83 (1954).
- (19) Vlugter, J.C., Waterman, H.I., and Westen, H.A. van, *J. Inst. Petroleum Technol.* 18, 735-50 (1932).
- (20) Vlugter, J.C., Waterman, H.I., and Westen, H.A. van, *J. Inst. Petroleum Technol.* 21, 661-76 (1935).
- (21) Ward, A.L., and Kurtz, S.S. Jr., *Ind. Eng. Chem. Anal. Ed.* 10, 559-76 (1938).

PRODUCTION OF PIPELINE GAS BY BATCH
HYDROGENOLYSIS OF OIL SHALE

by

E. B. Shultz, Jr. and H. R. Linden
Institute of Gas Technology
Chicago, Illinois

ABSTRACT

The conversion of oil shale to high heating value gases by direct hydrogenation was investigated to determine if the production of pipeline gas by this method was feasible and if it offered potential advantages over alternate methods for utilization of the large reserves of this fossil fuel. Data on the batch hydrogenolysis of a 22.9 gal. per ton Fischer assay Colorado oil shale were obtained at a maximum reactor temperature of 1300°F., maximum pressures of 1200 to 5700 p.s.i.g., hydrogen-shale ratios equivalent to 50 to 200 per cent of stoichiometric requirements for complete conversion of the organic carbon plus hydrogen content to methane, and for three particle size ranges. Nearly complete conversion of organic carbon and hydrogen to a fuel gas with a heating value of over 800 B.t.u. per standard cubic foot was obtained in relatively short residence times at temperatures of 1200° to 1300°F., with only little formation of carbon oxides from mineral carbonate decomposition. In view of the relatively low material costs, these results indicate that serious consideration can be given to supplementing the future supply of natural gas with synthetic high heating value gas from oil shale, particularly in areas served by long-distance transmission lines passing in the vicinity of the Colorado deposits.

NOT FOR PUBLICATION

Presented Before the Division of Gas and Fuel Chemistry
American Chemical Society
Chicago, Illinois, Meeting, September 7-12, 1958

PRODUCTION OF PIPELINE GAS BY BATCH HYDROGENOLYSIS OF OIL SHALE

E. B. Shultz, Jr. and H. R. Linden
Institute of Gas Technology
Chicago, Illinois

An exploratory investigation has been made of the dry, high-pressure hydrogenolysis (hydrogasification) of oil shale as part of a continuing program concerned with the production of natural gas supplements and substitutes from liquid and solid fossil fuels.

Previous publications in this series have dealt with the high-pressure hydrogasification of petroleum oil, bituminous coal and lignites, and pure compounds related to petroleum oils.^{4,13,14} The purpose of the present work was to determine if the recovery of the organic constituents of oil shale in the form of high heating value gas would provide an attractive alternative to the conventional approach of maximizing liquid products recovery. Results indicated that rapid, and nearly complete conversion of the organic carbon plus hydrogen content of oil shale to a high methane and ethane content gas of over 800 B.t.u./SCF (standard cubic foot at 60°F., 30 inches of mercury pressure, saturated with water vapor) heating value can be obtained at relatively moderate temperatures and pressures.

A Colorado oil shale of 22.9 gal. per ton Fischer assay was used throughout the study, since this material appeared representative of the Green River formation deposit of Northwestern Colorado estimated to contain about 1260 billion barrels of oil.⁶

An indication of the need for development of economical methods for the production of pipeline gas from the large reserves of solid fossil fuels can be obtained from a recent study of factors influencing United States crude oil and natural gas production.⁵ The results of this study show that on the basis of an estimate of average drilling return (ratio of established reserves to footage drilled), domestic crude oil prices would have to reach \$6 per barrel to achieve an ultimate recovery of 160 billion barrels, and that at a maximum price of \$4 per barrel only 140 billion barrels would be ultimately recovered. These crude oil prices were computed after allowing for natural gas revenues ranging from 50 cents per barrel at present, to over \$1 per barrel at the time ultimate crude oil recovery reaches 160 billion barrels. Since 88 billion barrels of domestic crude oil had already been discovered at the end of 1957, this would correspond to additional discoveries of only 52 billion barrels at a maximum price of \$4 per barrel, or 72 billion barrels at a maximum price of \$6 per barrel, assuming average drilling return. At an expected average future recovery of 6000 cubic feet of natural gas per barrel of crude oil,^{5,18} the total additional gas supply, including present reserves of 247 trillion cubic feet,¹ would then be about 560 and 680 trillion cubic feet, respectively. This is substantially less than a recent estimate of 1200 trillion cubic feet (corresponding to an ultimate crude oil recovery of 250 billion barrels), based on geological factors without consideration of economic limitations on exploration and drilling.^{7,18}

Thus, if increased importation of relatively low-cost foreign crude is permitted, lack of economic incentives may retard development of a major portion of potential domestic crude oil reserves. Oil shale would correspondingly gain in importance as an alternate source

of pipeline gas in view of the large and well-known proved reserves, approaching in magnitude the thermal value of economically recoverable coal reserves.^{11,12}

APPARATUS AND PROCEDURE

The one-liter Autoclave Engineers high-temperature, high-pressure reactor used in previous batch hydrogenolysis studies was used in this work.^{13,14} The procedure was essentially the same as described in the pure compound study.¹⁴ The reactor was charged at room temperatures and placed in the rocking furnace, which was also at room temperature. Heating at full input (4.5 kw.) was maintained throughout the rising temperature portion of the run, with temperature rising at about 9°F. per minute. Simultaneous temperature and pressure measurements were taken, and gas samples were obtained at intervals throughout the course of each run which consisted of a 128 to 152 minute period required to reach the nominal temperature of 1300°F., and an additional 30 minute period at 1300°F. In all cases reaction was initiated well below 1300°F.; the initiation of rapid gasification appeared to correlate with the appearance of a well-developed temperature dip at 1025°F. In accordance with previous practice, this was designated the initial gasification temperature for oil shale and was arbitrarily used as a zero time base for the space-time yield calculations. Feed and residue shale samples were subjected to sieve analysis, and to ultimate analysis for total carbon and hydrogen. Mineral carbon was determined gravimetrically from the carbon dioxide evolved with acid, in a technique employed by the Bureau of Mines Experiment Station, Laramie, Wyoming; organic carbon was obtained by difference.¹⁷ Carbon dioxide liberation values determined from residue shale analyses were found to be uniformly greater than values obtained from gas analysis data, because of continued evolution of carbon dioxide after runs were terminated; conclusions concerning carbon oxides formation were drawn from product gas yields and compositions.

Product gas samples were analyzed with a Consolidated Engineering Co. Model 21-103 mass spectrometer; heating values and specific gravities were calculated from the analyses. Product gas volumes and heating values were calculated at 60°F., 30 inches of mercury absolute pressure, and saturation with water vapor, assuming the ideal gas law. Specific gravities were calculated on a dry basis from the average molecular weight of the gas referred to air of molecular weight 28.972. Initial hydrogen volumes were obtained by direct measurement; the reactor was charged with shale and hydrogen to the desired pressure, and the hydrogen was slowly vented through a wet test meter. Use of compressibility data at room temperature permitted the calculation of reactor free space when charged with shale. Product gas volumes during the course of the run at temperatures of 950°F. and above were calculated from observed temperatures and pressures and the initial reactor free space, assuming ideal gas behavior. Previous work with coal has shown that gas volumes calculated by this method agree with values measured by wet test meter, with a deviation of about 3 per cent.¹³ Further, the reasonably close agreement of reported organic carbon and hydrogen conversions based on computed product gas volumes, and organic carbon conversions based on residue ultimate analyses, supports the use of pressure-temperature-reactor volume measurements with assumption of ideal gas behavior. The feed shale analysis is given in Table 1, and the effects of process variables are shown in Tables 2, 3, and 4, and Figures 1 and 2.

Table 1.-ASSAY AND ANALYSIS OF U. S. BUREAU
OF MINES OIL SHALE SBR58-40X

Fischer Assay ^a	
Oil, wt. %	8.8
Water, wt. %	1.2
Spent shale, wt. %	88.0
Gas + loss, wt. %	2.0
Total	100.0
Oil, gal./ton	22.9
Water, gal./ton	3.0
Sp. gravity of oil, 60°/60°F.	0.917-0.918

Carbon-Hydrogen Analysis ^b	
Carbon, wt. %	
Mineral	4.88
Organic	10.52
Total	15.40
Hydrogen, wt. %	1.59
Ash, wt. %	68.98
Mineral CO ₂ , wt. %	17.88

Sieve Analysis ^c	
40-100 Mesh Sample	
Runs 3, 4, 5, 10, 11	
U.S.S. Sieve	Wt. %
+40	0.8
40-50	25.3
50-60	20.0
60-70	19.1
70-80	16.7
80-100	13.6
-100	4.5
Total	100.0

Sieve Analysis ^d	
5-20 Mesh Sample	
Run 8	
U.S.S. Sieve	Wt. %
+5	4.6
5-8	41.3
8-10	4.7
10-12	8.4
12-14	8.1
14-16	13.4
16-18	0.6
18-20	13.2
-20	5.7
Total	100.0

Sieve Analysis ^e	
140-325 Mesh Sample	
Run 9	
U.S.S. Sieve	Wt. %
+140	3.2
140-170	24.5
170-200	0.4
200-230	32.8
230-270	11.2
270-325	0.2
-325	27.7
Total	100.0

- a) Average of U. S. Bureau of Mines Runs 53456 and 53457.¹⁷
- b) Average of U. S. Bureau of Mines Runs 10291 and 10292.¹⁷
- c) I.G.T. Lab. No. 3910.
- d) I.G.T. Lab. No. 4012.
- e) I.G.T. Lab. No. 4013

Table 3.-EFFECTS OF HYDROGEN FEED RATIO ON HYDROGASIFICATION OF OIL SHALE

	RUN 11 - 0.100 lb. ORGANIC C+H, 50% OF STOICHIOMETRIC				RUN 5 - 0.025 lb. ORGANIC C+H, 200% OF STOICHIOMETRIC			
	1	2	3	4	1	2	3	4
Feed shale weight, lb	1025	1075	1200	1300	1290	1290	1290	1298
Organic C+H, lb.	205	245	320	405	4075	4075	4075	2040
Feed hydrogen	93	103	107	127	157	177	177	165
Initial pressure, p.s.i.g.								
Feed ratio								
% of stoichiometric ^a	51.5							
SCF/lb. of organic C+H	15.78							
SCF/ton of shale	3822							
Operating Results								
Reactor temperature, °F.	950	1025	1075	1200	1300	1290	1290	1295
Reactor pressure, p.s.i.g.	2050	2450	2545	3230	4055	4145	4075	2080
Time above room temp., min.	93	103	107	127	147	157	177	2040
Time to start run temp., (1300°F.) min.								
Product gas yield ^b								
SCF/lb. org. C+H	15.76	17.44	17.52	20.54	24.30	24.42	24.56	56.42
SCF/ton of shale	3817	4224	4244	4974	5886	5915	5949	13662
Net B.t.u. recovery	490	1511	2332	3582	5656	3423	3330	4366
M.B.t.u./ton of shale	11.2	31.7	49.5	72.3	76.7	70.8	68.8	104.0
Gasification of organic C+H in shale, % of total ^b								
Gasification of organic C in shale, % of total ^d								
Gaseous hydrocarbon space- time, reactor-hr.								
Thermal space-time yield, M.B.t.u./cu.ft. reactor-hr.								
Spent shale, wt. % of shale charged								
Material balance, %								
Product Gas Properties								
Composition, mole %								
N ₂ + CO	2.4	3.6	4.4	3.3	4.1	5.4	6.1	8.6
H ₂	5.1	6.1	6.1	10.0	13.8	16.9	16.1	5.4
CH ₄	85.1	67.2	49.6	3.2	3.8	4.7	5.3	4.1
C ₂ H ₆	3.5	10.4	18.3	71.4	75.4	74.0	71.6	31.9
C ₃ H ₈	1.9	5.9	10.4	10.1	2.0	0.6	0.4	50.7
C ₄ H ₁₀	1.6	4.4	7.2	0.5	0.1	0.1	0.1	3.2
Higher paraffins	1.0	2.1	2.8	0.2	0.1	0.1	0.2	0.1
CH ₄								
Higher olefins								
Benzene								
Toluene								
Total	100.0	100.0	100.0	100.0	100.0	100.0	100.0	100.0
Heating value, B.t.u./SCF	449.2	646.8	837.1	965.6	835.4	785.2	765.1	692.0
Specific gravity (air = 1)	0.238	0.411	0.565	0.728	0.712	0.708	0.719	0.466

a) Stoichiometric for complete conversion of organic C + H in shale to methane.
 b) Calculated from observed reactor pressure and temperature, and initial reactor free volume, assuming ideal gas law.
 c) Product of gas yield and heating value, less thermal input of feed hydrogen.
 d) Calculated from carbon analysis of residue.
 e) Value doubtful.

Table 4.-EFFECTS OF PARTICLE SIZE RANGE ON HYDROGASIFICATION OF OIL SHALE

	RUN 8 - 5 TO 20 MESH PARTICLE RANGE				RUN 9 - 140 TO 325 MESH PARTICLE RANGE			
Feed Shale Charge weight, lb.	0.4129	0.4129	0.4129	0.4129	0.4129	0.4129	0.4129	0.4129
Organic C+H, lb.	0.0500	0.0500	0.0500	0.0500	0.0500	0.0500	0.0500	0.0500
Feed rate, lb./hr.	725	725	725	725	740	740	740	740
Initial pressure, p.s.i.g.	103.2	103.2	103.2	103.2	103.0	103.0	103.0	103.0
Feed ratio	31.64	31.64	31.64	31.64	31.54	31.54	31.54	31.54
% of stoichiometric C+H	7663	7663	7663	7663	7639	7639	7639	7639
SCF/lb. of organic C+H	850	1085	1075	1200	1300	1298	1300	1300
SCF/ton of shale	1800	2075	2015	2400	2400	2385	2400	2400
Operating Results	68	100	107	125	140	150	170	170
Reactor temperature, °F.	--	--	--	0	30	30	30	30
Reactor pressure, p.s.i.g.	31.44	32.34	31.60	31.68	32.58	33.16	34.02	34.02
Reactor space-time, min. (1300°F.), min.	7614	7832	7653	7672	7891	8031	8239	8239
Product gas yield, ^b SCF/ton of shale	425	1948	2725	4062	4191	4017	3739	3739
Net B.t.u. recovery, M B.t.u./ton of shale	10.6	42.4	60.0	87.4	95.5	93.4	88.4	88.4
Gasification of organic C+H in shale, % of total	--	--	--	--	--	--	93.5	93.5
Gas in shale, % of total	--	--	--	--	--	--	--	--
Gaseous hydrocarbon space-time yield, SCF/cu.ft. reactor-hr.	--	--	104.7	58.7	45.2	39.2	29.0	29.0
Thermal space-time yield, M B.t.u./cu.ft. reactor-hr.	--	--	257.2	90.7	57.8	45.1	30.9	30.9
Spent shale, wt. % of shale charged	--	--	--	--	--	--	79.1	79.1
Water balance, %	--	--	--	--	--	--	98.9	98.9
Proximate analysis, %								
Composition, mole %								
N ₂ + CO	1.1	2.9	3.8	6.4	8.1	7.0	6.3	6.0
CO ₂	1.6	2.0	2.6	5.3	10.9	13.9	17.3	15.7
H ₂	92.8	77.2	66.1	33.4	15.2	9.1	5.9	4.8
CH ₄	1.3	7.9	12.6	33.5	52.0	62.8	68.7	66.0
C ₂ H ₆	0.5	4.6	7.4	19.8	12.8	6.4	1.4	1.6
C ₃ H ₈	0.4	3.0	5.0	0.7	0.2	0.2	--	--
Higher paraffins	0.3	0.2	0.3	0.1	--	--	--	--
Alkynes	0.3	0.5	0.5	0.2	--	--	--	--
Higher olefins	0.7	0.6	0.3	0.4	0.8	0.6	0.4	0.4
Benzene	100.0	100.0	100.0	100.0	100.0	100.0	100.0	100.0
Total	377.2	561.5	676.0	848.5	841.4	805.0	750.9	750.9
Heating value, B.t.u./SCF	0.147	0.296	0.393	0.585	0.698	0.717	0.733	0.733
Specific gravity (air = 1)								

a) Stoichiometric for complete conversion of organic C + H in shale to methane.
 b) Calculated from observed reactor pressure and temperature, and initial reactor free volume, assuming ideal gas law.
 c) Product of gas yield and heating value, less thermal input of feed hydrogen.
 d) Calculated from carbon analysis of residue.

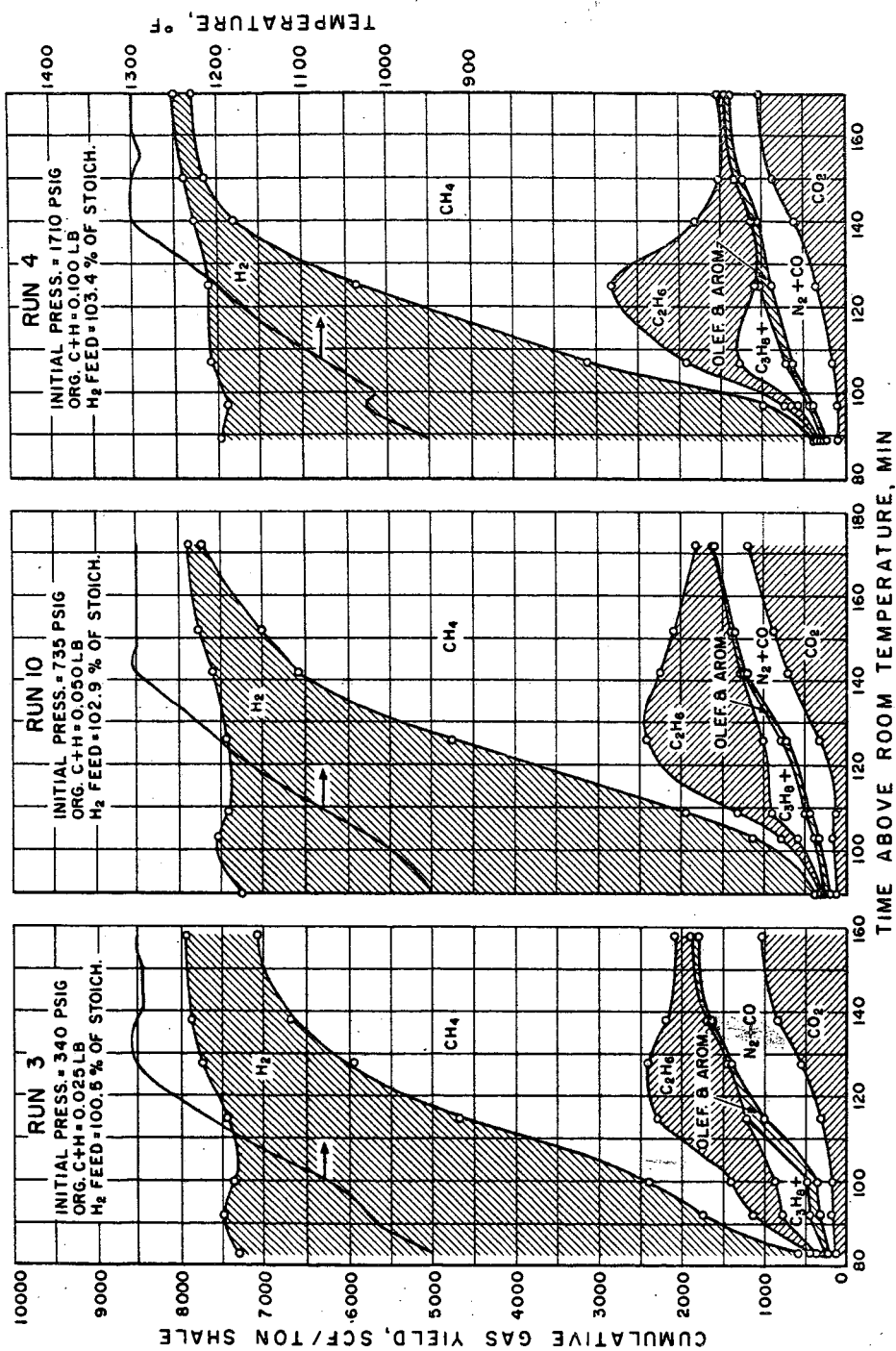
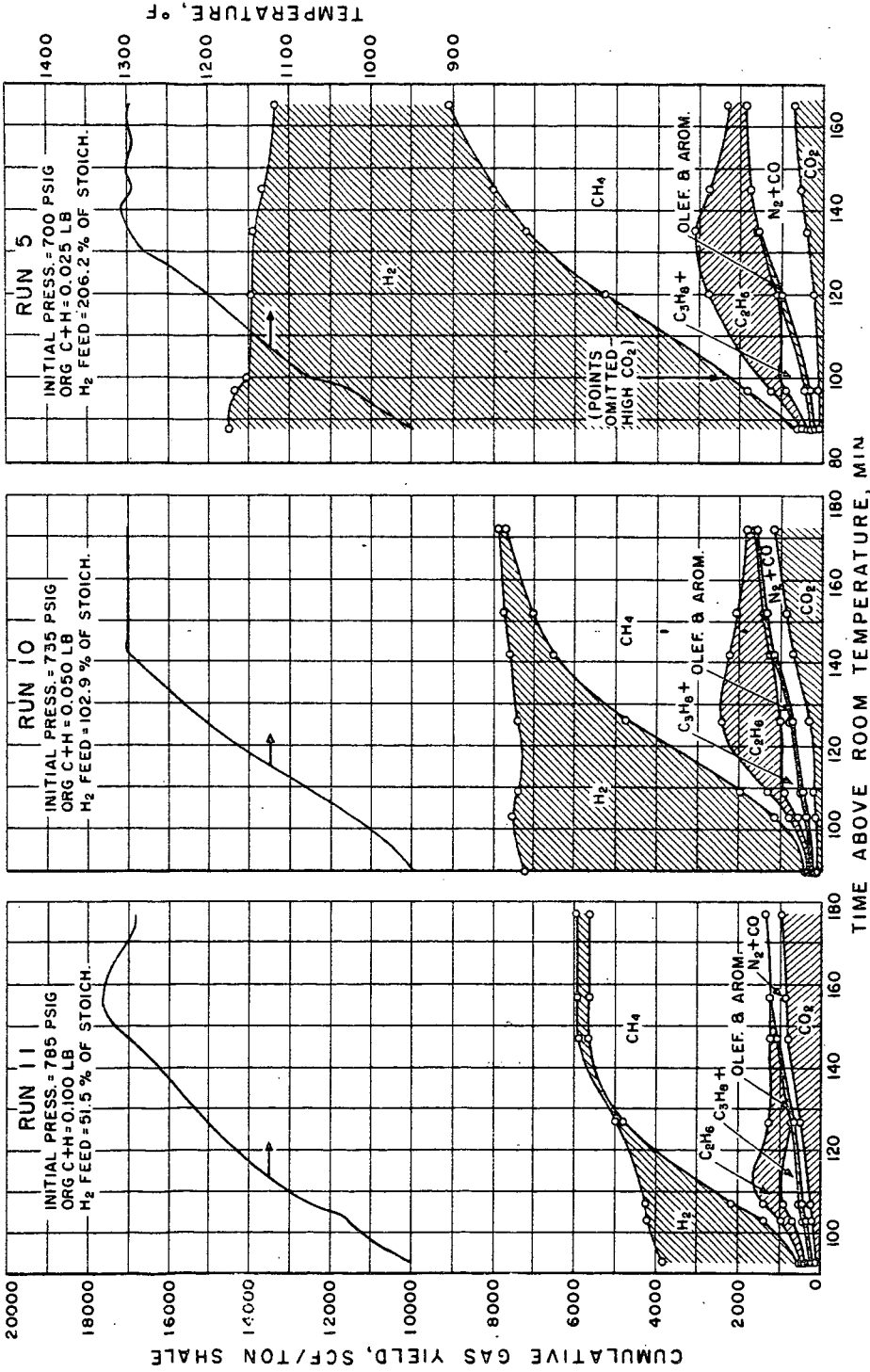


FIG. 1.-EFFECTS OF PRESSURE ON HYDROGASIFICATION YIELDS OF 22.9 GAL./TON FISCHER ASSAY OIL SHALE



TEMPERATURE, °F

TIME ABOVE ROOM TEMPERATURE, MIN

Fig. 2.-EFFECTS OF FEED RATIO ON HYDROGASIFICATION YIELDS OF 22.9 GAS./TON FISCHER ASSAY OIL SHALE

EFFECTS OF PRESSURE

At all three pressure levels studied, 340, 735 and 1710 p.s.i.g. initial pressure (1215, 2430 and 5540 p.s.i.g., respectively, upon attainment of 1300°F.), the results showed that high heating value product gases were obtained at high organic carbon-plus-hydrogen conversions as the nominal run temperature of 1300°F. was approached; product gas dilution with carbon oxides was not excessive and practically no liquid products were formed (Table 2). The spent shale was free flowing and had virtually the same sieve analysis as the charge.

Rapid attainment of high conversions of the organic matter to gas (primarily methane, ethane and propane) at temperatures of only 1200° to 1300°F. was primarily responsible for the low evolution of mineral carbon oxides⁹; this differs significantly from the results obtained in high-temperature retorting at low pressures and in the absence of hydrogen.^{2,18} Although higher pressure would be expected to suppress carbon dioxide evolution, the apparent yield and mole per cent of carbon dioxide was not affected significantly by pressure level (Figure 1). However, total yields of carbon oxides were decreased at the higher pressures, reflecting the decrease in carbon dioxide conversion to carbon monoxide by the reaction $\text{CO}_2 + \text{H}_2 \rightarrow \text{CO} + \text{H}_2\text{O}$, as the hydrogen content of the product gas decreased. Even at the lowest pressure level, total carbon oxides content was only 22.4 mole %. (The reported $\text{N}_2 + \text{CO}$ contents were primarily carbon monoxide.)

The hydrocarbon hydrogenolysis reactions, and the sequence of appearance of the stable intermediates in methane production from higher molecular weight carbon-containing materials (such as oil shale kerogen), corresponded closely to those observed in hydrogenolysis of petroleum oils¹³ and pure compounds related to petroleum oils.¹⁴ Propane and higher paraffin hydrocarbons formed in earlier portions of each run were soon hydrogenolyzed with increasing appearance of ethane and methane. Ethane yields and concentrations in turn passed through maxima with increases in time and temperature, as methane, the stable final product, continued to increase. Maximum ethane yields were observed at attainment of 1200°F. at all pressures (Figure 1). The effect of pressure increase was to increase the rate of ethane production below 1200°F. and the rate of ethane disappearance to methane above 1200°F. Methane yields were considerably increased above 1200°F. with increases in pressure, accompanied by increases in conversions and space-time yields. Increased hydrogen consumptions at higher pressures, together with lower carbon oxide yields and higher methane yields resulted in considerable increases in product gas heating values. For example, heating values of 792, 871 and 908 B.t.u./SCF were observed at attainment of 1300°F. as pressure was increased from 1215 to 2430 to 5540 p.s.i.g., respectively (Table 2).

At the two higher pressures studied, as well as in other runs carried out at 100% of stoichiometric feed ratio, the gasification of organic carbon-plus-hydrogen decreased slightly at temperatures of 1200° to 1300°F., accompanied by a decline in gas heating value in excess of that corresponding to increased carbon oxide formation. This indicates that insufficient hydrogen may have been present in the later portions of these runs to prevent a small amount of carbon formation from product hydrocarbons. This effect appeared to be greater at higher pressures, due to decreased hydrogen concentrations brought about by the higher hydrogen consumptions characteristic of higher pressure operation.

EFFECTS OF HYDROGEN-SHALE FEED RATIO

Figure 2 presents gas yield data at hydrogen-shale feed ratios of 50% (Run 11), 100% (Run 10) and 200% (Run 5) of stoichiometric requirements for conversion to methane; complete results for Runs 11 and 5 are given in Table 3, and for the key test, Run 10, in Table 2. At temperatures below 1200°F., the extent of gasification at 50% of stoichiometric hydrogen-shale feed ratio was approximately the same as at the higher feed ratios so that, in the absence of excess hydrogen dilution, earlier formation of high heating value product gas occurred. However, at the higher temperatures, conversions were reduced substantially by decreases in hydrogen supply, but not proportionally to reductions in feed ratio. For instance, at 1300°F., gasification of organic carbon and hydrogen was 77 weight % at 50% of stoichiometric, 90 weight % at 100% of stoichiometric, and complete at 200% of stoichiometric feed ratio. Considerable vapor-phase carbon formation was indicated during the later portion of the run at 50% of stoichiometric, and none at 200% of stoichiometric. This compares with evidence of only limited vapor-phase carbon formation, indicated by a gradual decline in conversion and product gas heating value, late in the course of the run at 100% of stoichiometric feed ratio.

Pressure levels for Runs 10 and 5 at 100% and 200% of stoichiometric feed ratio, respectively, were quite comparable, permitting a direct evaluation of the effect of hydrogen concentration on carbon oxides formation. Total carbon oxide yields were about the same for these two runs, but increased hydrogen concentration at 200% of stoichiometric feed ratio caused much greater conversion of evolved carbon dioxide to carbon monoxide.

Ethane yields were increased by increases in feed ratio from 50% to 200% of stoichiometric; however, ethane contents were greatest at 100% of stoichiometric feed ratio. Dilution of the product gas with excess hydrogen reduced the ethane content at 200% of stoichiometric, and pyrolysis reactions favoring methane over ethane formation reduced the ethane content at 50% of stoichiometric.

EFFECTS OF PARTICLE SIZE RANGE

In view of the substantial cost of oil shale size reduction,¹⁰ it would be desirable to utilize relatively large particle sizes if a practical hydrogenolysis process can be developed for moving- or fixed-bed operation. In Table 4, it can be seen that insignificant effects on gas yields and composition resulted from a variation in particle size range from 5-20 mesh to 140-325 mesh.

COMMERCIAL POSSIBILITIES

Production of pipeline gas from oil shale may be preferable to liquid fuel production because of higher conversion of organic matter (90-100 weight % for hydrogasification, compared to about 80 weight % conversion to liquid and gaseous products in conventional retorting²) and elimination of costly liquid product refining operations. Hydrogasification, in addition to producing a free-flowing residue containing little organic matter, also yields only negligible quantities of liquid products. This differs from oil hydrogasification^{13, 14} and pyrolysis of crude shale oil,⁹ where substantial quantities of liquid byproducts are formed. Absence of agglomeration problems should permit the development of continuous moving- or fluid-bed oil shale hydrogasification processes. Fixed-bed operation would have the advantage of reduced feed preparation costs. Hydrogen requirements could be met with conventional catalytic steam reforming and carbon

oxide removal processes, utilizing a portion of the purified product gas for feed and fuel.

On the basis of the results with 22.9 gal. per ton shale at 50 to 100% of stoichiometric feed ratios, about 4900 to 6600 SCF/ton of 1000 B.t.u./SCF equivalent gas can be produced with 3800 to 7600 SCF/ton of hydrogen feed. Total product gas requirements for hydrogen production, including all fuel requirements, will be about 1900 to 3800 SCF/ton, leaving a net 1000 B.t.u./SCF equivalent gas yield of 2800 to 3000 SCF/ton. Heat requirements for the shale processing step, estimated from gas combustion retort data³, will be about 500,000 B.t.u./ton, so that if product gas is used as a source of heat, a net gas yield of 2300 to 2500 SCF/ton would finally be obtained. At 50 cent/ton mining cost and 25 cent/ton crushing cost,¹⁰ this would result in a raw material cost of 30 to 33 cents/1000 SCF of 1000 B.t.u./SCF gas equivalent for 22.9 gal. per ton shale. Large deposits of shale average 30 gal. per ton or more,⁹ so that raw material cost could be reduced to less than 30 cents/MCF with the richer shale.

Existing pipeline systems and requested extensions could supply the major West Coast and Middle West marketing areas with pipeline gas produced in Colorado. With adequate storage, already under consideration by Congress, the flow of the Colorado river is adequate to provide water for a 2 million barrel per day oil shale industry, which is equivalent to about 8 billion cubic feet per day of net pipeline gas production.¹⁰

CONCLUSIONS

Nearly complete conversion of the organic matter of a typical Colorado oil shale to high methane and ethane content, high heating value fuel gases has been achieved in batch hydrogenolysis at 1200° to 1300°F. in the presence of sufficient hydrogen to convert the organic carbon and hydrogen to methane. Liberation of mineral carbon dioxide was kept at a low level by operation at these relatively low temperatures. Particle size range variations from 5-20 mesh to 140-325 mesh had no significant effect on gasification rates and yields. Increases in pressure to 5500 p.s.i.g. resulted in more rapid formation of high heating value gas, higher gas yields and lower total yields of carbon oxides. However, pressure increases above 2000 to 2500 p.s.i.g. did not appear to afford advantages commensurate with the cost increases that would be involved in a commercial application. Hydrogen feed of twice the stoichiometric requirements for methane formation resulted in complete conversion of organic carbon content, but excess hydrogen diluted the product gas. Hydrogen feed of one-half of the stoichiometric requirements resulted in lower conversions and some vapor-phase carbon deposition, but pyrolysis reactions brought about high yields of high heating value gases at 1200°F. before appreciable carbon deposition appeared to begin. Low hydrogen concentrations in the product gas slowed conversion of carbon dioxide to carbon monoxide, an undesirable reaction which consumes feed hydrogen. Although fuel gases of pipeline quality were produced in this study without further treatment, it would probably be economic to remove carbon dioxide before high-pressure transmission. On the basis of these results, high heating value gas production by hydrogasification of oil shale with hydrogen produced from a portion of the product gas appears both technically and economically feasible. In view of the large reserves of oil shale, vastly exceeding estimated ultimate crude oil reserves and approaching in magnitude the thermal value of economically recoverable coal reserves, serious consideration to this alternate source of pipeline gas should be given in studies of future gas supply.

ACKNOWLEDGMENT

This study was conducted as part of the basic research program of the Institute of Gas Technology with funds provided by its Members and Contributors. M. A. Elliott, director of the Institute and H. M. Henry, president of the N.E.G.E.A. Service Corporation were very helpful in formulating the program. H. M. Thorne, Chief of Oil-Shale Research, Region III, Bureau of Mines, made the oil shale supply and analyses available and contributed valuable information required for the study. The batch hydrogenation tests were performed by R. F. Johnson. D. M. Mason and J. E. Neuzil provided the analytical data.

LITERATURE CITED

- (1) Amer. Gas Assoc., Amer. Petroleum Inst. and Canadian Petroleum Assoc., "Proved Reserves of Crude Oil, Natural Gas Liquids and Natural Gas in the United States and Canada, December 31, 1957," No. 12, The Societies, New York and Calgary, Alberta, 1957.
- (2) Brantley, F. E. and others, "High Temperature Shale Oil," Ind. Eng. Chem. 44, 2641-50 (1952).
- (3) Cameron, R. J. and Guthrie, B., "Oil from Shale," Chem. Eng. Progr. 50, 336-41 (1954).
- (4) Channabasappa, K. C. and Linden, H. R., "Fluid-Bed Pretreatment of Bituminous Coals and Lignite-Direct Hydrogenation of the Chars to Pipeline Gas," Ind. Eng. Chem. 50, 637-44 (1958).
- (5) Davis, W., "A Study of the Future Productive Capacity and Probable Reserves of the U. S.," Oil Gas J. 56, 105-19 (February 24, 1958).
- (6) Donnell, J. R., "Preliminary Report on Oil-Shale Resources of Piceance Creek Basin Northwestern Colorado," U. S. Geological Survey Bulletin 1042-H, Govt. Print. Office, Washington, D. C., 1957.
- (7) Hill, K. E. and others, "Future Growth of the World Petroleum Industry," The Chase Manhattan Bank, New York, 1957.
- (8) Jukkola, E. E. and others, "Thermal Decomposition Rates of Carbonates in Oil Shale," Ind. Eng. Chem. 45, 2711-14 (1953).
- (9) Linden, H. R. and others, "High Temperature, Vapor-Phase Cracking of Hydrocarbons," Ind. Eng. Chem. 47, 2467-82 (1955).
- (10) Prien, C. H. and Savage, J. W., "A Shale-Oil Industry is on its Way," Chem. Eng. Progr. 52, 16-J-26-J (1956).
- (11) Rubel, A. C., "Shale Oil - as a Future Energy Resource," The Mines Magazine 45, 72-76 (1955) October.
- (12) "Shale, Coal Gas to Supplement Natural," Oil Gas J. 56, 110-11 (April 7, 1958).
- (13) Shultz, E. B., Jr., Channabasappa, K. C. and Linden, H. R., "Hydrogasification of Petroleum Oils and Bituminous Coal to Natural Gas Substitutes," Ind. Eng. Chem. 48, 894-905 (1956).
- (14) Shultz, E. B., Jr. and Linden, H. R., "Batch Hydrogenolysis Reactions of Pure Compounds Related to Petroleum Oils," Ind. Eng. Chem. 49, 2011-16 (1957).
- (15) Sohns, H. W. and others, "Entrained-Solids Retorting of Colorado Oil Shale-Equipment and Operation," Ind. Eng. Chem. 47, 461-64 (1955).
- (16) Terry, L. F. and Winger, J. F., "Future Growth of the Natural Gas Industry," The Chase Manhattan Bank, New York, 1957.
- (17) Thorne, H. M., Bureau of Mines Experiment Station, Laramie, Wyoming, Private Communication, February, 1958.
- (18) Tihen, S. S. and others, "Entrained-Solids Retorting of Colorado Oil Shale-Product Yields and Properties," Ind. Eng. Chem. 47, 464-68 (1955).

PERFORMANCE OF SUPPORTED NICKEL CATALYSTS IN CYCLIC
STEAM REFORMING OF NATURAL GAS

by
J. M. Reid and D. M. Mason
Institute of Gas Technology
Chicago, Illinois

ABSTRACT

Comparatively little data are available regarding the performance of catalysts in the cyclic steam-hydrocarbon reforming process used by the utility gas industry on the Eastern Seaboard, and more extensively in Europe and Asia. In this study, several commercial types of supported nickel catalysts having either alumina or magnesia as the base material were subjected to cyclic process conditions in a laboratory reforming apparatus. Catalyst performance and catalyst life were significantly affected by the oxygen which was present during the heating portion of the cycle. Unlike the continuous steam-hydrocarbon reforming process used extensively by the chemical industry for production of hydrogen and ammonia synthesis gas, performance of the cyclic process was not found to be singularly dependent on the activity of the catalyst for the steam-hydrocarbon reaction, but rather under certain conditions to be controlled by the rates of oxidation and reduction of the nickel. In these tests, life of alumina-supported catalyst was related to the formation of an unreactive compound between nickel oxide and the support. Life of the magnesia-supported catalyst was related to solid solution formation between nickel oxide and the support. The inadequacy of present manufacturing specifications and testing procedures for nickel catalyst for cyclic reforming is illustrated by these results.

NOT FOR PUBLICATION

Presented Before the Division of Gas and Fuel Chemistry
American Chemical Society
Chicago, Illinois Meeting, September 7-12, 1958

PERFORMANCE OF SUPPORTED NICKEL CATALYSTS IN CYCLIC
STEAM REFORMING OF NATURAL GAS

J. M. Reid and D. M. Mason
Institute of Gas Technology
Chicago, Illinois

INTRODUCTION

Catalytic steam reforming of natural gas and other low molecular weight hydrocarbons is a well established process.^{6,29,32,33,40,41} It has been applied extensively in the chemical industry where large quantities of hydrogen are required, as in the case of ammonia synthesis. A few installations have also appeared in the utility gas industry for the production of low heating value fuel gases.^{1,18,21}

The process is carried out in a tube furnace in which preheated steam and hydrocarbon are passed through externally heated catalyst-filled tubes. The hydrocarbon and steam react to produce hydrogen, carbon monoxide and some carbon dioxide. This reaction is highly endothermic. Reaction temperatures range from about 1200°F. to 1800°F. and pressures from atmospheric to several atmospheres. The most commonly employed catalyst is reduced nickel oxide supported by a high surface area refractory material; nickel concentrations range from several weight percent to more than 30.

Performance of these catalysts has been extensively investigated.^{5,30,31} In addition to process conditions, the major factors influencing the catalyst behavior have been shown to be poisons such as sulfur compounds contained in the feed streams, and physical properties of the catalyst such as surface area, porosity and crystallite size. With proper control of process variables, the catalyst appears to have essentially unlimited life in commercial operation.

Cyclic Reforming

Prior to World War II, the utility gas industry in the United States was based almost entirely on carburetted water gas produced from coke, steam and oil in cyclic apparatus. The availability of low-cost natural gas to major population centers through long distance pipe lines constructed in the post-war era made processes based on solid fuel economically unfavorable. Where conditions warranted the continued distribution of low heating value gas, it was necessary to find some means for converting natural gas. The catalytic steam reforming process was ideally suited for this purpose. However, the process as developed by the chemical industry is carried out in continuous tube furnaces. To adapt this process to the gas industry would require the capitalization of entire new manufacturing plants to replace the existing carburetted water gas plants. A more attractive scheme for the utilities was made possible by the United Gas Improvement Company, which pioneered the development of the cyclic reforming process in the United States.^{20,26,34,35,42,44} The cyclic process could be carried out by a relatively low-cost modification of the existing carburetted water gas equipment. As a result, 17 cyclic process installations are in use in the eastern part of the United States.^{13,25}

The Cyclic Catalytic Reforming (CCR) process differs from the conventional continuous process, basically, only in the manner in which the heat requirements are supplied. First, the catalyst bed located in one of the refractory-lined shells from the carburetted water gas apparatus is heated to reaction temperature by the passage of hot products of combustion supplied by either oil or gas burners. This is followed by a reforming step in which steam and hydrocarbon are passed through the catalyst bed. The heat stored in the refractory shapes used for process steam preheat and in the catalyst bed during the heating step is used during the reforming step. Steam purges are normally used to separate the heating and reforming steps. The entire cycle sequence is generally completed in less than five minutes.

The catalyst employed in the cyclic reforming process is similar to continuous reforming catalyst in that it is metallic nickel supported by a refractory material. Properties of the refractory support are necessarily more stringent for the cyclic process because of the thermal shock associated with cyclic heating and cooling of the catalyst bed and because of a tendency for the bed to lift or move slightly with cyclic flow changes. The material used almost universally in commercial operation consists of fused spheres 1/2 to 1 inch in diameter, of impure alumina (90%) having medium porosity (30-40%). The catalyst is prepared by impregnating the spherical support with a nickel salt solution and then decomposing the nickel salt to nickel oxide by heating in air to about 600°C.

Performance of the catalyst has been commercially acceptable for utility operation, but the catalyst has decidedly short life compared to catalysts used in the continuous reforming process.²⁵ Ordinarily more than 50% of the original catalyst activity is lost after 2000 to 4000 hours of operation with one inch diameter catalyst. For 1/2-inch diameter catalyst, where relative light catalyst loading is used, somewhat longer life is obtained. Plant capacity is obviously affected by loss in catalyst activity, and replacement of at least part of the catalyst is required annually.

Efforts to improve catalyst performance in the cyclic process have recently become of considerable interest to utility companies using the CCR process.²⁵ In addition, extension of the CCR process to liquid hydrocarbon operation and the development of several new gas manufacturing processes which incorporate in some form the principles of cyclic catalytic steam reforming of hydrocarbons have focused attention on the performance of catalyst under cyclic conditions.^{3, 11, 22, 28, 43} In a recent study at the Institute of Gas Technology, the cyclic performance of several supported nickel catalysts was investigated under closely controlled conditions in the laboratory. It was the object of this study to determine the factors unique to the cyclic process which governed catalyst performance and were responsible for relatively short catalyst life. Significant results of this study are presented here.

EXPERIMENTAL

This study was limited to commercial catalysts containing approximately 5 weight per cent nickel. Support materials were either fused alumina (α - Al_2O_3) or fused periclase (MgO). All of the catalyst pellets were in the form of nominal 1-inch diameter spheres except for one sample with high-purity alumina support which consisted of irregularly shaped, 1-inch lumps. Only the lower purity alumina base catalyst contained magnesium oxide promoter. Properties of the

unused catalysts are shown below.

Catalyst Designation	A	B	C	D
Acid Soluble Nickel, wt. %	5.14	4.48	4.99	5.16
Magnesium Oxide Promoter, wt. %	1.81	None	None	None
Support Composition, wt. %				
Al ₂ O ₃	86.85	99+	— 0.3 —	—
MgO	--	--	— 95.5 —	—
SiO ₂	12.90	--	— 3.0 —	—
CaO	--	--	— 1.0 —	—
Fe	0.25	--	— 0.2 —	—
Pellet Shape	Sphere	Irregular	Sphere	Sphere

Catalyst nickel concentration data appearing throughout this paper refer to that nickel portion of the catalyst which was soluble in nitric acid. The nickel content was determined by boiling a ground (minus-100 mesh) sample with concentrated nitric acid until the disappearance of brown fumes, followed by filtration and gravimetric determination by a standard dimethylglyoxime method.

X-ray diffraction patterns of the catalysts were obtained by the Debye-Scherrer powder camera method.

Reforming tests were conducted in the apparatus shown in Figure 1. The reactor consisted of a 3.125-inch I.D. x 102-inch long, Type 310 stainless steel tube with a centrally located 0.675-inch O.D. thermowell of the same alloy inserted through the bottom. The reactor tube was suspended in a Smith alloy wound electric furnace with four independently controlled heating zones. The temperature in each zone was regulated by potentiometric temperature indicator-controllers in combination with chromel-alumel thermocouples. The control thermocouple was welded to the outside skin of the reactor tube at the center of each heating zone. Additional chromel-alumel thermocouples located in the internal thermowell were used to measure the catalyst temperature at three points within the bed and the feed gas stream temperature immediately before entering the bed.

Provision was made to weigh distilled water, which was fed by a chemical proportioning pump through an electrically heated steam generator to the top of the reactor tube. Natural gas was fed from high-pressure cylinders through a pressure regulator and gas meter to the top of the reactor tube, where it was mixed with the steam feed. Product gas was withdrawn from the bottom of the reactor tube through a water-cooled tube and shell condenser, where excess steam was removed. The cooled product gas stream was measured with a second gas meter before being discharged through a back-pressure regulator to the sampling system. All measured gas volumes were corrected to standard cubic feet (SCF) at 60°F., 30 inches of mercury pressure, and saturated with water vapor. A side stream of the product gas was collected for a recording calorimeter and for Orsat and mass spectrometer analyses.

For each reforming test a 0.1 cubic foot sample of catalyst was placed in the lower two heating zones of the reactor furnace and formed a 24-inch deep bed. Inert periclase spheres were used below the catalyst to properly space the bed in the reactor tube.

The apparatus as described was suitable for conducting the continuous reforming process. For cyclic operation, additional equipment was required. Provisions were made for supplying and metering both nitrogen (for purging) and air in a manner similar to the natural gas feed system. The natural gas, nitrogen and air feed lines were equipped with electrically operated solenoid valves which were opened and closed by a repeat cycle sequence timer. The steam feed system, reactor and product gas handling system were identical for cyclic

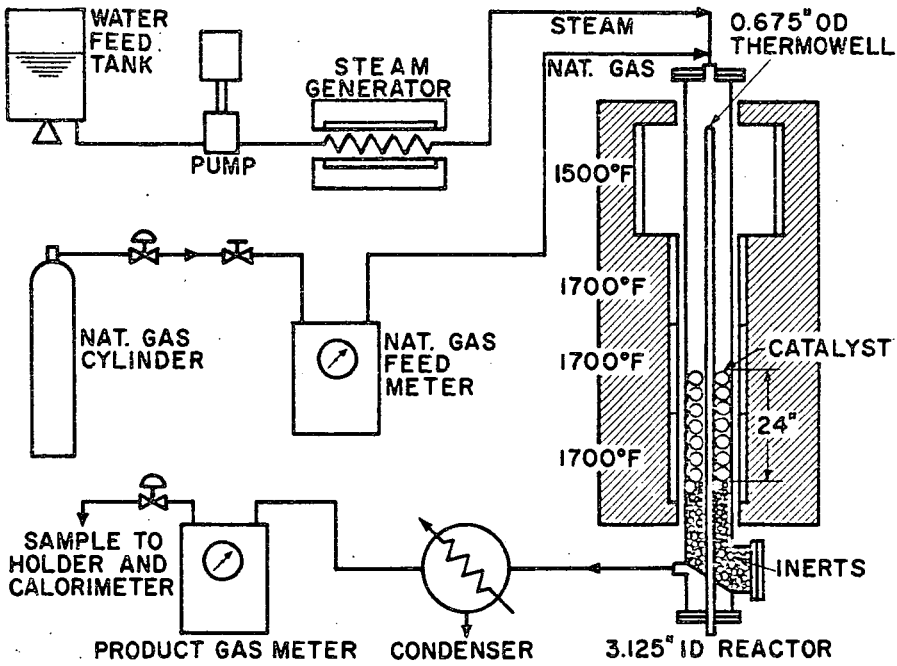


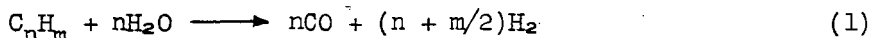
Fig. 1.-LABORATORY REFORMING UNIT

operation as for continuous reforming tests. A simple switching system made it possible to change from continuous operation to cyclic operation without interruption.

Reforming tests were long enough to insure attainment of equilibrium. The test period was normally about three to four hours after steady state was reached.

FACTORS INFLUENCING CATALYST ACTIVITY IN CYCLIC REFORMING

In the continuous reforming process the catalyst is at all times in the reduced state and at a constant temperature. The major reaction which is affected by the condition of the catalyst is that between the hydrocarbon and steam:



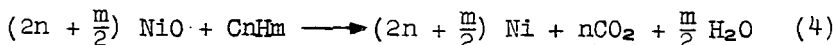
Subsequent reaction between part of the product carbon monoxide and steam has little influence on reaction (1) or on the ability of the catalyst to promote reaction (1):



The overall catalyst performance is therefore governed by the ability of the catalyst to promote the steam-hydrocarbon reaction at the temperature maintained in the catalyst bed.

Cyclic reforming is an exceedingly complex process by comparison. Neither catalyst temperature nor composition of the atmosphere remain constant. In a single cycle the catalyst is first heated, then cooled; oxidized, then reduced. The extent of these changes varies widely in actual practice. In some cases, combustion is controlled during the heating portion of the cycle so that the combustion products contacting the catalyst are essentially neutral. The quantity of catalyst which is oxidized in this instance is small. Another method of operation employs a certain amount of excess air in the combustion products to take advantage of the heat released in the catalyst bed by combustion of nickel metal.⁷ Other forms of cyclic reforming require the passage of undiluted air through the catalyst during the heating cycle.²² In all methods of operation, process heat is stored in the massive catalyst bed during the heating period for use during the make period. The catalyst, therefore, undergoes a significant change in temperature throughout the cycle.

Because of the changes in atmosphere throughout the cycle, other reactions besides reaction (1) occur in the cyclic process and are dependent upon the catalyst. Although the cyclic process is not fully understood, at least two other reactions of importance are those between metallic nickel and oxygen and between nickel oxide and a reducing agent.



Reaction (4) represents only the most probable stoichiometric relationship, and is not intended to indicate the actual mechanism of reduction in the process.

Other constituents of the reacting gases, such as sulfur compounds in the hydrocarbon feed, and nitric oxide in the combustion products used for heating, affect the process.

It is apparent that the overall catalyst performance in the cyclic process is governed by the behavior of the catalyst in all of the significant reactions which occur during the cycle, together with the change in catalyst temperature over the course of a cycle. The rates of one or more of these reactions may be controlling for a selected cycle so that the process is not singularly dependent on reaction (1) as in the case of continuous reforming.

To determine the extent to which the overall catalyst performance in cyclic operation differs from continuous reforming, a series of cyclic tests were made in the laboratory reforming apparatus at reactor tube wall temperatures from 1400°F. to 1900°F. (Table 1). The catalyst samples used were first determined to have approximately equal activity for continuous reforming at a set of standard activity test conditions in the same apparatus (see Table 2). The cycle simulated conditions for a process presently under development at the Institute.^{2a} After each cyclic test, the activity of the catalyst was again checked at continuous conditions to ascertain that no permanent change in the catalyst had occurred during the course of the tests. Overall catalyst performance is illustrated by Figure 2, in which the percentage of hydrocarbon conversion is plotted against reactor tube wall temperature. It can be seen that although the activity of all of the catalyst samples was considered equivalent for the continuous process, under cyclic conditions their performance differed widely. Not only were the levels of hydrocarbon conversion different for each catalyst, but the effect of temperature on conversion varied significantly for the different catalysts.

Several general characteristics of catalyst behavior under cyclic conditions can be observed from the data in Table 1 and Figure 2. The magnesia-supported catalysts used in this study were less effective for cyclic reforming than were the alumina-supported catalysts. Not only did the magnesia-supported catalysts (curves C(b) and D, Figure 2) give lower conversion at equivalent temperature and natural gas feed space velocity than did the alumina supported catalysts (curves A and B), but the decrease in conversion with reduction in temperature was also much more severe.

There was also considerable evidence that the portion of nickel entering into oxidation and reduction reactions during the cycle was greater for the alumina supported catalysts. This was indicated by the catalyst temperature, carbon dioxide-carbon monoxide ratio in the product gas, and agreement between the quantities of water decomposition calculated from hydrogen and oxygen balances. In several instances with the alumina-supported catalyst, especially at high reactor temperatures (see Runs 19, 20, 28 and 29, Table 1), the catalyst bed temperature approached or exceeded the reactor tube wall temperature, indicating a sizable release of exothermic reaction heat from oxidation of metallic nickel. In these same instances, the ratio of carbon dioxide to carbon monoxide in the product gas was considerably higher than the carbon oxides ratio normally resulting from water-gas shift reaction (2). This is due to carbon dioxide formation at the beginning of the cycle by reaction (4) in which nickel oxide is reduced to metallic nickel. The quantity of water decomposition for the process calculated from both hydrogen and oxygen balances should agree if only reactions (1) and (2) were significant. In the runs where oxygen was transferred by the catalyst, the calculated quantity of steam decomposition based on a hydrogen balance appears lower than actual. Conversely, the oxygen content of carbon dioxide formed by reaction (4) will make the calculated quantity of steam decomposition based on an oxygen balance appear higher than actual. These observations in

Table 1.-RESULTS OF CYCLIC REFORMING TESTS IN LABORATORY REFORMING UNIT

Catalyst Designation Test No., IGT Sample No., Promoter	A		B		C		D	
	18 3624	19 3931	20 4023	28 None	29 None	10 None	12 None	16 None
Support Material and Nominal Size	MGO		1" Alumina		1" Magnesia		1" Magnesia	
Total Acid Soluble Nickel, wt. %	5.14		4.46		4.99		5.16	
Condition	New Used ^a		New Used ^a		Used ^a		New Used ^a	
Operating Conditions	480		480		480		480	
Pressure, lb./sq. in.	20		20		20		20	
Natural Gas Feed, %	60		60		60		60	
Air Feed, %	20		20		20		20	
N ₂ Purge, %	0		0		0		0	
Reactor Pressure, inches Hg	29.48		29.87		29.80		29.57	
Reactor Tube Wall Temperature, °F	120		120		120		120	
Reactor Tube Wall Temperature, °C	50		50		50		50	
Catalyst Bed Volume, cu.ft.	24		24		24		24	
Temperature, °F, Top	0.1		0.1		0.1		0.1	
Temperature, °F, Middle	1365		1396		1540		1598	
Temperature, °F, Bottom	1460		1515		1620		1653	
Steam Feed, lb./cu.ft. catalyst-hr.	1440		1860		1620		1620	
Steam/Natural Gas Molar Ratio	55.2		56.2		56.4		56.5	
Natural Gas Feed, SCF/cu.ft. catalyst-hr.	2.68		2.77		2.78		2.78	
Air Feed, SCF/cu.ft. catalyst-hr.	4089		4347		4205		4196	
N ₂ Feed, SCF/cu.ft. catalyst-hr.	1420		1419		1475		1430	
Operating Results	2236		1771		2242		2223	
Space Time Yield, SCF/cu.ft. catalyst-hr.	4.22		3.25		4.10		4.23	
Expansion, SCF/cu.ft. catalyst-hr.	1.239		0.220		1.031		0.744	
Contraction, SCF/cu.ft. catalyst-hr.	1.350		1.527		1.271		1.320	
Calculated from Hydrogen Balance	1.229		0.256		1.123		0.964	
Calculated from Oxygen Balance	1.350		1.527		1.271		1.320	
Carbon Balance, %	100		100		100		100	
Hydrocarbon Conversion, %	93.5		98.7		86.1		99.0	
Product Gas Properties ^d								
Hydrogen	73.9		65.6		72.5		71.2	
Methane	1.6		0.4		0.5		0.5	
Ethane	0.0		0.0		0.0		0.0	
Other Hydrocarbons	0.0		0.0		0.0		0.0	
Carbon Monoxide	18.4		14.4		17.0		15.2	
Carbon Dioxide	0.7		0.9		0.7		0.8	
Nitrogen	100.0		100.0		100.0		100.0	
Total	301		288		307		292	
Heating Value, B.t.u./SCF	0.344		0.448		0.348		0.351	
Specific Gravity, Air = 1	88.5		85.1		88.5		85.1	
Natural Gas Properties ^d								
Hydrogen	88.5		85.1		88.5		85.1	
Methane	5.0		5.0		5.0		5.0	
Ethane	1.9		2.1		1.9		2.1	
Propane	0.51		0.62		0.51		0.51	
Butane	0.04		0.05		0.04		0.04	
Pentane	0.02		0.02		0.02		0.02	
Hexane	0.16		0.16		0.16		0.16	
Carbon Dioxide	3.0		3.0		3.0		3.0	
Helium	100.0		100.0		100.0		100.0	
Total	100.0		100.0		100.0		100.0	
Heating Value, B.t.u./SCF	0.627		0.643		0.627		0.643	
Specific Gravity, Air = 1	0.627		0.643		0.627		0.643	

a. The same catalyst sample was used for tests 17, 19 and 20. The same catalyst sample was used for tests 21, 22 and 23. The same catalyst sample was used for tests 28 and 29. Preceding each test the catalyst was first burned off with air for approximately 30 minutes at 1700°F, tube wall temperature and then checked for activity under continuous reforming conditions at 700 SCF/cu.ft. catalyst-hr. natural gas space velocity and 1700°F, tube wall temperature. In each case the activity was equivalent to that of the new catalyst.

b. Operating results for cyclic operation are based on product gas volumes calculated from the feed gas and product gas compositions assuming 100% carbon balance.

c. Percentage disappearance of carbon (as hydrocarbon) from the feed gas.

d. Mass spectrometer analysis.

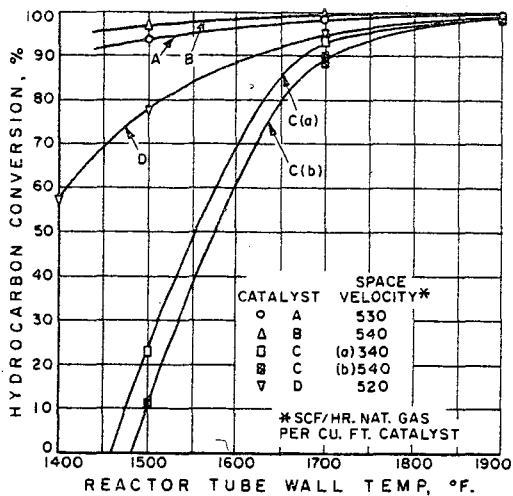


Fig. 2.-COMPARISON OF REFORMING CATALYST PERFORMANCE IN CYCLIC LABORATORY OPERATION

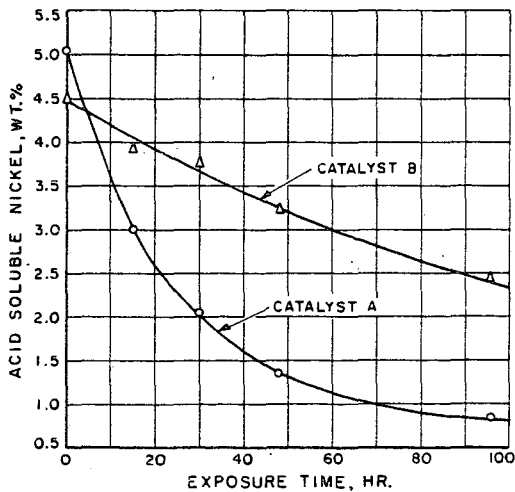


Fig. 3.-DECREASE IN CONCENTRATION OF ACID SOLUBLE NICKEL IN ALUMINA SUPPORTED CATALYSTS ON EXPOSURE AT 1800°F IN AIR

the case of the alumina-supported catalyst seem to indicate higher rates of oxidation and reduction of nickel than occurred with the magnesia-supported catalyst.

It can also be noted that the general level of hydrocarbon conversion and the apparent quantities of nickel cyclically undergoing oxidation and reduction were higher for the high purity, unpromoted alumina-base catalyst (B) than for the lower purity alumina-supported, magnesia-promoted catalyst (A). It is not possible to draw conclusions regarding the effect of base impurities and promoter from these data, however.

Overall catalyst performance as shown in Figure 2 does not indicate the specific effect of individual catalyst properties, but rather reflects the cumulative effect of the complex factors influencing cyclic reforming operation which are not readily apparent from characteristics of the catalyst under continuous reforming conditions. One might conclude from these data that high catalyst performance under cyclic conditions is closely related to the susceptibility of the catalyst to oxidation and reduction of its nickel content. This conclusion would seem logical, since it is evident that the steam-hydrocarbon reaction (1) is primarily dependent upon the presence of some form of metallic nickel as the catalytic agent.

Recent work in the field of solid state physics dealing with the relationships between the electronic properties of semiconductor metal oxides and their catalytic behavior has shed additional light on the factors which influence the oxidation and reduction reactions of nickel.^{4,10,12,36,37,45,46,47} These factors can be summarized as follows:

- a) Source of nickel oxide. Nickel oxide prepared from different nickel salts can differ significantly in chemical properties.^{2,27}
- b) Treatment of nickel oxide. Temperature, pressure and atmospheric exposure have been demonstrated experimentally to change the susceptibility of nickel oxide to reduction by hydrogen.^{2,9,18,27} It has been found that the combination, sequence, duration and rate of change of treatment conditions are all important in determining its behavior during subsequent reduction.¹⁸ Thus the treatment of nickel oxide during preparation of the catalyst, and the treatment received in operation in the cyclic process, are both important in determining its behavior.
- c) Promoters or impurities in the nickel oxide. Studies have shown that the inclusion of foreign metal ions in the crystal lattice of nickel oxide has a pronounced effect on its chemical reactivity, including reduction to metallic nickel.^{8,19,37}
- d) Support material. The susceptibility of nickel oxide to reduction by hydrogen is influenced by the electronic nature of an adjacent material, even though there is no chemical reaction or solid solution between the two materials.^{14,38,39}

It should be noted that the foregoing factors are all related to changes in, or variations of, the crystal structure of nickel oxide. Present-day considerations in the manufacture of supported nickel reforming catalysts include nickel concentration and distribution, support porosity, surface area and the mechanical properties of the support. The selection of promoters is based largely on initial activity considerations. Little attention, however, is given to

conditions controlling the crystal structure of the nickel and nickel oxide. In view of the significance of the oxidation-reduction reactions in the cyclic process, these factors should not be overlooked. A combined effort is presently under way by members of the utility gas industry, equipment constructors and catalyst manufactures to develop suitable standards for catalyst specifications and to improve the performance and life of the catalyst. In this connection Milbourne has recently suggested an oxidation rate determination test as a method of evaluating cyclic reforming catalysts.²⁵ This approach seems to have merit in view of the data shown here.

PERMANENT LOSS OF CATALYST ACTIVITY

In the continuous reforming process the catalyst, as long as it is not poisoned by sulfur or similar impurities in the feed stream, apparently has unlimited life. Since this has not been the case in commercial operation of the cyclic reforming process it was suspected that loss of catalyst activity in cyclic use was related to the operating differences in the two processes already cited. These are cyclic variation in atmosphere and catalyst temperature which are not encountered in continuous reforming. All types of catalyst employed in the cyclic process have been subject to permanent loss in activity, although not necessarily at the same rate. For example, 1-inch diameter alumina-base promoted catalyst, and 1-inch diameter magnesia-base unpromoted catalyst have been observed to lose a major part of their activity after 2000 to 4000 hours of operation. On the other hand, some 1/2-inch alumina base unpromoted catalyst has been reported to have given essentially constant performance for about 20,000 hours.²⁵

Effect of Oxygen

Since the atmosphere in the continuous reforming process is always reducing, an investigation was made of the effect of an oxidizing atmosphere on the catalyst. A series of tests was made in the laboratory reforming apparatus with both magnesia-supported and alumina-supported catalyst. Each catalyst was treated for 4 to 6.5 hours in a stream of air at 1700° and 1900°F. reactor tube wall temperature. Before and after each exposure, an activity test was made at comparable continuous reforming conditions. Results of these tests are shown in Table 2.

With the alumina-supported catalyst (A, Tests 4, 5 and 6), little change in reforming activity was observed even after exposure at 1900°F. Chemical analysis of the catalyst following final exposure indicated a nitric acid soluble nickel concentration of 4.08 weight per cent, compared to 5.14 weight per cent before exposure. An x-ray diffraction pattern of the catalyst after exposure contained lines corresponding to nickel aluminate (spinel) which were not present in the pattern of the new catalyst. It appeared that some of the nickel content of the catalyst had formed an insoluble spinel compound with the support material during the period of exposure, but that the reduction in concentration of available nickel was not sufficient to significantly affect the reforming activity.

With the magnesia-supported catalyst (C, Tests 1, 2 and 3), no reduction in reforming activity was observed after exposure at 1700°F., but following exposure at 1900°F. the reforming activity was approximately 2/3 that of the original catalyst. Chemical analysis indicated a nitric acid soluble nickel concentration of 4.63 weight per cent following final exposure compared to 4.99 weight per cent in the new catalyst. The x-ray diffraction pattern of the exposed catalyst

contained only lines corresponding to periclase (MgO). With the magnesia-supported catalyst, exposure in air at elevated temperature had a more serious effect on reforming activity than in the case of the alumina-supported catalyst, although the reduction in nitric acid soluble nickel content was less, and no compound formation was detected for the magnesia catalyst. An examination of the phase diagram for the nickel oxide-magnesium oxide system^{23,24} does not indicate the existence of a compound; however, Holgersson and Karlsson confirmed the existence of a completely miscible system of solid solutions between these two materials.¹⁵ Since both nickel oxide and magnesium oxide have face-centered cubic lattices with nearly the same unit cell length, low concentrations of solid solution, if present, would probably not be detectable in the x-ray diffraction pattern.

Although the specific relation between catalyst changes and reforming activity was not defined in these tests, the indications fit the circumstances. In the case of the alumina-supported catalyst, combination of the nickel content with the alumina support to form spinel would be expected to reduce reforming activity, since spinel compounds are very unreactive, and reduction to metallic nickel with hydrogen or hydrocarbons would be unlikely. In the case of the magnesia-supported catalyst, solution of the nickel content in the unreactive magnesium oxide lattice could easily make the nickel unavailable for reduction by hydrogen or hydrocarbons. Both cases would be unique to the cyclic reforming process, since either would proceed only with nickel present as nickel oxide.

Spinel

Additional tests were conducted to determine if the rate of spinel formation was rapid enough to contribute materially to loss of catalyst activity at conditions of the cyclic reforming process. Samples of both the high purity alumina-base unpromoted catalyst (B), and the lower purity alumina-base magnesia-promoted catalyst (A), were crushed to pass 100 mesh. Each catalyst was heated to 1800°F. in an electric furnace for an extended period in contact with air. At intervals, samples were withdrawn for determination of nitric acid soluble nickel concentration. The change in nitric acid soluble nickel content with time of exposure is shown in Figure 3.

After 96 hours at the test conditions both catalysts showed a marked decrease in the concentration of acid soluble nickel. It is interesting to note the difference in rate of decrease for these two catalysts. In curve B for the high-purity alumina support the rate of decrease was almost a linear function of time. Since only nickel oxide and alumina were present in this catalyst, nickel aluminate would be the only suspected compound which would lower the concentration of acid soluble nickel. This was confirmed by the x-ray diffraction pattern of the catalyst after exposure for 96 hours. Only lines corresponding to α -alumina, nickel oxide and spinel were detected. No spinel lines were observed in the pattern for the new catalyst. Curve A for the lower purity alumina base catalyst shows a different time-nickel concentration relationship. The decrease in acid soluble nickel content was very rapid initially, but approached the rate in curve B after about 30 hours. The major materials present in this catalyst in addition to alumina and nickel oxide were 12.90 weight per cent silica in the support, and 1.8 weight per cent magnesia added as promoter by coimpregnation as nitrate with the nickel. An x-ray diffraction pattern of this catalyst indicated that the silica was in the form of aluminum silicate ($3Al_2O_3 \cdot 2SiO_2$). In addition to spinel lines, the pattern of the catalyst after 96 hours of exposure contained unidentified lines corresponding to 5.4, 4.7 and 1.84A. These do

not correspond to any nickel compound for which x-ray data are readily available. The difference between curves A and B could be attributed either to the formation of insoluble nickel compounds in addition to nickel aluminate, or to an increased rate of formation of nickel aluminate due to the presence of silica or magnesia.

Solid Solutions

To determine the relationship between catalyst activity and the possible formation of solid solutions between nickel oxide and the magnesia catalyst support as indicated by the atmosphere tests described above, a number of samples of the same magnesia-supported catalyst C having various operating histories and showing different levels of activity under comparable continuous reforming conditions were subjected to microscopic analysis. Descriptive data for the samples selected are itemized below:

IGT Sample No.	3623	3664	3635	3665
Acid Soluble Nickel, wt. %	4.99	4.47	4.63	4.01
Approximate Relative Continuous Reforming Activity, %	100	120	70	15
History	New	29 hours Pilot Plant in Tube Operation Furnace at 1400- 1660°F.	Oxidized for 9.5 hours at 1700- 1900°F.	29 hours Pilot Plant Operatic at 1830- 1890°F.

For each sample the catalyst pellet was impregnated with Canada balsam, after which a thin section through the center was prepared. Photographs of the sections made with transmitted light are shown in Figures 4, 5, 6 and 7. The original pore structure of the support material was preserved and shows as white areas in these photographs.

In Figure 4, the new catalyst, two distinct phases are apparent; a colorless isotropic phase having an index of refraction slightly below that of a 1.74 immersion medium (refractive index of periclase: 1.734-1.737) and a black opaque phase (nickel oxide). The nickel oxide is concentrated near the surface of the pellet and especially around the perimeter of the larger pores. Particle size of the periclase ranged from a maximum of approximately 50 microns down to a very fine dust. The nickel oxide particle size was too small to be determined.

Figure 5 shows a section of the catalyst after brief cyclic operation in a pilot plant at relatively low temperature. The activity under continuous reforming conditions in the laboratory apparatus was found to be noticeably higher than that of the new catalyst. Two phases are apparent, as in the new catalyst. However, the nickel oxide seems to be more uniformly distributed throughout the pellet, and instead of being concentrated around the pore perimeters it appears to have diffused into a thin layer in the grain boundary surrounding each periclase crystallite. Some grains have a refractive index slightly above 1.74, whereas others have a refractive index lower than 1.74. Since nickel oxide has a refractive index of 2.37, the grains with a refractive index higher than 1.74 undoubtedly contain nickel oxide in solid solution. Solid solution formation in this sample is evidently in initial stages and far from complete.

Figure 6 shows a section of the catalyst following air treatment in the laboratory reforming apparatus at 1900°F. reactor tube wall

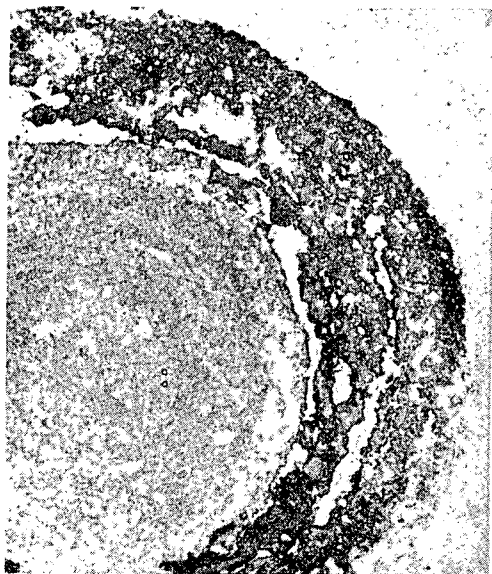


Fig. 4.-NEW CATALYST C,
RELATIVE ACTIVITY = 100%



Fig. 5.-USED CATALYST C,
RELATIVE ACTIVITY = 120%

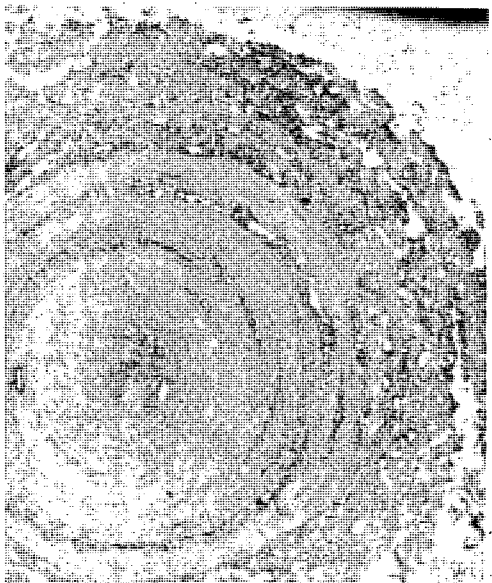


Fig. 6.-TREATED CATALYST C,
RELATIVE ACTIVITY = 70%

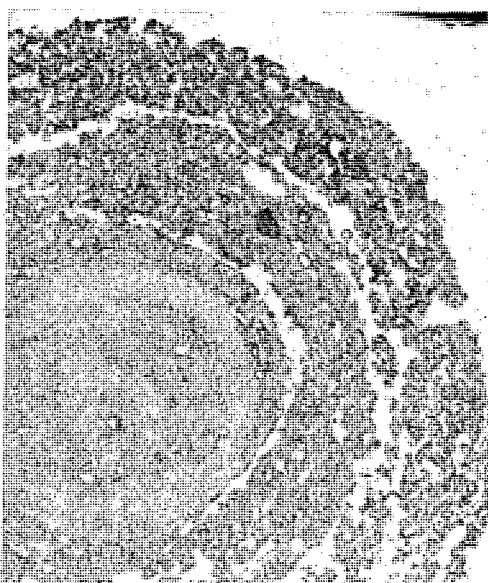


Fig. 7.-USED CATALYST C,
RELATIVE ACTIVITY = 15%

temperature (Test 3, Table 2). This sample was found to have approximately $2/3$ of the activity of the new catalyst. Two phases can be detected in this sample, although the amount of black opaque phase has greatly diminished. Only a few grains were observed with an index of refraction less than 1.74, indicating a substantial amount of solid solution formation.

Figure 7 shows a sample of catalyst which was subjected to high temperatures in cyclic pilot plant operation. The activity of this material under continuous reforming conditions was very low, estimated at about 15% of the new catalyst. Only one phase can be detected in this sample, the nickel oxide phase having completely disappeared. Refractive indices of all grains were well above 1.74, indicating that solid solution of the nickel oxide in magnesia was essentially complete. No grains with an index of refraction greater than 1.78 were observed, indicating that the solutions formed were always dilute in nickel oxide. The largest particle size in the sample was approximately four times that in the new catalyst, indicating that some recrystallization may have occurred.

This series of analyses seems to indicate the path of the change which occurs in the magnesia-supported catalyst with use. It is interesting to note that the early changes in structure corresponding to nickel oxide migration throughout the pellet, and incomplete solid solution formation, are accompanied by an increase in reforming activity rather than a decrease. This result agrees with the findings of Hüttig with mixtures of metal oxide catalyst.¹⁷ Hüttig describes a series of states that occur during the formation of a solid solution from a mixture of metal oxides. The initial states constitute diffusion of the more mobile lattice over and around the less mobile lattice. Hüttig relates the highly disordered condition which is created to increased catalytic activity. The final state, constituting the complete solution and filling in of lattice defects, he relates to diminishing catalytic activity.

CONCLUSIONS

It appears from the results of this study that the factors which influence overall performance of the catalyst in the cyclic reforming process, as well as catalyst life, are quite different from significant factors for the continuous reforming process. For this reason, catalyst properties which have generally been considered desirable in continuous reforming catalysts may not be satisfactory for the cyclic process. Likewise, the methods commonly used to evaluate catalyst performance for continuous reforming do not appear adequate to predict the behavior of catalysts under cyclic conditions.

Although the cyclic process is extremely complex, the data from this study lead to several general conclusions regarding performance of supported nickel catalysts of the type employed in commercial practice. First, the susceptibility of the nickel content of the catalyst to rapid oxidation and reduction appears to be closely related to good overall reforming efficiency in cyclic operation. Second, catalyst activity is decreased by any changes which result in decreasing the amount of nickel available for oxidation and reduction. For alumina-supported catalysts a major factor contributing to loss in activity appears to be the formation of spinel by reaction between nickel oxide and the support. For magnesia-supported catalysts a similar effect appears to result from solution of nickel oxide in the support. In both instances, the undesirable changes must occur during the heating portion of the cycle, when all or part of the nickel is present as the oxide.

Many other factors may contribute to short catalyst life in the cyclic reforming process. One for which very little specific data are available is the effect of coatings built up on the surface of the catalyst with use, from dust constituents in the combustion air, or from ash content of oil feed or fuel. Additional studies will be necessary to define these effects, as well as to determine methods for improving catalyst performance and life.

ACKNOWLEDGMENT

This study was conducted under the sponsorship of the Gas Operations Research Committee of the American Gas Association with funds provided by the Association's Promotion-Advertising-Research Plan. Permission for publication of this paper and the guidance given by the Project Supervising Committee under the chairmanship of A. R. Belyea and with the assistance of N. K. Chaney are gratefully acknowledged. The authors wish to express their appreciation to the many staff members of the Institute of Gas Technology who contributed to this work. The counsel of H. R. Linden, Research Director, was especially helpful. J. S. Griffith of the Armour Research Foundation of the Illinois Institute of Technology conducted the petrographic analysis of catalysts (the results of which are presented in this paper). Catalyst samples for this study were supplied by Catalysts and Chemicals, Inc., The Harshaw Chemical Company and Westvaco Mineral Products Division of the Food Machinery and Chemical Corporation.

LITERATURE CITED

- (1) Barnes, J. M. and Bergey, E. S., "Eastern Utility Installs Catalytic Reforming Units," Gas 33, 39-42 (1957) December.
- (2) Benton, A. F. and Emmett, P. H., "The Reduction of Nickelous and Ferric Oxides by Hydrogen," J. Amer. Chem. Soc. 46, 2728-37 (1924).
- (3) Calderwood, G. L., "The 'ONIA-GEGI' Process for Cyclic Catalytic Cracking of Liquid Hydrocarbons," Paper CEP-58-11, Operating Section, American Gas Association, 1958.
- (4) de Boer, J. H. and Verwey, E. J. W., "Semiconductors with Partially and Completely Filled 3d-Lattice Bands," Proc. Phys. Soc. (London) 49, 59-73 (1937).
- (5) Dirksen, H. A., Linden, H. R. and Pettyjohn, E. S., "Cracking Catalyst Activity in the Presence of Hydrogen Sulfide," Institute of Gas Technology Research Bulletin No. 4 (1953) February.
- (6) Eickmeyer, A. G. and Marshall, W. H., Jr., "Ammonia Synthesis - Gas Generation by Pressure Reforming of Natural Gas," Chem. Eng. Progr. 51, 418-21 (1955).
- (7) Erickson, H. V. and Hartzel, F. W. (to United Gas Improvement Co.), "Method of Carrying out Catalytic Reactions," U. S. Patent 2,759,805 (August 21, 1956).
- (8) Fensham, P. J., "Solid Solutions of Lithium Oxide in Nickel Oxide," J. Amer. Chem. Soc. 76, 969-71 (1954).
- (9) Foex, M., "Property Anomalies Accompanying λ -Type Transformations of Nickel Oxide," Bull. Soc. Chim. France, 373-79 (1952).
- (10) Garner, W. E., "Adsorption and Catalysis on Oxides," Discussions Faraday Soc. 8, 211-15 (1950).
- (11) Glover, C. B., "New Developments in the U.G.I. Cyclic Catalytic Reforming Process," A.G.A. Proceedings-1955, 829-33.
- (12) Gray, T. J. and Darby, P. W., "Semi-Conductivity and Catalysis in the Nickel Oxide System," J. Phys. Chem. 60, 209-17 (1956).
- (13) Griggs, E. R., "Operating Experience with the C.C.R. Set at Paterson, N. J.," A.G.A. Proceedings-1954, 740-48.
- (14) Hill, F. N. and Selwood, P. W., "Structure and Activity of Supported Nickel Catalysts," J. Amer. Chem. Soc. 71, 2522-29 (1949).
- (15) Holgersson, S. and Karlsson, A., "X-Ray Examination of a System of Mixed Crystals with Monoxide Components," Z. Anorg. Allgem. Chem. 182, 255-71 (1929).
- (16) Horsfield, S. W., "Reforming Natural Gas by the Continuous Catalytic Cracking Process," A.G.A. Proceedings-1951, 591-601.
- (17) Hüttig, G. F., "Catalytic Activity and Composition of Oxide Systems," Discussions Faraday Soc. 8, 215-22 (1950).
- (18) Igaki, K., "The Electric and Magnetic Properties of Nickel Oxide," Bull. Naniwa Univ. A3, 113-23 (1955).
- (19) Innes, W. B., "Catalyst Carriers, Promoters, Accelerators, Poisons and Inhibitors," in Emmett, P. H., "Catalysis," Vol. 1, pp. 245-314; Reinhold, New York, 1954.
- (20) Janeway, P. W., Jr. (to The United Gas Improvement Co.), "Method for Making Gas Rich in Hydrogen," U. S. Patent 2,743,171 (April 24, 1956).
- (21) King, G. R., "Install Modern Catalytic Reformers," A.G.A. Monthly 37, 33-36 (1955) September.
- (22) Knoblock, K. D., "Duluth Plant for Regenerative Catalytic Reforming of Liquid Hydrocarbons," Paper CEP-58-5, Operating Section, American Gas Association, 1958.
- (23) Landholt-Bornstein, "Physikalisch-Chemische Tabellen," 3rd Erg., Vol. 1, p. 453, Springer Verlag, Berlin, 1935.

- (24) Levin, E. M., McMurdie, H. F. and Hall, F. P., "Phase Diagrams for Ceramists," p. 54, The American Ceramic Society, Columbus, Ohio, 1956.
- (25) Milbourne, C. G., "CCR Catalyst Developments," Paper presented at A.G.A. Operating Section Conference, May 8, 1958, New York.
- (26) Milbourne, C. G. and Glover, C. B., "Cyclic Catalytic Reforming Process," Ind. Eng. Chem. 49, 387-91 (1957).
- (27) Prasad, M. and Tendulkar, M. G., "The Preparation and Properties of Nickelous Oxide," J. Chem. Soc. 1403-07 (1931).
- (28) Reid, J. M., Bair, W. G. and Linden, H. R., "Production of High-Btu Oil Gas in a Cyclic-Regenerative Pilot Unit with Hydrogen as Carrier Gas," Paper CEP-57-14, Operating Section, American Gas Association, 1957.
- (29) Reidel, J. C., "Ammonia Manufacture by Gas Reforming," Oil Gas J. 54, 106-07, 110, 113 (1956) March 26.
- (30) Riesz, C. H., Dirksen, H. A. and Kirkpatrick, W. J., "Sulfur Poisoning of Nickel Catalysts," Institute of Gas Technology Research Bulletin No. 10 (1951) September.
- (31) Riesz, C. H., Dirksen, H. A. and Pleticka, W. J., "Improvement of Nickel Cracking Catalysts," Institute of Gas Technology Research Bulletin No. 20 (1952) October.
- (32) Riesz, C. H., Komarewsky, V. I., Kane, L. J., Estes, F. and Lurie, P., "Catalytic Gasification of Higher Hydrocarbons," A.G.A. Monthly 28, 159-64, 190 (1946).
- (33) Riesz, C. H., Lurie, P. C., Tsaros, C. L. and Pettyjohn, E. S., "Pilot Plant Catalytic Gasification of Hydrocarbons," Institute of Gas Technology Research Bulletin No. 6 (1953) July.
- (34) Schlegel, C. A., "The UGI Cyclic Catalytic Reforming Process Reforming Natural Gas," Paper presented at New England Gas Association, Operators' Section Meeting, January 18, 1950, Boston, Mass.
- (35) Schlegel, C. A., "The Cyclic Catalytic Reforming Process for Reforming Natural Gas," Gas 26, 26-29 (1950) February.
- (36) Schwab, G. M., "Experiments Connecting Semiconductor Properties and Catalysis," in Conference on the Physics of Semiconductor Surfaces, R. H. Kingston, Editor, "Semiconductor Surface Physics," pp. 283-96, Univ. of Pennsylvania Press, Philadelphia, 1957.
- (37) Schwab, G. M. and Block, J., "Oxidation of Carbon Monoxide and Decomposition of Nitrous Oxide on Defined Semiconducting Oxides," Z. Physik. Chem. 1, 42-62 (1954).
- (38) Selwood, P. W., Hill, F. N. and Boardman, H., "A New Magnetic Effect Applied to the Structure of Catalytically Active Solids," J. Amer. Chem. Soc. 68, 2055-59 (1946).
- (39) Selwood, P. W. and Lyon, L., "Structure of Oxide Catalyst Systems," Discussions Faraday Soc. 8, 222-30 (1950).
- (40) Shearon, W. H., Jr. and Thompson, H. L., "Ammonia at 1000 Atmospheres," Ind. Eng. Chem. 44, 254-64 (1952).
- (41) Sherwood, P. W., "Water Gas from Methane," Petroleum Processing 5, 1308-11 (1950).
- (42) Smoker, E. H., "The UGI Cyclic Catalytic Reforming Process--Recent Developments," A.G.A. Proceedings-1952, 843-44.
- (43) Smoker, E. H., "Experiences in the Production of High Btu Gas from Naptha and Kerosene Using the UGI Cyclic Catalytic Reforming Process," A.G.A. Proceedings-1953, 852-53.
- (44) Taussig, J. H., Jr. (to The United Gas Improvement Co.), "Method of Reforming Gaseous Hydrocarbons," U. S. Patent 2,665,979 (January 12, 1954).
- (45) Taylor, H. S., "Catalysis: Retrospect and Prospect," Discussions Faraday Soc. 8, 9-18 (1950).

- (46) Vol'kenshtein, F. F., "The Mechanism of Catalytic Action by Semiconductors," Izvest. Akad. Nauk. SSSR, Otdel, Khim. Nauk. (1957) 924-28, No. 8.
- (47) Wright, R. W. and Andrews, J. P., "Temperature Variation of the Electrical Properties of Nickel Oxide," Proc. Phys. Soc. (London) 62A, 446-55 (1949).

ABSTRACT

APPLYING FUNDAMENTAL CONCEPTS
TO THE ENGINEERING DESIGN OF APPLIANCE BURNERS

by Walter B. Kirk and James C. Griffiths
American Gas Association Laboratories
Cleveland, Ohio

Fundamental concepts relating burner design factors and gas composition to the conventional flame characteristics of lifting, yellow tipping, and flashback are discussed.

Design relationships are developed from the basic critical boundary velocity gradient theory with respect to lifting flames. Such burner design factors as port size, depth, and spacing; port loading and primary aeration; and gas composition are taken into account.

Not for Publication
Presented Before the Division of Gas and Fuel Chemistry
American Chemical Society
Chicago, Illinois, Meeting, September 7-12, 1958

APPLYING FUNDAMENTAL CONCEPTS
TO THE ENGINEERING DESIGN OF APPLIANCE BURNERS

by Walter B. Kirk and James C. Griffiths
American Gas Association Laboratories
Cleveland, Ohio

There are many areas in the gas industry where there is a definite need to bridge the gap between fundamental concepts and engineering application. As an example, the design of atmospheric gas burners for domestic appliances requires a judicious balance of opposing characteristics. A design directed toward eliminating any propensity for lifting flames might introduce a tendency for yellow tipping flames, or a design for high primary air injection could be liable to flashback. A knowledge of the quantitative effects of all pertinent variables is, therefore, necessary to achieve a desired balance in design. The following is an attempt to interpret fundamental concepts in such a manner that they might be easily applied in the engineering design of burner port areas.

The nature of the port area for any given application is dictated by limiting conditions which produce critical flame characteristics such as lifting, yellow tipping, and flashback. A typical flame characteristic diagram is shown in Figure 1, which describes limiting conditions in terms of primary aeration, expressed as a per cent of the air required in a stoichiometric mixture and port loading in Btu per hour per square inch of port area. Any change in variables such as port size, depth, or spacing will displace these limit curves so as to either increase or decrease the area of the stable, blue flame zone. Ideally, of course, this zone should be as large as possible.

The flame characteristic diagram for a given burner operating on a given gas is fixed. If at any time the operating point of the burner, as defined by port loading and primary aeration, lies above the lifting limit curve, lifting flames will occur. When the operating point lies below the yellow tip limit, the flames will exhibit yellow tips, and flashback will take place if the operating point lies to the left of the flashback limit curve.

The general effects of burner design variables and gas composition on these limiting flame characteristics have been known for many years. Lifting tendencies are reduced by the use of larger, deeper, more closely spaced ports. Yellow tipping of flames, on the other hand, is reduced by using smaller, more widely spaced ports. The use of several rows of ports generally raises the yellow tip limit, but does not affect lifting tendencies, provided even distribution of air-gas mixture to all the ports is provided. Port depth does not appear to have an effect on yellow tipping tendencies. Flashback tendencies appear to be reduced by the use of smaller, deeper ports. The use of closer port spacings apparently results in a hotter operating burner head temperature, which in turn promotes flashback. At the same air-gas mixture temperature, however, port spacing does not appear to affect flashback.

Burning velocities of fuel gases affect lifting and flashback tendencies. Slower burning gases are more critical in regard to lifting flames, while flashback occurs more readily with faster burning gases. Each fuel gas has its own yellow tipping characteristics.

Lifting and flashback are flame stability phenomena. As such, they are dependent on the relative velocities of air-gas mixture flowing out of the port, and the counter propagation of flame into the air-gas mixture in the ports and burner head. With normal flames, equilibrium between these opposing factors generally takes place a short distance above the burner port. This distance between the burner port and the base of the flame is generally referred to as the "dead space".

Yellow tipping, on the other hand, is a completely different phenomenon. Each fuel gas requires a certain amount of air to completely eliminate yellow tips from appearing in its flames. This air can be obtained either as primary air or as secondary air diffusing to the point where yellow tips appear in the flames. Port size, spacing, and the number of rows of ports affect the degree to which secondary air can be utilized to eliminate yellow tipping. This, in turn, determines the primary air necessary to make up a deficiency of secondary air, and hence establishes the so-called yellow tip limit of the burner.

Extensive studies of flame characteristics and burner design have been made at the A.G.A. Laboratories, the U. S. Bureau of Mines, and other institutions. In February, 1958, A.G.A. Laboratories Research Bulletin 77, "Influence of Port Design and Gas Composition on Flame Characteristics of Atmospheric Burners", was published. This bulletin not only describes recent burner design studies, but correlates the results of those studies with the results of previous investigations. For the purposes of the present discussion, only lifting characteristics of flames will be considered.

The critical boundary velocity gradient theory was used as a basis of studies of lifting flames. This theory states that blowoff (lifting) will occur when the flow velocity gradient at the wall of a port exceeds the burning velocity at all points around the port.

The expression for the boundary velocity gradient, g , is derived by equating the pressure drop per unit length of channel to the retarding viscous force at the wall per unit length of channel:

$$\mu g 2 \pi R = \left(\frac{\Delta P}{L} \pi R^2 \right) = C_f V^2 / 4 \pi R^3 \quad (1)$$

where:

- μ = viscosity, pound second per square foot,
- g = boundary velocity gradient, 1/sec,
- R = port radius, feet,
- $(\Delta P/L)$ = pressure drop per unit length of port, pounds per square foot per foot,
- C_f = mass density, slugs per cubic foot,
- f = friction factor, dimensionless, and
- V = volumetric flow rate, cubic feet per second.

Introducing Reynolds' number as $Re = 2 V C_f / \mu \pi R$, equation (1) becomes:

$$g = \frac{f V Re}{16 \pi R^3} \quad (2)$$

Equation (2) is, therefore, a generalized equation for the boundary velocity gradient. Substituting the Hagen-Poiseuille relationship for parabolic (laminar) flow, $f = 64/Re$, in equation (2) obtains:

$$g = \frac{4 V}{\pi R^3} \quad (3)$$

This is the expression for the boundary velocity gradient for deep circular ports. If the value of the volumetric flow at a condition of lifting flames, V_L , is substituted in equation (3), the equation then defines the critical boundary velocity gradient for lifting, g_L , for deep circular ports.

It should be emphasized that this critical boundary velocity gradient for lifting is a fundamental characteristic of the given gas, and as such is independent of burner design. In other words, for any given primary aeration, there is a definite critical boundary velocity gradient at which lifting will occur, regardless of the design of the port. Advantage can be taken of this fact to obtain expressions relating port geometry to lifting flames for shallow and non-circular port forms.

Equation (3) may be expressed in terms more generally used in the gas industry as:

$$g = \frac{1.92 I a (1 + A/G)}{\pi R^3 H} \quad (4)$$

where:

- g = boundary velocity gradient, 1/sec,
- I = port loading, Btu per hour per square inch of port area,
- a = port area, square inches,
- A/G = air-gas ratio,
- R = port radius, feet, and
- H = heating value of fuel gas, Btu per cubic foot.

For an individual port, $a = \pi R^2$ and equation (4) reduces to:

$$g = 1.92 \frac{I}{R} \left(\frac{1 + A/G}{H} \right) \quad (5)$$

At the limiting conditions for lifting flames for a given fuel gas and a given primary aeration, the fraction $(1 + A/G)/H$ is a constant, K, so that equation (5) can be further reduced to:

$$K g_L = \frac{3.84 I_L}{D} \quad \text{for deep circular ports} \quad (6)$$

where:

- K = a function of the primary aeration and heating value, $H/(1 + A/G)$,
- g_L = critical boundary velocity gradient for lifting, 1/sec,
- I_L = port loading at the lifting limit, Btu per hour per square inch of port area, and
- D = port diameter, inches.

The critical boundary velocity gradient for a given gas with a given primary aeration is a constant. Equation (6) then states that the limiting port loading at the lifting limit is directly proportional to the port diameter.

The equation also indicates that lifting limit curves (plotting per cent primary aeration versus port loading) would be parallel curves. Figure 2 demonstrates that this is true for port sizes which might be used in contemporary drilled port burners.

It will be noted that the lifting limit curve in Figure 2 for the 1/4 inch diameter port is not parallel to the other curves, but falls off more abruptly at higher port loadings. Uneven distribution of air-gas mixture flow velocities in larger ports lowers the lifting limit of that port. Lifting will occur at any point around the port rim where the critical boundary velocity gradient for lifting is reached, even though flames may be stable at all other points around the port. In calculating port loading, even distribution must be assumed and the port loading obtained simply by dividing the heat input by the port area. Uneven distribution resulted in "incipient lifting", i.e., lifting at one point on the port with the flame hanging on to the remainder of the port rim. This condition was also noted with large rectangular ports. Within the port sizes generally used in contemporary drilled port burners (No. 50 to No. 20 DMS), however, parallel lifting limit curves for different port diameters were observed.

It is possible, therefore, to represent the lifting limits of various individual ports of various sizes by a single limit curve by plotting ϕI_L versus primary aeration at lifting, where I_L is the limiting port loading and ϕ is a multiplying factor dependent on the port geometry. For deep circular ports, ϕ would equal $1/D$, where D is port diameter.

It was also observed that parallel lifting limit curves were obtained for various port depths, up to a limiting depth. The lifting limit of ports deeper than this limiting depth were found to be the same. Figure 3 illustrates a typical example of this trend. Similarly, parallel lifting limit curves were observed for rectangular ports of various widths, lengths, and depths, when two of these geometric factors were held constant and the third varied. It appeared, then, that geometric multiplying factors could be obtained for these various port designs so that a single lifting limit curve could be used for all such port designs.

As a first step in these determinations, the critical boundary velocity gradient for Cleveland natural gas was calculated (by use of equation (3)) from observed lifting limits with very deep ports. All of these lifting studies were made with a relatively cold burner, since this is the most critical condition for lifting flames. Figure 4 shows these critical boundary velocity gradients for Cleveland natural gas.

Equation (2), when applied to a condition of lifting flames, can be modified to include a term for port loading to become:

$$\epsilon_L = \frac{f \text{ Re } I_L^a}{16 \pi R^3} \times \frac{1 + A/G}{H} \times \frac{1728}{3600} \quad (7)$$

At any given primary aeration for Cleveland natural gas, equation (7) would reduce to:

$$K g_L = \frac{0.06 f Re I_L}{D} \quad (8)$$

where:

D = port diameter, inches, and
 K = a function of the given primary aeration.

The values of f at lifting conditions for various port geometries were then evaluated by observing the lifting limits for a number of ports. For each corresponding value of primary aeration at the lifting condition, values of the critical velocity gradient, g_L , were picked from the curve of Figure 4. Values of f could then be solved for in equation (8), since all of the other factors in the equation are known from measurement.

Figure 5 shows the observed empirical relationship between the expression f Re and port geometry for various circular ports. The horizontal segment of the curve represents data obtained with relatively deep ports in which laminar flow takes place. The sloped portion of the curve, which can be represented by the expression $f = 305 D/Re \sqrt[4]{d}$, applies to relatively shallow ports. Substitution of the latter relationship in equation (8) obtains:

$$K g_L = \frac{18.3 I_L}{\sqrt[4]{d}} \quad \text{for shallow circular ports} \quad (9)$$

As was previously pointed out, the critical boundary velocity gradient for a given gas and primary aeration is a function of the burning characteristics of the gas, and as such is independent of the port geometry. Thus, equations (6) and (9) can be equated so that:

$$\frac{3.84 I_L}{D} \quad \text{for deep circular ports} = \frac{18.3 I_L}{\sqrt[4]{d}} \quad \text{for shallow circular ports} \quad (10)$$

If the multiplying factor (ϕ) for deep circular ports is taken as $\phi = 1/D$, then this factor for shallow circular ports would be $\phi = 4.77/\sqrt[4]{d}$.

It is realized that the transition from "deep" to "shallow" circular ports takes place in a gradual process, rather than at a sharp breaking point. This transition zone is illustrated in Figure 5 by the curved line joining the straight horizontal and sloped lines. It was found, however, that an arbitrary limiting point could be determined by the intersection of the extensions of the straight horizontal and sloped lines of Figure 5. The "deep" port multiplying factor can be used with good accuracy for ports to the left of this arbitrary point, and the "shallow" port expression can be used for ports to the right of this point.

A similar treatment was made with rectangular ports, and empirical geometrical multiplying factors were determined. Expressions obtained for the factor ϕ , for circular and rectangular ports are summarized in the following:

$$\text{Deep circular ports } (D/\sqrt[4]{d} < 0.21), \quad \phi = \frac{1}{D} \quad (11)$$

$$\text{Shallow circular ports } (D/\sqrt[4]{d} > 0.21), \phi = 4.77/\sqrt[4]{d} \quad (12)$$

$$\text{Deep rectangular ports } (\frac{De}{d} < 1.0), \phi = \frac{1.44 (n + 1)}{n \sqrt{W}} \quad (13)$$

$$\text{Shallow rectangular ports } (\frac{De}{d} > 1.0), \phi = \frac{2.88\sqrt{W}}{d} \quad (14)$$

where:

- D = port diameter of circular ports, inches,
- d = port depth, inches
- De = equivalent port diameter of rectangular ports,
inches = $2 n W / (n + 1)$,
- W = rectangular port width, inches, and
- n = ratio of rectangular port length to width.

These expressions for ϕ were applied to all the lifting limit data observed for Cleveland natural gas with individual ports to obtain the average generalized lifting limit curve illustrated in Figure 6. For port sizes generally used in contemporary burners, the observed lifting limits generally fell within 3 percentage units of primary aeration of the curve.

The use of multiple drilled ports affects the lifting limit of a burner. In general, closer port spacing raises the lifting limit. Of course, there is a maximum port spacing above which the ports can be considered to act as individual ports. This effect is apparently due to a reduction in the quenching of the flame reaction by the surrounding air above the port.

A simple experiment at the A.G.A. Laboratories illustrated this effect. An electrically heated coil was placed around a port. The coil was so spaced that it would not ignite the air-gas mixture issuing from the port. The lifting limit of the port was raised considerably when the coil was heated electrically.

With a multiple drilled port burner, adjacent flames apparently create the same effect as the heated coil. The end ports of bar burners, which are influenced by adjacent ports on only one side, generally lift first. Some such lifting can be tolerated if combustion or carryover is not impaired when the burner is first lighted. Because of this, the lifting limit of multiple port burners was arbitrarily chosen as the point at which three or four of the end ports lifted.

Figure 7 illustrates that lifting limit curves for multiple port burners were found to be essentially parallel curves. A multiplying factor can then be determined for various port spacings in order to obtain a single lifting limit curve.

The values of these factors, in relation to the individual port curve of Figure 6, were determined to be: 0.88 for 1/4 inch or greater; 1.0 for 3/16 inch; 1.12 for 1/8 inch; and 1.82 for 1/16 inch spacing of ports edge-to-edge.

The use of multiple rows does not appear to affect lifting characteristics, provided the port spacing multiplying factor for the smallest spacing between ports (whether in the rows or between rows) is used in entering Figure 6.

It has been observed that within the span of port loadings generally used in contemporary drilled port burners (10,000 to 60,000 Btu per hour per square inch of port area), lifting limit curves for various gases were essentially parallel curves. This trend was noted in burner port design studies conducted at the U. S. Bureau of Mines, and in investigations conducted at the A.G.A. Laboratories. Figure 8 illustrates the lifting limits obtained for various gases at the U. S. Bureau of Mines.

Thus, the lifting characteristics of a fuel gas may be expressed in terms of an equivalent rate factor relative to the lifting characteristics of a reference gas. The effects of gas composition on lifting characteristics were calculated for a limited number of gases. The principle involved, however, can be applied to other gases which might be used in the field. Information which can be used to determine the equivalent rate factor for a number of gases can be found in several publications. Two such publications are the U. S. Bureau of Mines' Report of Investigation 5225, "Fundamental Flashback, Blowoff, and Yellow Tip Limits of Fuel Gas-Air Mixtures", and A.G.A. Laboratories Research Bulletin 36, "Interchangeability of Other Fuel Gases with Natural Gas". The method of using the information contained in these reports is described more fully in A.G.A. Laboratories Research Bulletin 77.

Tables have been prepared which relate the lifting characteristics of designs generally used in contemporary burners to those of an arbitrarily chosen reference burner.

Several factors affecting the lifting characteristics of burners are still relatively unexplored. Uneven distribution of air-gas mixture to the ports will always result in a lower lifting limit than values calculated from the equations previously discussed. Port loading must be considered as simply the total heat input to the burner divided by the total port area in design calculations. Overrated ports will, therefore, lift at a lower primary aeration than the calculated value.

The design methods described in A.G.A. Laboratories Research Bulletin 77 are for open room conditions. Combustion chamber environment has some effect on lifting characteristics. A current water heater research investigation at the A.G.A. Laboratories is considering this aspect of the problem.

Burner design research is a continuing process. By applying fundamental concepts, the engineering design of appliance burners is, with time, becoming less of an art and more of a science.

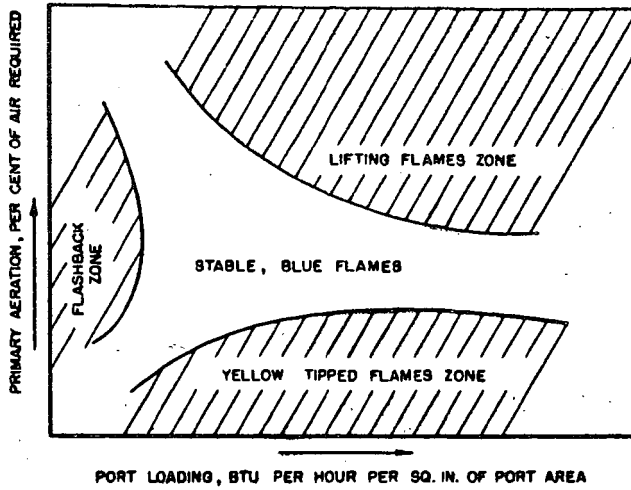


Figure 1 Typical Flame Characteristics Diagram, Showing Lifting, Yellow Tipping, and Flashback Limit Curves.

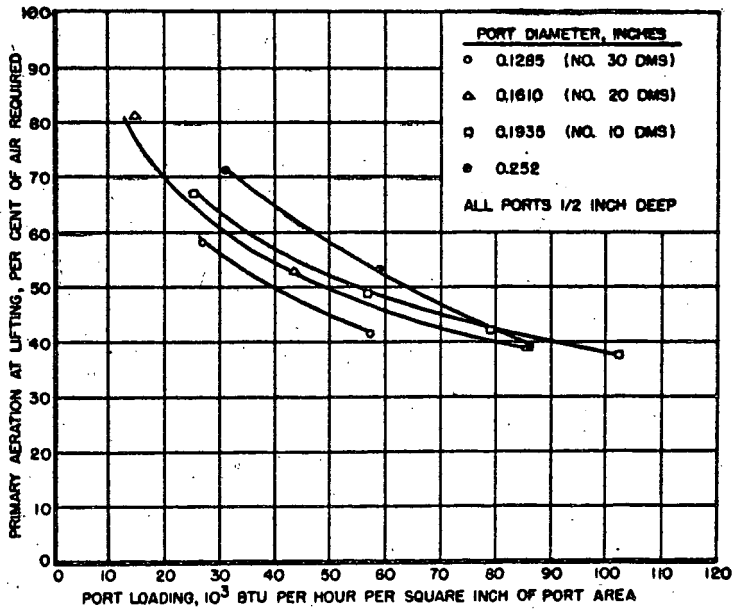


Figure 2 Lifting Limits of Various Individual Circular Ports with Cleveland Natural Gas.

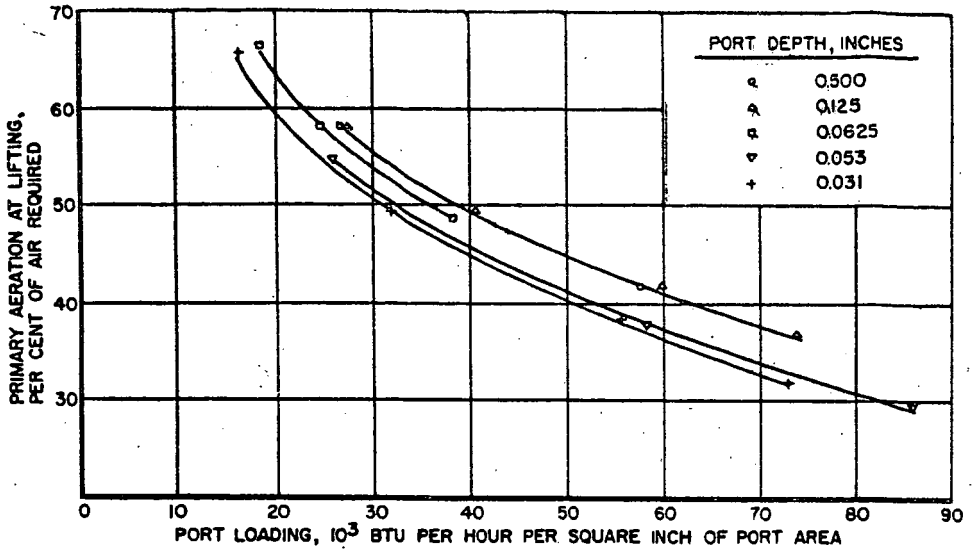


Figure 3 Lifting Limits of a No. 30 DMS Drilled Port with Various Port Depths with Cleveland Natural Gas.

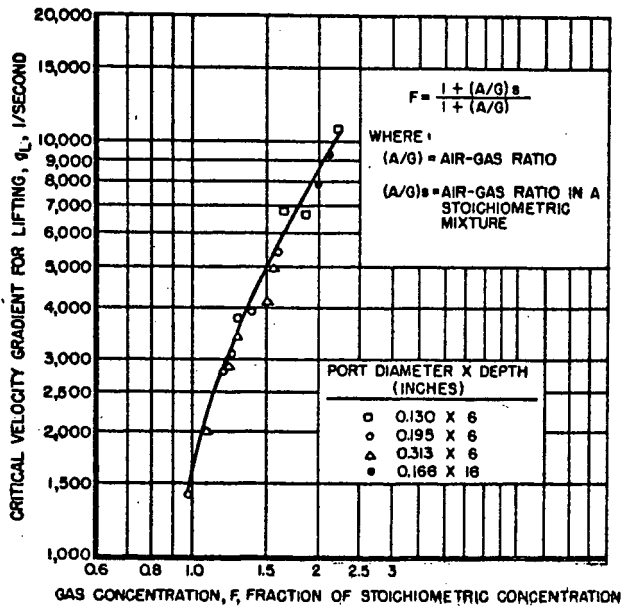


Figure 4 Critical Lifting Boundary Velocity Gradient for Cleveland Natural Gas.

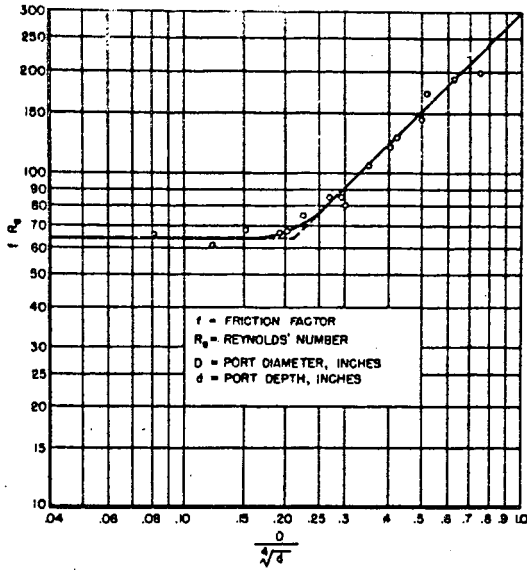


Figure 5 Friction Factors for Various Deep and Shallow Circular Ports with Cleveland Natural Gas at the Lifting Limit.

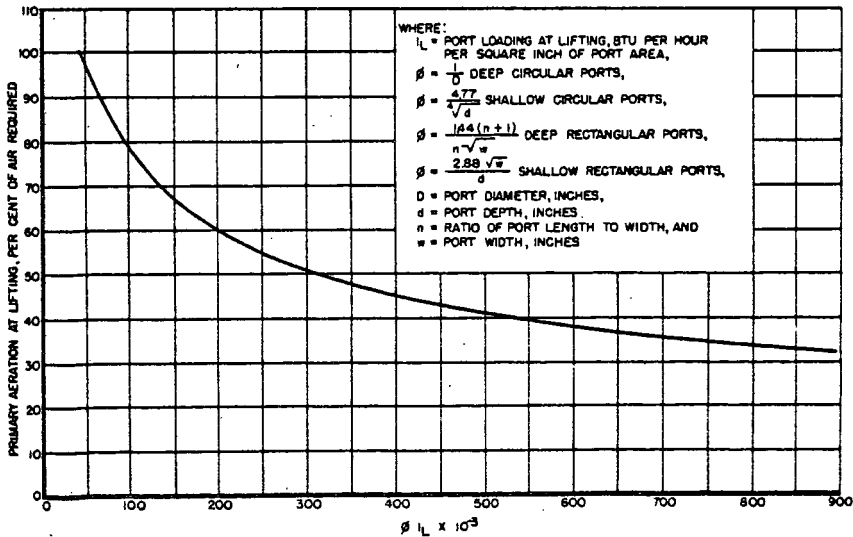


Figure 6 Lifting Limits of Slotted and Circular Ports with Cleveland Natural Gas.

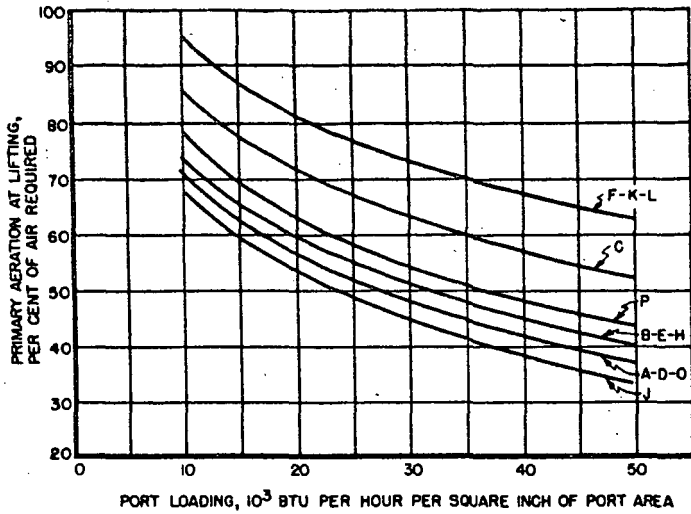


Figure 7 Lifting Limit Curves with Cleveland Natural Gas for Experimental, Multiple Port Burners.

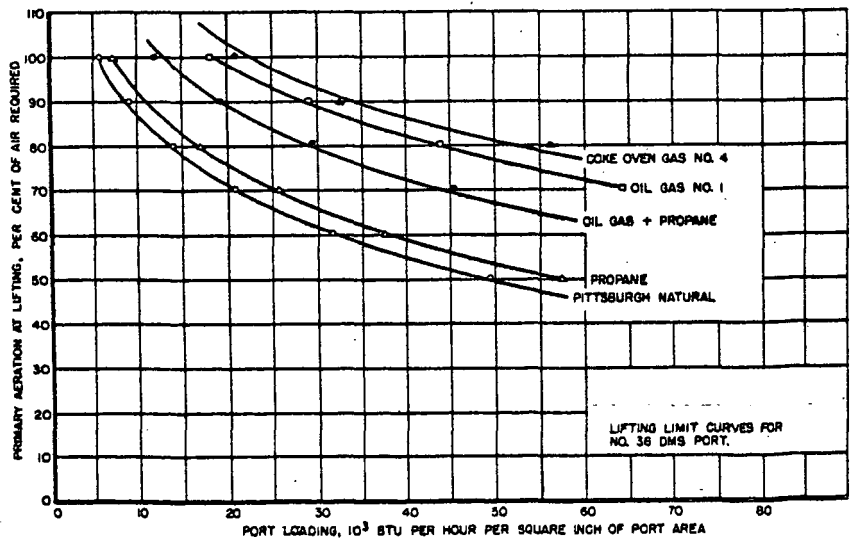


Figure 8 Lifting Limits Obtained at the U. S. Bureau of Mines for Various Fuel Gases.

Measurement of the Thermal Properties
of Carbonaceous Materials

By

J. D. Batchelor, P. M. Yavorsky and E. Gorin

CONSOLIDATION COAL COMPANY
Research and Development Division
Liberty, Pennsylvania

ABSTRACT

Three parameters of interest for thermal processing of carbonaceous materials have been studied. The mean specific heat capacity from room temperature to temperatures of 500° to 900°F have been shown to range from 0.54 to 0.41 for coal from the Pittsburgh Seam and 0.28 to 0.31 for its LTC char. These measurements were made in a simple high temperature calorimeter. The thermal conductivity of coal-char-pitch briquets was found to follow a pattern similar to coal being coked, exhibiting a 20-fold increase in value from room temperature to hot coke temperature. The conductivities were measured by a very direct method using a compensated conductometer. An estimation of the surface film heat transfer coefficient for fluidized solid heating of an immersed sphere was carried out experimentally using the unsteady state heating curve. Values for h of the order of 30 Btu/hr ft² F° were obtained which are consistent with the range generally found in the literature for wall and tube coefficients.

Not for Publication
Presented Before the Division of Gas and Fuel Chemistry
American Chemical Society
Chicago, Illinois, Meeting, September 7-12, 1958

Measurement of the Thermal Properties
of Carbonaceous Materials

J. D. Batchelor, P. M. Yavorsky and E. Gorin

CONSOLIDATION COAL COMPANY
Research and Development Division
Library, Pennsylvania

INTRODUCTION

Many of the processes for the treatment of coal, either in present day use or under development, involve thermal conversion. One such process, the forming of coal-char briquets, is discussed in a companion paper. It is obviously desirable, in the development of such processes, to have available thermal data on the materials being handled. The work described here was designed to supply such thermal data for carbonaceous materials of interest. Heat capacity measurements have been made on a bituminous coal from the Pittsburgh Seam and its low temperature char. Thermal conductivity measurements have been carried out on a coal-char-pitch briquet. Finally, an estimate has been made of the heat transfer film coefficient from a fluidized heating medium to a spherical briquet. This latter work was carried out so that the thermal parameters could be applied to the calculation of heating rates for carbonaceous briquets, an application which is described in another paper.

Literature Survey

The heat capacity data for coal recorded in the literature have been reviewed by Clendenin, et al.³ In this review a correlation equation for the specific heat capacity of moisture-free coal is presented, based on data for 23 American bituminous coals. The equation relates heat capacity to temperature and volatile matter content as follows:

$$C = 0.200 + 0.0015 \text{ V.M.} + 0.00088 t$$

where V.M. = percentage volatile matter on a moisture-free basis
t = temperature, °C

This equation cannot be expected to hold into the temperature range in which coal becomes plastic. In fact the very limited data included in the correlation for temperatures above 100°C make its use above about 150°C an extrapolation that may not be justified.

The heat capacity of a bituminous coal within its plastic range may be a somewhat variable quantity depending upon the definition of the quantity and the method of measurement. The literature contains numerous papers devoted to the measurement of two heat quantities. One, the total "heat of carbonization", is defined to include all the sensible and reaction heats involved in carbonization; the other, often called the "heat of decomposition", refers to the reaction heats only after the sensible heats have been removed by calculation or by the use of a differential calorimetric method. The most notable of the data in the literature

are those of Terres and co-workers¹¹⁻¹⁵, Davis, et al.⁴⁻⁶, Weyman¹⁶, and Burke and Parry². Work has also been reported upon the heat capacity of chars produced from coal by thermal treatment¹³. In general, the data found in the literature fall short of providing applicable and consistent data for materials typical of Pittsburgh Seam bituminous coal.

Published information on the thermal conductivity applicable to materials with which we deal is also very meager. By the time our work had progressed to conductivity measurements, we were primarily interested in compactions of coal, char and pitch. Data on coals and cokes are summarized by Clendenin, et al.³, but again these data are principally low temperature measurements below 100°C. Some data by Terres¹¹ cover the whole coking range, but since the values are reported as "mean" conductivities they probably represent average values over a wide temperature range. Millard⁶ has published conductivity data for beds of granulated coal (and coke, subsequently produced) over a 100-900°C temperature range. While the experimental unit used by Millard was adequate for measurements on packed beds, it was not applicable to solid compactions. Work by Birch and Clark¹ on the conductivity of rock samples up to 900°F provided the basic design for the conductometer used in our work.

No work has been found in the literature which predicts directly the surface film heat transfer coefficient between fluidized solids and small spheres immersed in the bed. Numerous investigations and correlations are available for heat transfer coefficients between fluidized solids and the walls of the containing vessel and some work is reported for internal tubes. No effort has been made to critically evaluate all this information, but the range of values for h thought to be applicable is from 20 to 50 Btu/hr ft² F°.

Heat Capacity Measurements

Method

A variation of the standard calorimetric method of mixtures was used in this work. The bituminous coal samples under study were known to undergo irreversible changes upon thermal treatment in the temperature range of interest; for this reason, it was essential that a high temperature calorimeter be used in which the sample is heated and the calorimeter cooled. This procedure is exactly the opposite of the one generally used in which a hot sample is cooled in a cold calorimeter. The method adapted measured the total heat required to raise the sample from room temperature to the temperature investigated; sensible and reaction heats are thus lumped together. This is the important quantity, however, for most practical applications.

The use of a high temperature calorimeter made it impractical to reduce the thermal losses to a negligible level. Instead, it was necessary to control and standardize the losses at a reasonably high level. In an effort to keep the unit as simple as possible, an unsteady state method was used, in which the effect of an added sample on the normal cooling curve of a heated metal block was observed. This method proved adequate, and allowed the use of simple equipment; however, considerable care and extensive calculation were needed to produce these satisfactory results.

The heart of the calorimeter was an aluminum block 1-1/2" o.d. by 2-7/8" long with an axially bored hole 3/4" in diameter and 2-1/2" deep. Six holes were drilled on a 1-1/8" circle in the top of the block; two of these holes were tapped

for support rods, and the other four were used as thermocouple wells 1/2", 1", 1-1/2" and 2" deep, respectively. This aluminum block was wound with a resistance wire heater and suspended by small iron rods from a transite disc. The block was hung down into a glass Dewar flask, which in turn was placed in a tube furnace. The furnace temperature was controlled at a level near the operating temperature of the block to reduce the heat loss. A "seal-ring" of transite, slightly smaller than the inside diameter of the Dewar flask, was placed between the block and its supporting disc. This "seal-ring", which contained an electric heater powered from a constant voltage source, was provided to reduce the end losses upward from the block and to improve the temperature symmetry of the system. A long glass tube was used to provide an inlet path for the test samples. A nitrogen purge was metered in near the bottom of the Dewar flask to insure an inert atmosphere. The calorimeter is shown assembled in Figure 1.

The thermocouple circuits used to get a sensitive measure of the temperatures of the system consisted of two 4-element thermo-piles made of iron-constantan. The four hot junctions of one thermo-pile were placed in the holes drilled in the aluminum block, and because of their spacing in the block yielded a good average temperature directly. These junctions had to be insulated electrically from the block, and this was done with a bead of aluminum cement to which a little water-glass had been added. The hot junctions of the second thermo-pile were held about 1/16" away from the inner wall of the Dewar flask, spaced at 90° around the block at a level near the middle of the block. The sensitivity of each of these thermo-piles, between 500° and 900°F, is of the order of 0.12 millivolt per degree Fahrenheit, so that by measuring each output to the nearest 0.01 millivolt with a Leeds and Northrup portable potentiometer the temperatures within the block and external to it could be determined to the nearest 0.1°F.

In the normal experimental procedure, the outer furnace and the seal ring heater were used to establish an elevated "steady state" temperature in the calorimeter block. From this level the block heater was used to raise the block temperature to a level about 20°F higher. After conditions were steady at this upper temperature level, the block heater was switched off, and the block allowed to cool towards its lower steady state temperature. After about three minutes had elapsed a powdered solid sample, held in a small aluminum foil cylinder about 5/8" diameter and 1-1/2" long, was dropped into the block. The block and external temperatures were read alternately, each on a 30-second schedule, until the cooling rate became relatively small so that less frequent readings were sufficient.

The calculation of the effect of the added sample required that a "normal cooling curve be determined for each temperature level without any sample addition or other external stimulus. By graphical differentiation of the block temperature curve during "normal" cooling, the block cooling rate was plotted as a function of the instantaneous temperature difference between the block and its surroundings. At each level a good straight line relation existed, as predicted by the simple Newtonian cooling law; a typical plot is shown in Figure 2. The slope of this line depends on the properties of the system, but the intercept depends, principally, on the input to the seal ring heater. When used as a correction of the observed cooling after a sample has been added to the calorimeter block, this Newtonian plot must be extrapolated into the heating domain where $\frac{dt_{\text{block}}}{dt}$ is positive and

$(t_{\text{block}} - t_{\text{external}})$ is negative. To prove that this extrapolation was reasonably accurate, a dry ice pellet was added at one temperature level to force the block temperature below the external temperature; the observed heating rate for the block was just that predicted by extrapolation.

A typical pair of temperature curves for a run in which a solid sample was added is shown in Figure 3. For selected values of time the temperature driving force, ($t_{\text{block}} - t_{\text{external}}$), was noted and the normal cooling rate determined from the Newtonian plot. The integral expression, $\int \left(\frac{dt_{\text{block}}}{d\theta} \right)_{\text{normal}} d\theta$, was

determined graphically for each run, and served as a correction for the observed temperature drop of the block. The corrected temperature effect of the sample was the algebraic difference of the observed temperature drop and this integral normal temperature drop: The corrected temperature effect should approach a steady final value after a reasonable period of time, as shown in a typical curve in Figure 4. In some cases in which no final steady value was approached, it was necessary to shift the Newtonian cooling plot, holding its slope constant, until the total effect was forced to level off. This forced balance was equivalent to assuming that the seal ring heater input varied while the insulating properties of the system did not. This assumption appeared reasonable since the corrections were random and no aging trend was noticed during the period spent on measurements at a given temperature level.

After the total corrected effect of a sample on the calorimeter block was found, the remaining calculations were familiar. Powdered Al_2O_3 , a substance of known heat capacity, was run to establish a calorimeter constant. The heat capacities of other materials were determined by using this calibration as a reference.

Results

The heat capacity of a Pittsburgh seam coal (38.6% V.M. and 7.0% ash, from the Arkwright mine in West Virginia) was determined to a maximum temperature of 800°F. Swelling and frothing of the coal made it impossible to use higher temperatures. A char produced from this coal by fluidized carbonization at 950°F was used for measurements to 890°F. This Arkwright char contained 13.2% V.M. Magnesium oxide was used as a secondary standard to check the accuracy of the method, by comparison between observed and literature values for heat capacity from 650° to 800°F. The results for these three materials is shown in Figure 5; the mean specific heat capacities are, of course, averaged from room temperature to the final temperature plotted.

Most points on the curves shown in Figure 5 are the average of two or more determinations. The variability of individual values from the mean was generally less than 2% for the heat stable materials, but rose as high as 5% in one instance for the coal sample in the middle of the plastic temperature range. The agreement between the observed and literature values for MgO adds confidence in the method.

For comparison with data found in the literature, two other curves are shown in Figure 5. One represents the values that would be predicted by applying the equation derived by Clendenin, et al.³; the other curve is from data by Porter and Taylor⁹, these data being the highest temperature values included in the correlation of Clendenin. No comparable data are available for char.

The data obtained here by use of a high temperature calorimeter apply to the particular case in which the sample is heated very rapidly and the products of carbonization are carried out of the system. This corresponds quite well to the pattern in fluidized low temperature carbonization of coal, the application for which these data were originally determined, but may differ substantially from the heating regime in some other processes. Reaction effects, particularly from extensive secondary reaction of the tar products, may cause some variance in total specific heat capacity under other treatment conditions.

Thermal Conductivity Measurements

Method

Absolute thermal conductivities of a material are best determined by direct measurement of the temperature gradient which exists for a known rate of heat transfer across a unit area of material under steady state conditions. From the Fourier heat transfer equation

$$\frac{dq}{d\theta} = k A \frac{dt}{dx}$$

the thermal conductivity can be calculated directly. The thermal conductometer used in this work was modeled after one described by Birch and Clark¹, and allowed us to measure these needed factors for compactions made of char, coal and pitch.

A cross-sectional view of the conductometer is shown in Figure 6. The location of the lead-in wires has been omitted. The apparatus was symmetrically square about the vertical axis. The specimen was a flat slab approximately 2" square and 1/2" thick, cut from a single large briquet, or formed of close fitting rectangular sections from small briquets. It was placed between the heater block and cooling plate, both of which are made of copper to assure an even temperature distribution. A 30-gauge nichrome wire heating element in the heater block held its temperature about 10°C above that of the cooling plate when a steady state was reached. Measurement of this temperature difference across the specimen was made with thermocouples placed at positions indicated by the heavy dots. Provided that there is no heat transfer from the heater block other than through the specimen, the conductivity is simply calculated. The condition of no extraneous heat loss from the block was approached as closely as possible by use of a thermal guard dome of copper which covered the heater block as shown. The guard dome contained a heating element by which the dome's temperature was adjusted to equal the temperature of the heater block. Heat losses to the surroundings then came from the guard dome and not from the heater block. Lateral heat losses from the specimen were minimized by the guard ring of insulating material (transite) that surrounds the specimen. Small ceramic spacers prevented accidental metal-to-metal contact between the dome and heater block.

The entire conductometer was enclosed in a steel box which was purged with nitrogen to prevent oxidation of the copper or the specimen at high temperatures. The entire unit was immersed in a fluidized sand bath to provide the controlled elevated ambient temperatures.

Stable power for the heater block was provided by two six-volt storage batteries in series. The current was manually controlled with rheostats to give the desired temperature differential across the specimen. With currents of 100-200 milliamperes in the block heater, there was no discernible drift in the current during the course of a measurement. The less critical power for the guard dome was provided by a Variac with a rheostat for fine control. A type K Leeds and Northrup potentiometer was used for accurate measurement of the thermocouple potentials and the voltage and current of the heater block. Voltage measurements across a standard one-ohm resistor in the heater circuit gave direct measurements of the heater current.

Results

Thermal conductivities were determined for sections of briquets made from coal, char and pitch. The composition was 25% coal (Pittsburgh Seam from Montour

mine in Western Pennsylvania), 63.5% low temperature char produced from this coal by fluidized carbonization at 950°F and 11.5% pitch. These briquets were pre-coked at several temperature levels, their conductivity measured at that temperature, and then also at lower temperatures. This procedure separately demonstrates both the effect of coking on conductivity at a particular temperature and the temperature dependence of conductivity of specifically coked briquets. These data are plotted in Figure 7.

Trustworthy results could not be obtained at temperatures above 1600°F on the fully coked briquets because adequate fluidized sand furnace temperature control was not realized. However, the values obtained at other temperatures on this fully coked material allow a reasonable extrapolation of the curve to 1800°F.

Figure 8 shows a comparative plot of the present data with those presented by Millard⁸ for coal. Millard made no attempt to explain the difference in the conductivities of the two coals, which came from different mines. It is readily seen from the plot that there is no radical difference in the briquet conductivity as compared to the coals. Both materials show a very large increase in conductivity with temperature and a marked increase with degree of coking.

Estimation of Surface Film Coefficient for Heating With Fluidized Solids

The application of the thermal parameters reported above very often requires the estimation of a surface film heat transfer coefficient pertinent to the thermal system to be used. One of the thermal arrangements of interest for the carbonization of briquets is the heating with circulating, hot fluidized solids. Considerable work has been done by the authors and their associates on the treatment of carbonaceous briquets in this type of system. In an effort to bring order and predictability to some of the results noted, and further to check the validity of assumed values of the heat transfer film coefficient used in machine calculations made on this type system (reported in a companion paper), an experimental method for the estimation of the film coefficient was tested. This experimental method is simple, especially so under the special conditions in which it has been applied here. The results obtained represent only a rather cursory examination of the transfer coefficient, but it is felt that the method deserves description.

The method used was to observe the temperature rise of spherical objects after immersion in a constant temperature, fluidized sand bath. Although, generally speaking, the use of an unsteady state system leads to a relatively low degree of precision, it is also true that these measurements are rapid and may be made quite well in a very simple system, much simpler than would be needed for steady state measurements.

Examination of mathematical expressions for this system showed that in order to relate these results to the film coefficient it was necessary to restrict our attention to materials and temperature ranges for which the thermal diffusivity may be treated as a constant. In these cases, the Fourier equation can be solved analytically. A solution which has been published may then be applied to this problem^{7,10}. This solution reduced further to a very simple form for the case of objects with a high thermal conductivity such as aluminum or copper ($Nu \ll 1$).

Under these specific conditions the temperatures of the center and surface, respectively, of a sphere of radius r_0 at initial temperature T_1 which is suddenly surrounded by a medium at a constant temperature T_0 are given by the equations

$$Y_{r_0} = \left(\frac{T_c - T}{T_0 - T_1} \right)_{r_0} = e^{-3Nu\theta}$$

$$Y_{r=r_0} = \left(\frac{T_0 - T}{T_0 - T_1} \right)_{r=r_0} = \sqrt{3Nu} e^{-3Nu\theta}$$

The Nusselt number, Nu , is defined as

$$Nu = \frac{hr_0}{k}$$

and θ is a dimensionless time = $\frac{\alpha t}{r_0^2}$ or $\frac{k t}{\rho c_p r_0^2}$

The Nusselt number can be very simply determined in this case by plotting experimental values of $\ln Y$ versus θ . A straight line should be obtained whose slope is $-3 Nu$. This is true for both the center and surface temperatures.

Experimentally, all measurements were made by plunging an aluminum sphere into an 8" diameter fluidized sand bath. An aluminum sphere was chosen so that the simplified form of the Fourier solution equation could be applied; i.e., the thermal conductivity of aluminum is high and almost exactly independent of temperature, and the thermal diffusivity is relatively constant. It was assumed that the nature of the sphere's surface was unimportant to the result, so that values of h calculated here would be applicable to carbonaceous briquets.

Two thermocouples were used to sense the temperatures of interest in the sphere, one attached to the surface and one placed in a small hole bored to the specimen center. Small diameter thermocouple wire (28 gauge) was used to minimize error caused by heat conduction down the wire. A third thermocouple in the fluidized sand bath was used to sense and control its temperature. All three temperatures were recorded on a multi-point strip chart recorder. All the tests used a nominal fluidized sand temperature of 1000°F.

Five tests were run using a 2" sphere. Four of these tests were made using a fluidization velocity (superficial) of 0.6-0.7 feet per second; one test used a reduced linear velocity of 0.34 fps. Single tests were made with a 1" and a 3" sphere. A typical plot of the temperature history recorded by the thermocouple placed at the center of the sphere is shown in Figure 9.

A plot of the temperature approach data used for the estimation of some of the film coefficients, h , is shown in Figure 10. Straight lines are obtained as predicted by the special solution for the basic Fourier equation. Similar results may be obtained when the surface temperature is treated in a similar manner, but the surface temperature is more difficult to measure with precision.

The lines in Figure 10 do not show the unit value of y -intercept as predicted by theory. Part of the cause of this discrepancy is thought to be a thermocouple error caused by conduction of heat down the thermocouple wire, thus producing high temperature readings. It can easily be shown that the total heat conducted down the wire is a negligibly small fraction of that conducted through the aluminum. Further, it can be shown that if the thermocouple error is proportional to the temperature difference between the surroundings and the center of the sphere (a logical assumption), then only the intercept of the Fourier solution equation is shifted and its slope is unaffected.

The calculated values of the film coefficient, h , are listed in Table I. The precision of the replicate tests on the 2" inch sphere is not the best, but the results are consistent and reasonable. The test made at a reduced fluidizing velocity shows a somewhat lower value for h , which is also reasonable.

Table I

Experimental Values of Heat Transfer Coefficient
Between Fluidized Sand and Aluminum Spheres

Thermal Parameters for Calculations: $k = 117 \text{ Btu/hr. ft. } ^\circ\text{F}$
 $a = 3.33 \text{ ft.}^2/\text{hr.}$

Run No.	Sphere Diameter	Fluidization Velocity	Fluidized Sand Temperature	Calculated Heat Transfer Coefficient, h
Al-1	3"	0.72 ft/sec	950°F	38 Btu/hr ft ² F°
Al-2	2"	0.72	1000°F	31
Al-3	1"	0.72	1050°F	27
Al-4	2"	0.61	985°F	36
Al-5	2"	0.61	990°F	34
Al-6	2"	0.34	980°F	23
Al-7	2"	0.61	950°F	30

The values measured here might be expected to lie in the upper range of values reported because of the high density of the fluidized sand; on the other hand, the fluidization velocities used were rather low, especially for a dense solid, and this factor would lower the value of h . The average value of h measured here is about 30 Btu/hr. ft.² F°, and thus well within the range of 20-50 Btu/hr. ft.² F° chosen for the calculations of heating rates of carbonaceous briquets in fluidized solids systems.

SUMMARY

The various thermal data reported here are not entirely comparable in terms of materials and temperature ranges. However, they all bear directly on the problem of heat transfer to carbonaceous briquets containing coal, char and pitch. The heat capacity data measured for coal and char may be combined with values in the literature for pitch to provide composite values applicable to briquets. The thermal conductivity data were obtained directly on briquet samples. The heat transfer film coefficient, h , was estimated for a metal of high thermal conductivity (aluminum) for simplicity, but no reason is apparent why this external factor cannot be applied directly to the heating of carbonaceous shapes of much lower conductivity. These data have been used for machine computations of briquet heating rates as reported in a companion paper.

BIBLIOGRAPHY

- 1 Birch, F. and Clark, H., Am. J. of Sci., 238, 529 (1940).
- 2 Burke, S. P., and Parry, V. F., Ind. Eng. Chem., 19, 15-20 (1927).
- 3 Clendenin, J. D., Barclay, K. M., Donald, H. J., Gillmore, D. W., and Wright, C. C., Trans. of the Seventh Annual Anthracite Conf. of Lehigh University, May 5-6, 1949, Bethlehem, Pennsylvania.
- 4 Davis, J. D., Ind. Eng. Chem., 16, 726-30 (1924).
- 5 Davis, J. D. and Place, P. B., Ind. Eng. Chem., 16, 589 (1924).
- 6 Davis, J. D., Place, P. B. and Edeburn, P., Fuel, 4, 286-99 (1925).
- 7 Ingersoll, L. R., Zobel, O. J. and Ingersoll, A. C., "Heat Conduction". University of Wisconsin Press, Madison, Wisconsin (1954).
- 8 Millard, D. J., J. Inst. of Fuel, 28, 345 (1955).
- 9 Porter, H. C. and Taylor, G. B., Ind. Eng. Chem., 5, 289-93 (1913).
- 10 Schneider, P. J., "Conduction Heat Transfer". Addison-Wesley Press, Cambridge, Massachusetts (1955).
- 11 Terres, E., Proc. Second Intern. Conf. Bituminous Coal, 2, 657-84 (1928).
- 12 Terres, E., et al., Beiheft Z. Ver. Deut. Chem., No. 10, Angew Chem., 48, 17-21 (1935).
- 13 Terres, E. and Biederbeck, H., Gas und Wasserfach, 71, 265-8, 297-303, 320-5, 338-45 (1928).
- 14 Terres, E. and Meier, M., Gas und Wasserfach, 71, 457-61, 490-5, 519-23 (1928).
- 15 Terres, E. and Voituret, K., Gas und Wasserfach, 74, 98-101, 122-8, 148-54, 178-82 (1931).
- 16 Weyman, G., Journal Soc. Chem. Ind., 39, 168-9 (1920).

FIGURE 1
CALORIMETER

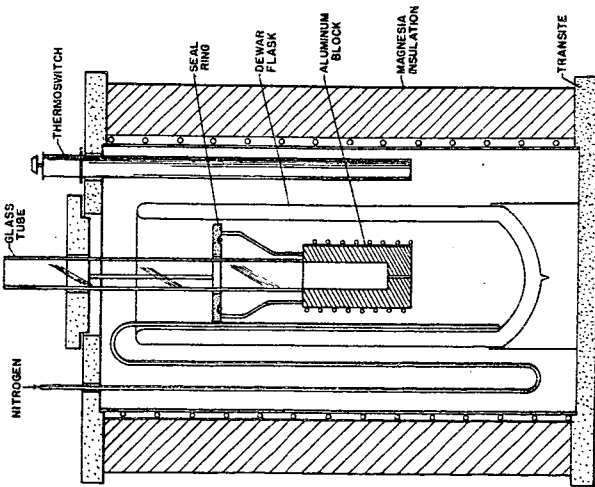


FIGURE 2
'NORMAL' COOLING CORRECTION LINE

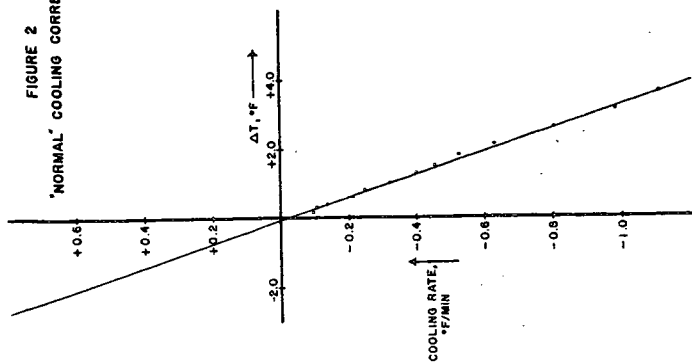


FIGURE 3
OBSERVED DATA FOR A CALIBRATION TEST

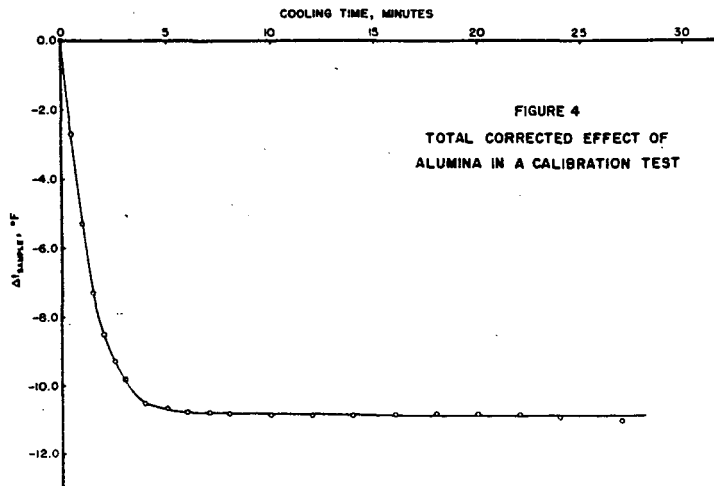
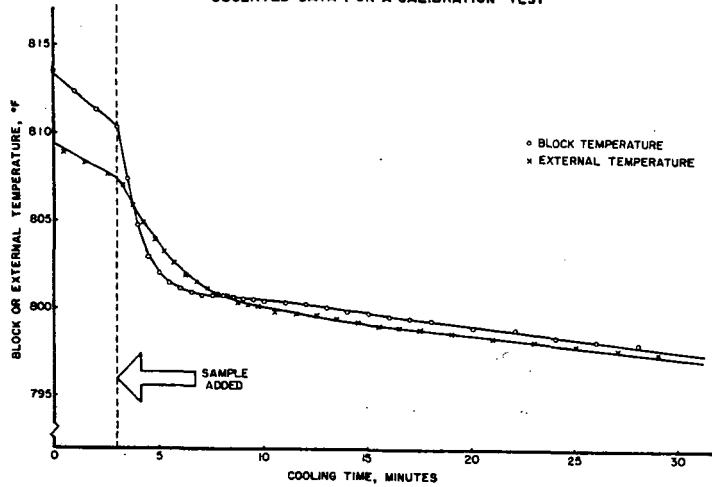


FIGURE 4
TOTAL CORRECTED EFFECT OF
ALUMINA IN A CALIBRATION TEST

FIGURE 5
MEAN SPECIFIC HEAT CAPACITIES OF COAL AND CHAR

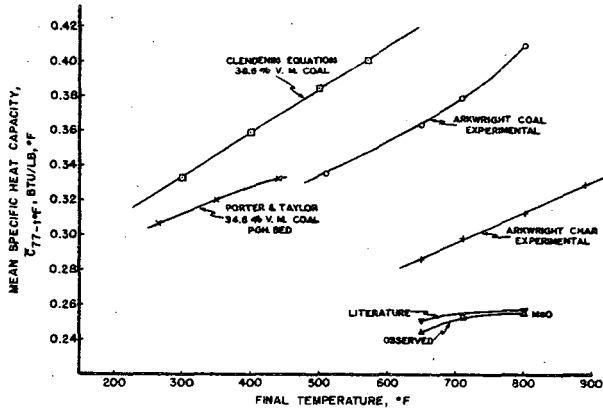


FIGURE 6
THERMAL CONDUCTOMETER

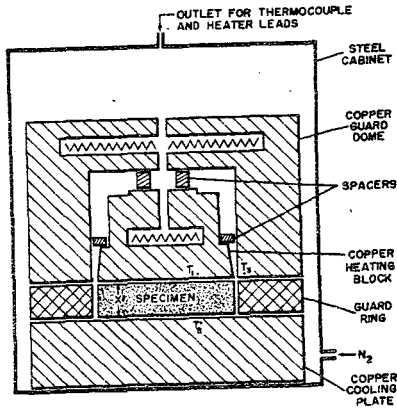


FIGURE 9
 CENTER TEMPERATURE OF ALUMINUM SPHERE
 HEATED BY FLUIDIZED SAND BED

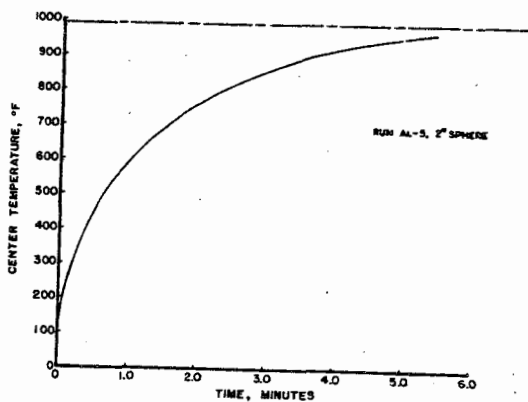
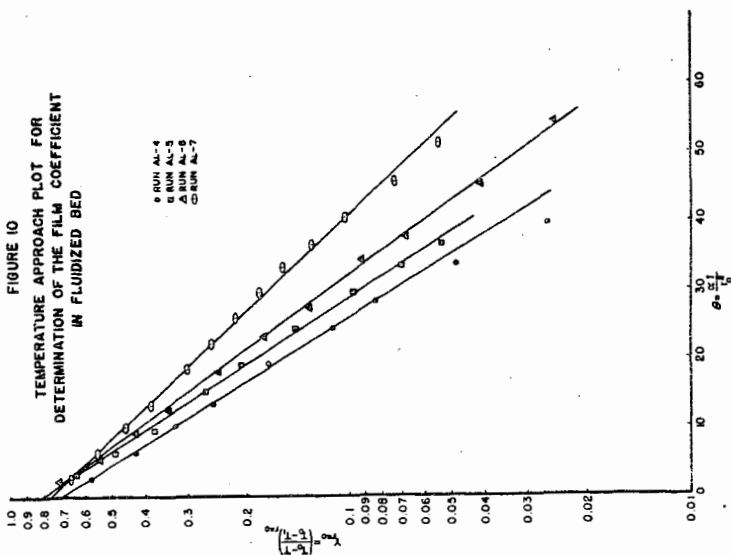


FIGURE 10
 TEMPERATURE APPROACH PLOT FOR
 DETERMINATION OF THE FILM COEFFICIENT
 IN FLUIDIZED BED



Heat Transfer and Associated Effects in
The Carbonization of Briquets

By

P. M. Yavorsky, R. J. Friedrich and E. Gorin

CONSOLIDATION COAL COMPANY
Research and Development Division
Library, Pennsylvania

ABSTRACT

Temperature-time patterns for the carbonization of coal-char briquets were computed with an electronic digital computer for various briquet sizes, film heat transfer coefficients and two shock heating methods - hot flue gas and hot fluidized solids. This represents solution of an unusual heat transfer problem wherein conductivity and specific heat are strong functions of temperature. Heating rate correlations evolved from the computed results permit extension of the data to conditions not included directly in the computations.

Combination of the thermal patterns with experimental briquet expansivity data yielded information on the relative magnitude of thermal stresses in briquets undergoing carbonization. Excessive stresses lead to deleterious briquet fracturing.

The assembled data supply the necessary background for estimation of operability limits for briquet carbonization by shock heating procedures and can be used to define physical conditions and dimensions in the design of carbonization units in formcoking processes.

Not for Publication

Presented Before the Division of Gas and Fuel Chemistry
American Chemical Society
Chicago, Illinois, Meeting, September 7-12, 1958

Heat Transfer and Associated Effects in
The Carbonization of Briquets

P. M. Yavorsky, R. J. Friedrich and E. Gorin

CONSOLIDATION COAL COMPANY
Research and Development Division
Library, Pennsylvania

INTRODUCTION

The work reported here is part of a program aimed at the development of a continuous process for the production of formcoke suitable for blast furnace use. The potential advantages of such a process are lower investment costs/ton of coke, the ability to utilize the vast reserves of non-metallurgical grade coal, and the production of a product coke having uniform size and quality.

Experimental work carried out in these laboratories has shown that such a process can be developed based on briquetting followed by continuous coking of the briquets. The briquets are formulated from low temperature char, coal and a pitch binder. The briquetting aspects of this program will be discussed in subsequent papers. The present paper is concerned with the carbonization of the briquets and particularly with heat transfer problems associated with this process.

The briquets require very critical control in the carbonization process to yield acceptable formcoke. On the one hand, shock heating is necessary to prevent plastic deformation, and on the other, too severe shock heating causes fracturing of the briquets. Deformation and binding of briquets would cause inoperability in any continuous process and fracturing of the formcoke into small pieces would make it unacceptable for blast furnaces.

There are two immediate objectives of this work. One is the determination of the heating rates in briquets subjected to various methods of shock heating. These rates are required for the rational design of large scale carbonizing equipment. The other objective is to determine, by way of calculated thermal patterns within briquets undergoing carbonization, the relative magnitude of thermal stresses. Excessive thermal stresses are believed responsible for deleterious fracturing. Knowledge of these stresses produced under various conditions and methods of shock heating would be useful in the selection of the most favorable process for producing intact formcoke. Some empirical data, gathered from small scale laboratory experiments, outline the general thermal regime required for successful carbonization of briquets. The calculated temperature distribution within these briquets during carbonization can thus serve as a guide for selection of processes and equipment for large scale equipment. The general principle that will be adapted, as will be discussed later, is that the temperature gradient within a briquet undergoing carbonization shall be no greater than that corresponding to the operability limits prescribed by small scale work.

Attainment of both of the above objectives hinges upon solution of the problem of heat transfer to and through a briquet. This problem defies solution in a rigorous analytical form because both the thermal conductivity and the specific heat are strongly temperature dependent, as is established in a companion paper.

Therefore, recourse was had to an approximation method or numerical solution of the differential equations which involved use of an IBM 650 Digital Computer. The machine computations were carried out at the University of Pittsburgh Computing Center and were programmed to define the thermal pattern in a briquet at various times as a function of briquet size, film heat transfer coefficient, and two shock heating methods - with hot flue gas and with hot fluidized solids. Estimation of the film coefficient for a heating medium then allows selection of the appropriate heating pattern for the briquets. An empirical correlation was derived from the computed results which relates the rate of heating of briquets to all the important variables. With the law of squares for heated bodies, the correlation permits rapid extrapolation to many heating cases not directly covered in the computer program. The accuracy of the correlation is within 5%.

Dilatometer measurements were made to determine the magnitude of thermal expansion and contraction that occurs during carbonization of briquets. By coupling these data with the computed thermal patterns, the relative magnitude of thermal stresses can be estimated from the Timoshenko theory of elasticity for heated isotropic and elastic bodies.

Direct experimental data for the temperature rise of the center of a heated briquet are compared with the computed results in a few cases where a comparison can be made. Reasonable agreement with the comparable cases lends some degree of confidence to the other computed results. Many of the briquet heating cases investigated by machine computation cannot be easily examined experimentally on a small scale.

THE PROBLEM AND GENERAL PROPERTIES OF THE SOLUTIONS

The problem of heat conduction in carbonaceous materials has been attacked previously. Burke¹ et al. discussed some years ago mathematical relationships for the rate of heat conduction through coal undergoing carbonization. However, in order to arrive at an analytical solution, these authors treated the case that corresponded to the illegitimate assumption that the thermal diffusivity, (α), was independent of temperature. A constant α for carbonaceous materials cannot be assumed. The strong temperature dependence of thermal conductivity (k) and specific heat (c) has been shown in a companion paper. α is given by $\alpha = k/\rho c$ where ρ is the density. The non-constant conductivity of coal was also reported by Millard² who attempted solution of the Fourier heat-flow equation by use of an electrical analog technique. He could obtain agreement between calculated data and experimental thermal patterns in a coke oven only by injecting sizable heats-of-carbonization into the calculations.

The problem that concerns us is to define the temperature profile as a function of time within a spherical briquet undergoing carbonization, taking full account of the temperature dependence of the thermal parameters - the conductivity and specific heat. Two different methods of direct shock heating are considered, namely, with hot gas and hot fluidized solids.

At least in principle, the problem can be handled by solution of the Fourier heat conduction equation. The equation, in polar coordinates, for the general case of a sphere wherein the thermal diffusivity is temperature dependent, is

$$\left(\rho c + T \frac{d(\rho c)}{dT}\right) \frac{\partial T}{\partial t} = k \left(\frac{\partial^2 T}{\partial r^2} + \frac{2}{r} \frac{\partial T}{\partial r} \right) + \frac{dA}{dT} \left(\frac{\partial T}{\partial x} \right)^2 \quad (1)$$

This equation must be solved with these boundary conditions:

$$T = T_1 \text{ at } t = 0 \text{ for all values of } r.$$

$$\text{and } h \frac{dT}{dr} = h(T_0 - T_1) \text{ at } r = r_0. \quad (2)$$

T_0 , the ambient temperature of the heating medium surrounding the briquet, varies unless the heat content of the medium greatly exceeds that of the briquet. The variation of T_0 with time can be derived from heat balance, yielding

$$dT_0 = \frac{3A}{r_0 M \rho c_0} (T_0 - T_1) dt \quad (3)$$

The above relation holds for continuous carbonization where concurrent flow of heating medium and briquets prevail. It also holds for batch carbonization where no temperature gradient exists within the heating medium.

It thus becomes evident, that solution of the heat flow equation (1), with the complex boundary conditions, as well as the non-constant parameters k and c , cannot be obtained by the usual analytical methods. A numerical method of solution is consequently necessary.

Although an analytical solution of the above equations cannot be obtained, certain interesting properties of the solutions follow from the form of equation (1) and the boundary conditions.

Let new variables be introduced, namely $X = r/r_0$, $t' = t/r_0^2$, and $h' = hr_0$. It can now be readily verified that the temperatures, as expressed in equations (1) and (2), become functions only of X , t' , k , h' , and M . It follows that the solution is a function only of X and t' if k , M , and hr_0 are maintained constant. Consequently, an equivalent temperature profile is established within a briquet at corresponding values of the relative radius X at a time inversely proportional to the square of the radius of the briquet. This is a more generalized expression of the law of squares which has been previously discussed² and will become useful later.

NUMERICAL ANALYSIS AND SOLUTIONS

Before proceeding with the numerical analyses, it is necessary to establish the values of the parameters needed. These parameters are for briquets of Pittsburgh Seam coal and product char.

The thermal conductivity measured as a function of temperature for briquets is reported in the companion paper. The specific heat for briquets was obtained from the additive equation for the components thus,

$$C_{\text{briq.}} = 0.115 C_{\text{pitch}} + 0.250 C_{\text{coal}} + 0.635 C_{\text{char.}}$$

where the numbers correspond to the weight fraction of the briquet components.

The specific heats of coal and char were taken from measurements given in the companion paper. The specific heat of pitch was taken from Hyman and Kay³. These data were adequate to cover the range from room temperature to 500°C. Above 500°C, it was assumed that the briquet was carbonized and the data of Terres⁴ for char and coke was used.

Graphical representations of the specific heat and thermal conductivity as functions of temperature were reduced to algebraic expressions primarily for purposes of machine computation. The graphs were fitted to polynomial equations by a standard least-squares sub-routine used in the IBM 650 Digital Computer. The analytical expressions were found to be

$$C(T) = 2.14 \times 10^{-1} + 6.19 \times 10^{-4} T + 1.40 \times 10^{-6} T^2 + 4.36 \times 10^{-9} T^3 + 2.61 \times 10^{-12} T^4 \quad (4)$$

for the specific heat of briquets and

$$k(T) = 2.74 \times 10^{-1} + 5.28 \times 10^{-4} T + 4.57 \times 10^{-6} T^2 + 3.85 \times 10^{-9} T^3 + 4.91 \times 10^{-12} T^4 \quad (5)$$

for the thermal conductivity of briquets. T is expressed in °C.

The coefficients and exponents were stored in the computer memory section. The appropriate values of C(T) and k(T) could be determined by the machine whenever needed in the overall computations.

The measured density of raw briquets is 0.8 gm/cm³. It was assumed not to change during carbonization. This assumption is acceptable since shrinkage compensates approximately for the loss in weight (volatilization) during carbonization.

Evaluation of the film coefficients is also explained in the companion paper. Values of 20 and 50 Btu/hr ft² F° were assigned for the computations on solids heating, to bracket expected values for heat transfer from fluidized solids to briquets. For the gas film heat transfer coefficient, 9.5 Btu/hr ft² F° was employed in the calculation of the heating rate of two-inch briquets by hot flue gas. This value derives from correlations by Gamson⁵ et al. and by Wilke⁶ et al. and corresponds to a flow rate of 375 lbs. gas/ft² hr. This is consistent with a physical situation in which a 15-ft. high shock heating zone, containing briquets, is injected with 2200°F flue gas and in which the briquet residence time is 80 minutes.

The problem of the rate of heating of briquets can be solved by application of numerical methods of analysis similar to the step methods described by Ingersoll⁷. In a generalized problem as complex as the one encountered here, hand calculations would become prohibitively long and tedious. Only the speed of modern computing machines allows one to consider attempting such numerical solutions. Machine computing time for a single set of conditions, a single heating case, was an hour and a half.

Initial attempts with the Digital Computer to solve the general numerical problem by applying "relaxation" operations to the step method⁷ proved impractical. Programming the machine to make judicious predictions of temperature changes for small time intervals was difficult and it required too much time in working through many erroneous guesses before striking upon ones sufficiently correct. Therefore, a "guess-free" step method was developed to translate the numerical procedure into a form more suitable for machine computations.

To facilitate numerical solution of this problem, the physical process of heat transfer is artificially resolved into two distinct, sequential processes - first, isothermal flow of heat from one section of matter to another for a short

time, and second, a resultant change in temperature of the section based upon its heat balance during the isothermal period. This artifice is most helpful in reducing the heat transfer problem into simple first order difference equations that are easily translated into the basic language of digital computation. In reality, the flow of heat and change of temperature are not sequential, as pictured here, but occur simultaneously, so that our solution of the problem is an approximate one, though of very close approximation. The numerical solution approaches the rigorous one as the increments of time and space that enter the computations are made smaller for if the increments become infinitesimals, the solution would be a true calculus integration of the differential equations. The use of an electronic digital computer, with its extremely rapid computation permits computation of a set of equations for a great number of very small time and space increments; thus, our solution is very nearly rigorous.

Definitions of symbolic terms used in the following calculations and discussions appear in the Appendix.

In this approximation method, a briquet is considered as being made up of ten concentric spherical layers having initial temperatures of ${}_1T_1, {}_1T_2 \dots {}_1T_{10}$. The briquet is heated by hot gas of initial temperature ${}_1T_0$. For the duration of a short time interval, Δt , these temperatures are assumed constant while heat conduction proceeds, the driving force being differences between ${}_1T_0, {}_1T_1 \dots, {}_1T_{10}$. The heat transferred is given by

$$g_{0,1} = \frac{({}_1T_0 - {}_1T_1) \Delta t}{\frac{\Delta r/2}{k({}_1T_1) a_1} + \frac{1}{h a_s}} \quad (6)$$

for the transfer from gas to the first layer, and by

$$g_{i,i+1} = \frac{k({}_iT_i) a_i ({}_iT_i - {}_iT_{i+1}) \Delta t}{\Delta r} \quad \text{for } i = 1 \dots 10 \quad (7)$$

for the transfer from layer to layer. The balance of heat left in i 'th layer at the end of a time interval is

$$\Delta g_i = g_{i-1,i} - g_{i,i+1} \quad (8)$$

which upon substitution of equations (6) and (7) leads to

$$\Delta g_0 = -g_{0,1} \quad (9)$$

for the gas since it can only lose heat. For the first layer, the heat balance is

$$\Delta g_1 = g_{0,1} - g_{1,2} = \frac{({}_1T_0 - {}_1T_1) \Delta t}{\frac{\Delta r/2}{k({}_1T_1) a_1} + \frac{1}{h a_s}} - \frac{k({}_1T_1) a_1 ({}_1T_1 - {}_1T_2) \Delta t}{\Delta r} \quad (10)$$

$$\Delta g_1 = B_0 ({}_1T_0 - {}_1T_1) - B_1 ({}_1T_1 - {}_1T_2)$$

where by definition

$$B_0 \equiv \frac{\Delta t}{\frac{\Delta r/2}{k({}_1T_1) a_1} + \frac{1}{h a_s}} \quad \text{and} \quad B_i \equiv \frac{k({}_iT_i) a_i \Delta t}{\Delta r} \quad \text{for } i = 1 \dots 10. \quad (11)$$

For the remaining layers, the residual heat in each layer is

$$\Delta g_i = B_{i-1} ({}_iT_{i-1} - {}_iT_i) - B_i ({}_iT_i - {}_iT_{i+1}) \quad (12)$$

Equations (9) through (12) now give the balance of heat lost by the gas and gained by each layer during the arbitrary short time interval, Δt . Now, the temperatures of the gas and layers are allowed to change by virtue of the heat lost or gained so that

$$\Delta q_0 = -m_0 c_0 ({}_1T_0 - {}_2T_0) \quad (13)$$

and

$$\Delta q_i = m_i c ({}_2T_i - {}_1T_i) \quad (14)$$

Elimination of Δq_0 from equations (9) and (13) and defining $A_0 = M_0 C_0$ yields

$$A_0 ({}_1T_0 - {}_2T_0) = B_0 ({}_1T_0 - {}_1T_1) \quad (15)$$

Elimination of Δq_i from equations (12) and (14) and defining $A_i = m_i c ({}_1T_1)$ yields

$$A_i ({}_2T_i - {}_1T_i) = B_{i-1} ({}_1T_{i-1} - {}_1T_i) - B_i ({}_1T_i - {}_1T_{i+1}) \quad (16)$$

Since the ${}_1T$ values are known from chosen initial conditions the ${}_2T$'s are the only unknowns involved in equations (15) and (16), both of which can be re-arranged to the form,

$$A_i {}_2T_i = B_{i-1} {}_1T_{i-1} - (B_{i-1} + A_i - A_i) {}_1T_i + B_i {}_1T_{i+1} \quad (17)$$

which is completely general if it is remembered that B_{i-1} does not exist when $i = 0$ and that B_0 has a different form than all the other B_i values (see equation (11)). Thus, the temperature of the gas, and of each layer in the briquet, at the end of the first time interval, are computed directly from equation (17). These end temperatures, (${}_2T_1$), then become the initial temperatures, (${}_1T_1$), for the next time interval, and the computations are repeated to determine the temperatures at the end of the second interval. Iteration of this procedure, for many time intervals, in the computer yields the temperature profile of the gas and the layers of the briquet as a function of time. Ten-second time intervals were used in computations for 2 and 3-inch briquets and one-second intervals for the 1-inch briquet.

Eight briquet heating cases were solved directly on the computer, covering variations of the following parameters, initial temperature of the heating medium, mass ratio of heating medium to briquets, film coefficient, and the briquet radius. The law of squares, mentioned earlier, can be used to apply the results to different size spheres by adjusting the value of h to maintain $hr_0 = \text{constant}$. The cases studied are outlined in Table I.

The first four cases, involving high initial temperatures and a low value of h describe shock heating with hot gas. The specific heat and molecular weight of the heating medium in these cases was chosen to correspond to that of flue gas.

The other cases in Table I describe carbonization of briquets with hot fluidized solids, such as char.

The temperature distribution patterns solved for the eight programmed cases are shown in Figures 1 through 8. Figures 1 through 4 show the distribution obtained for shock heating with hot gas. Figures 5 through 8 show the distribution for the cases where a fluidized solid heat carrier is used for shock heating. These figures illustrate immediately the heating times involved in carbonization of different size briquets under various conditions.

The time scale in each case is given for either a 1, 2 or 3-inch briquet as noted in the particular figure. The conversion factor to convert the time scale to other briquet sizes by the law of squares is also noted on each figure.

The expected qualitative trends are clearly in evidence upon close examination of these figures. A faster rate of heating is observed, other things being equal, when 1) the shock heating temperature is increased, 2) the film coefficient becomes larger and 3) the briquets become smaller.

Some of these trends can be demonstrated more quantitatively by combining the salient features for several cases on individual plots. Figure 9, for example, shows the effect of briquet size on the rate of rise of the briquet center temperature with various values of h . The law of squares states that the rate of temperature rise is inversely proportional to the square of briquet radius when $h r_0$ is constant. If h is held constant, the rate here does not decrease quite as rapidly. The rate, in this case, decreases roughly as the 1.75 power of the briquet radius. It is clear, that as h becomes very large, that the law of squares will again become valid. A very large value of h corresponds to the case in which the surface temperature is held equal to that of the heating medium. Conversely, as h becomes very small the temperature within the briquet will tend to become uniform at all points and the rate of temperature rise becomes inversely proportional to the first power of the briquet radius.

The effect of the value of the heat transfer coefficient on the rate of temperature rise of the surface and center temperatures for the case of a two-inch briquet may be seen in Figure 9. As the value of h increases beyond 50 Btu/hr ft²F the rate of temperature rise tends to become independent of h .

The effect of the film coefficient on the time required for the briquet center to reach a given temperature is illustrated in Figure 10. The time required to reach temperature again becomes independent of h for large values.

Some experiments were conducted to observe the temperature rise at the briquet center for comparison with the theoretical behavior. The experiments were arranged so that the results could be compared with Cases IV through VIII where char was used as the heating medium. These computed cases were set up with a decreasing temperature of the char from an initial value of 1350°F to a final equilibrium temperature of 1110°F. The above temperature pattern (set up as representative of a continuous process) could not be conveniently reproduced in the laboratory.

The experiments were, therefore, conducted at a uniform 1200°F in the 8" fluidized sand bath. A thermocouple was inserted into the center of the briquet which was plunged into the sand bath and the temperature history was continuously recorded.

Measurements of this kind were made with 1", 2" and 3" diameter spherical briquets. The linear fluidizing velocity of the sand bath was maintained constant at 0.26 fps for 1 and 2-inch briquets. In order to check the effect of linear velocity a second and higher velocity of 0.45 fps was also employed for the 2-inch briquets. Since no effect of fluidizing velocity was found in this range, three-inch briquets were measured only at 0.45 fps.

The experimental measurements are compared with the calculated rate of temperature rise in Figure 9 for all three briquet sizes. The curves shown are the calculated curves for different values of h as parameter.

It should be remembered here that the work reported in the previous paper for aluminum spheres indicates that the correct value of h is in the neighborhood of 30 Btu/hr ft².

It is seen that in all cases the rate of temperature rise initially is greater than the calculated figures. This phenomenon is undoubtedly mainly due to a conduction thermocouple error. This was shown by the following experiment. The exposed extrusions of a thermocouple injected into the center of a 2" briquet was heated electrically to 1100°F. Another unheated couple was inserted also to the briquet center at a 90° angle to the former one. It was found that the heated thermocouple would read as much as 100°F above the unheated couple. This much thermocouple error is sufficient to bring about agreement between the lower temperature experimental points and a calculated curve expected for an h of 30 for 2" briquets, as can be seen from Figure 9.

As the temperature of the briquet rises the thermocouple error naturally would diminish quite rapidly both because of the smaller temperature differential and the increase in thermal conductivity of the briquet material.

The lowest value of h available from the calculations for the 1" sphere is 40. Extrapolation by the aid of the curve shown in Figure 10 to an h value of 30 shows that quite good agreement exists between theory and experiment after allowing for the initial thermocouple error.

It is also noted in the case of the two-inch briquet, that the effect of fluidizing velocity on the experimental rate of temperature rise is negligible. It is seen likewise, that good agreement between theory and experiment is obtained after the temperature rises above 500°C by assigning a lower than predicted value of h of the order of 20.

The agreement at higher temperatures becomes rather poor in the case of the three-inch briquet since one must assign a value below 13 to h to obtain agreement in this case.

The explanation of this higher temperature discrepancy is thought to lie in the retarding effect of volatile matter release on the penetration of heat through the surface of the briquet; i.e., effectively on the value of h . This effect was neglected in the calculations because of the added complexity it would have introduced. It should be noted, however, that the rate of volatile matter release per unit of briquet surface increases proportionately to the briquet radius, making it more serious for the larger briquets.

EMPIRICAL CORRELATIONS FOR HEATING RATES

It is desirable, if possible, to have available a simplified correlation encompassing the calculated results. If such a correlation can be derived it would simplify extrapolation to cases that were not directly considered and the application of the calculated rate of heating to many design problems.

A correlation was developed to fit the four cases, V through VIII, considered for solids heated briquets. These cases correspond, for a two-inch spherical briquet, to a range of values for h of 20 to 75 Btu/hr ft² F°.

The correlation is based on the use of the empirical equation

$$\frac{dT}{dt} = K (T_s - \bar{T}) \quad (18)$$

\bar{T} is approximately the mean briquet temperature and T_s is the temperature of the fluidized solids medium. \bar{T} is exactly defined by the equation

$$\bar{T} = \bar{T}_0 + Q/\bar{C} \quad (19)$$

\bar{T}_0 is the initial briquet temperature, Q is the amount of heat absorbed by the briquet and \bar{C} is the mean specific heat of the briquet over the whole carbonization range. \bar{T} would be exactly equal to the mean briquet temperature if the specific heat of the briquet were independent of temperature, which it is not.

It is clear that equation (18) in view of equation (19) can also be written as follows

$$\frac{dQ}{d\bar{T}} = \bar{C} K (T_s - \bar{T}) \quad (20)$$

This equation is obviously fallacious since the exact equation is

$$\frac{dQ}{d\bar{T}} = 4\pi r^2 h (T_s - T_1) \quad (21)$$

Where T_1 is the temperature of surface of the briquet.

If equation (20) is valid, it can only mean that the increase in the thermal conductivity of the briquet with temperature, is such that \bar{T} follows, fortuitously, the relationship

$$\bar{T} = T_s - a (T_s - T_1) \quad (22)$$

The test for equation (18) is shown graphically in Figure 11 where the $\log (T_s - \bar{T})$ is plotted against time. The points shown are derived from the computed results of Cases V through VIII. In the particular cases studied here, heat balance considerations give rise to the relationship

$$T_s - \bar{T} = T_0 + 5.73 - 1.23 \bar{T} \quad (23)$$

T_0 is the initial temperature of the heating medium in degrees centigrade. The slope of the straight lines shown in Figure 11 are equal to K of equation (18) multiplied by 1.23.

It is clear that the correlation holds with adequate accuracy as noted by the linearity of the plots. The calculated slopes K' ($= 1.23 K$) are given for the different h values on the graph.

It now remains, to complete the correlation, to account for the variation of K with h and with briquet radius r . The variation with h , at constant r of one inch, is adequately expressed by the empirical equation

$$K = \frac{a h}{1 + b h} \quad (24)$$

where $a = .00834$, $b = .0369$, the time is in minutes and h has units of Btu/hr ft² F°.

The transposition of equation (24) to other briquet sizes is carried out readily by the law of squares. The final correlation is given below where r is in feet and t in minutes.

$$\frac{d\bar{T}}{dt} = \frac{6.93 \times 10^{-4}}{r^2} \left(\frac{h r}{1 + 0.443 h r} \right) (T_s - \bar{T}) \quad (25)$$

This equation fits the computer calculations shown in Figure 11 with an accuracy of 5%.

THERMAL STRESSES

Thermal stresses can arise during the coking operation as a result of the temperature distribution produced within the briquet combined with either a contraction or expansion of the briquet material. To provide a better understanding of the nature of the thermal stresses existing within the briquet, a brief dilatometer study was made of the thermal expansion and contraction characteristics of the briquet material.

The dilatometer used is simply an electrically heated vessel about 1 cm I.D. containing a 2 cm high sample. The sample supports a rod which is counter-balanced by a small weight attached to a string which presses over a pulley. The pulley is fitted with an indicating needle whose displacement can be calibrated in terms of linear expansion or contraction of the sample. Using a slow rate of heating, about 3 to 5 F° per minute, the sample is assumed to be at the same temperature as the container, and at essentially uniform temperature throughout.

The dilatometer studies were made on samples of briquets of material from Pittsburgh Seam coal, particularly from two of our West Virginia mines, the Arkwright and the Moundsville mines.

The results of two slow heating runs on material derived from Arkwright coal appear in Figure 12. In one case the sample was cut from a raw briquet and in the other case, loose mix (not briquetted) was used. The briquet sample contracted sharply at nominally 400 and 800°F, with an overall linear shrinkage of 9% upon calcination to 1500°F and subsequent cooling. The loose mix did not show as much shrinkage. This is probably a reflection of the less intimate contact of the particular ingredients in the mix. The coal and pitch may become coked as separate particles in the mix whereas they envelop or penetrate the char in the briquet making it one solid body upon coking.

Figure 13 shows the negative thermal expansion of a briquet sample of material from Moundsville coal. It had an overall shrinkage of 13.5% and exhibited an abrupt contraction at about 700 to 800°F as in the above Case...

Figure 14 shows the results of a run which is an attempt to simulate shock heating. The sample and container were set into the furnace at 1500°F which immediately dropped to ca. 1000°F, which is the shock heating temperature wanted. The furnace was maintained at this temperature for 20 minutes at which time the center of the sample was nearly at the same temperature as the wall (1000°F). The temperature was then raised to 1500°F. In this case the sharp contraction at about 800°F seen in Figure 1 was not evident, probably because the whole sample was not at that temperature at any one time.

It was hoped that use could be made of the above data with exact methods that are available for calculation of the thermal stresses developed within an isotropic and elastic body upon heating or cooling. The thermal stresses are a function of the temperature distribution within the body, the shape of the body, the coefficient of thermal expansion α , the modulus of elasticity E and Poissons number ν .

The tangential stress σ_t at a radial position r of a sphere of radius r_0 is given by the following expression due to Timoshenko⁸,

$$\sigma_t = \frac{\alpha E}{1-\nu} \left[\frac{2}{r_0^3} \int_0^r T r^2 dr + \frac{1}{r_0^3} \int_r^{r_0} T r^2 dr - T \right] \quad (26)$$

The expression for the case of a hollow sphere with an inner radius a and an outer radius b is given by Timoshenko³ as follows

$$\sigma_t = \frac{2\alpha E}{1-\nu} \left[\frac{2r^3 + a^3}{2(b^3 - a^3)r^3} \int_a^b T r^2 dr + \frac{1}{2r^3} \int_a^r T r^2 dr - \frac{1}{2} T \right] \quad (27)$$

The use of these expressions to calculate the exact magnitude of the stresses existing in briquets during coking is not possible. The main difficulty is that we are dealing with a material that is not homogeneous and that is changing in chemical and physical structure with time and temperature. Likewise, the physical parameters α , E , and ν are not known exactly. In fact, the above data show there is no constant α .

The briquets actually undergo shrinkage rather than expansion as the temperature rises due to the above mentioned physical changes. If we permit ourselves a rough approximation of the dilatometer results shown in Figure 24, the shrinkage may then be treated as linear with the temperature. Under such conditions the Timoshenko equation can be employed to calculate relative thermal stresses by treating the factor $(\alpha E/1-\nu)$ as an unknown parameter for different coking conditions, but which is assumed to be constant.

The briquet mix remains in a plastic condition due to softening of the pitch and coal until a rigid coke bond is formed. Therefore, thermal stresses can only be set up within the rigid portion of the briquet, while the inner plastic region undergoes relaxation of any imposed stresses by flow into the rigid shell. The problem can therefore be handled by application of equation (27) for the case of a hollow sphere.

The application of this method requires that a more or less arbitrary decision be made relative to the temperature at which plasticity of the mix disappears. It has been assumed in what follows that the mix becomes rigid at 800°F. This may be in some error, but definition of the solidification temperature is not too important, however, since we are merely concerned with relative stresses.

The method adopted therefore was to compute the relative thermal stress over the coked portion of the briquet, i.e., over the shell where the temperature was 800°F and higher as a function of time, coking conditions and briquet size. For simplicity, the calculations were restricted to computing the tangential stress at the surface of the briquet only. Under these conditions, it can be shown that equation (27) reduces to

$$\sigma_t = \frac{2\alpha E}{1-\nu} \left[\frac{3}{2(1-c^3)} \int_c^1 T y^2 dy - \frac{1}{2} T \right] \quad (28)$$

where $c = a/b$ and $y = r/b$. The computed temperature distribution patterns given in Figures 1 through 8 were employed with this equation to obtain the relative stress results discussed below.

The application of the Timoshenko equation to the calculation of thermal stresses can be readily criticized since the equations apply to an elastic body of constant chemical structure which is not the case here. It is clear, however, that

in any case the thermal stresses are greater the sharper the temperature gradients within the body. The Timoshenko equations merely provides a convenient framework upon which to make a semi-quantitative evaluation of relative thermal gradients for different heating patterns.

To establish a background of comparison for determining which relative stresses can be expected to exceed the fracturing limits, a successful regime that has been worked out experimentally for shock carbonization of briquets without fracturing follows. Intact and non-deformed two-inch formcoke has been produced by shock heating in a fluidized sand bath, provided that the sand temperature was within the range of 900 to 1150°F. The proper regime for hot gas formcoking is difficult, if not nearly impossible, to investigate on a laboratory scale.

The calculated relative thermal stress in 2-inch briquets heated with gas is shown as a function of the initial gas temperature in Figure 15. In all cases the equilibrium temperature was maintained near 1000°F by selection of the quantity of gas. The maximum thermal stress increases as expected with initial gas temperature, but at a relatively low rate.

The thermal stress for char heated briquets as a function of briquet size, time and film coefficient is shown in Figure 16. The equilibrium temperature in all cases was constant at 1100°F. It is noted that the thermal stress is of the same order, or higher, than in the gas cases even where 2600°F gas was used. One may conclude, at least tentatively, from this that two-inch briquets may be successfully coked without fracturing even when 2600°F gas is used.

The other relationships in Figure 16 show the anticipated increase in thermal stress with increasing briquet size using a fixed value of h . The major increase in maximum stress is between the one and two-inch size with a relatively small increase between two and three inches. This complies with experimental findings, that 1" briquets survive the successful regime established for 2" briquets.

Experimentally, it is difficult to produce fracture-free 3" carbonized briquets by shock heating in fluidized sand. The slight increase in thermal stress in going from 2 to 3" briquets, as shown in Figure 16, must be critical.

Certain qualitative conclusions are signified by these results. It is readily seen from equation (28) that if the temperature distribution within a briquet is identical with respect to the relative radius y that the thermal stress should be identical and independent of briquet size. The law of squares states that the temperature distribution versus y will go through exactly the same sequence when plotted against the reduced time scale t/r_0^2 if hr_0 is constant. Since the non-dependence of stress upon briquet size is not observed either experimentally or from the computed results (Figure 16) it can only be concluded that h does not decrease inversely with r . Actually, it is felt that h decreases less rapidly, and therefore, the thermal stress does increase with size.

ACKNOWLEDGEMENT

Thanks are extended to Dr. William Kehl and Nicholas Sabers of the University of Pittsburgh Computing Center for helpful discussions and the final detailed programming of the problem into computer language.

LITERATURE CITED

- 1 Burke, S. P. and Others. "The Physics of Coal Carbonization".
Am. Gas Assoc. Proc., 1930, p. 820 + p. 700 .A5p 1930.
- 2 Millard, D. J. "A Study of Temperature Conditions in a Coke
Oven". J. Inst. of Fuel, 28, 345 (1955).
- 3 Hyman, D. and Kay, W. B., Ind. Eng. Chem., 41, 1764 (1949).
- 4 Terres, E. and Biederbeck, H. "Specific Heat of Char".
Gas und Wasserfach, 71, 265-268, 297-302, 303-305,
338-345 (1928).
- 5 Gamson, B. W. and Others. "Correlation of Gas Film Coefficient".
Trans. of the Am. Inst. of Chem. Engrs., 32, 1 (1943).
- 6 Wilke, C. R. and Hougen, O. A. "Correlation of Gas Film
Coefficient". Trans. Am. Inst. Chem. Engrs., 41, 445
(1945).
- 7 Ingersoll, L. R. "Heat Conduction". Madison, Wisconsin
University of Wisconsin Press, 1954.
- 8 Timoshenko, S. "Theory of Elasticity". New York,
McGraw-Hill, 1934. QA 931 .T5.

APPENDIX

Definition of Symbolic Terms

- ${}_1T_0$ - Temperature of hot gas or hot fluidized solids at the beginning of a specified time interval.
- T_0 - Ambient temperature of heating medium.
- ${}_1T_i, i = 1 \dots n$ - Temperatures of spherical layers in a briquet of n layers, at the beginning of a time interval. n^{th} layer is center.
- ${}_2T_0$ - Temperature of hot gas or hot fluidized solids at the end of a specified time interval.
- ${}_2T_i, i = 1 \dots n$ - Temperatures of the briquet layers at the end of a specified time interval.
- Δt - Time interval in seconds.
- $Q_i, i + 1$ - Quantity of heat transferred during a time interval from the i layer to the $i + 1$ layer or from fluid medium to the first layer in the briquet if $i = 0$.
- r - Radius in general.
- Δr - Thickness of a briquet layer.
- r_0 - Radius of the solid spherical briquet.
- a_0 - Surface area of briquet.
- a_i - Effective heat transfer area for transfer from the $i-1$ to the i layer. It is given by $a_i = 4\pi r_{i-1} r_i$.
- ρ - Density of briquet material, assumed constant for the computer problem.
- m_i - Mass of briquet layer, taken as $(a_i \rho \Delta r)$.
- $k(T)$ - Thermal conductivity of briquet material, a function of temperature.
- $c(T)$ - Specific heat of briquet material, a function of temperature.
- h - Film heat transfer coefficient for transfer from gas or fluidized solids to the briquet.
- n - Number of layers in the briquet.
- α - $k/\rho c$, the thermal diffusivity. Also used for expansivity.
- M - Mass ratio of heating medium/briquet.
- Nu - Nusselt Number = $\frac{hr_0}{k}$

- θ - $\alpha t/r_0^2$.
- M_n - Roots of equation, $N_u = 1 - M_n \cot M_n$.
- \bar{T} - Mean Briquet Temperature.
- T_1 - Initial Briquet Temperature.

All other symbols identified as used.

Table I

Formcoking Cases for Which the Thermal Patterns Were Solved

Case	Heating Medium	Initial Temp. °F of Medium	Equil. Temp. °F	Mass Ratio, Medium Briquet	hrc Btu/hr ft sec	h → Btu/hr ft ² F°	
						for Briquets of 1" 2"	for Briquets of 1" 2"
I	Gas	2200	705	0.58	.079	19.0	9.5*
II	Gas	2200	1000	1.24	"	"	"
III	Gas	1800	1000	1.95	"	"	"
IV	Gas	2600	1000	0.91	"	"	"
V	Char	1350	1110	5.0	2.08	50.0*	25.0
VI	Char	1350	1110	5.0	4.16	100.0	50.0*
VII	Char	1350	1110	5.0	6.24	150.0	75.0
VIII	Char	1350	1110	5.0	1.67	40.0	20.0*

-103-

* Identifies h and size used in machine computation of the case. Case also fits for the other two sizes given with the adjusted h as listed.

FIGURE 2
TEMPERATURE PATTERNS IN
FORMING
CASE II

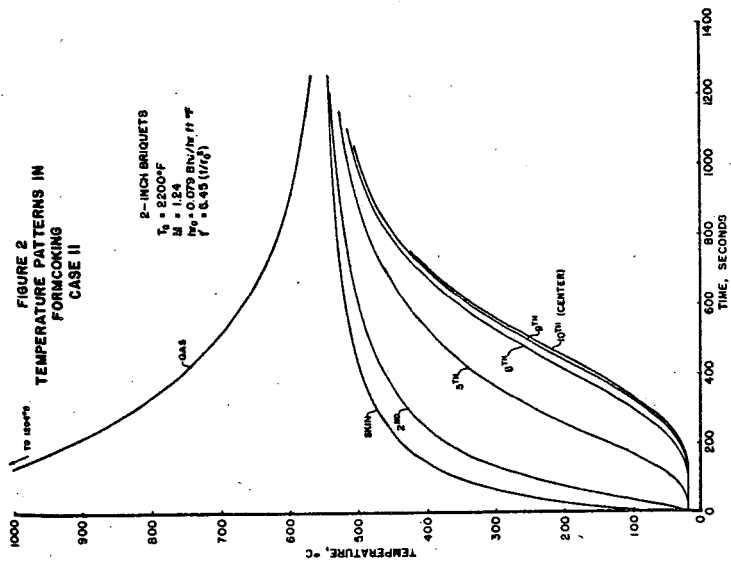
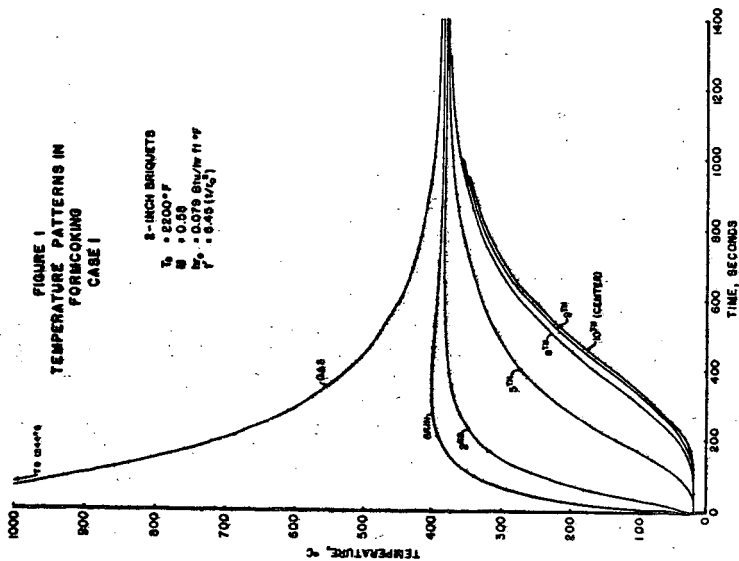
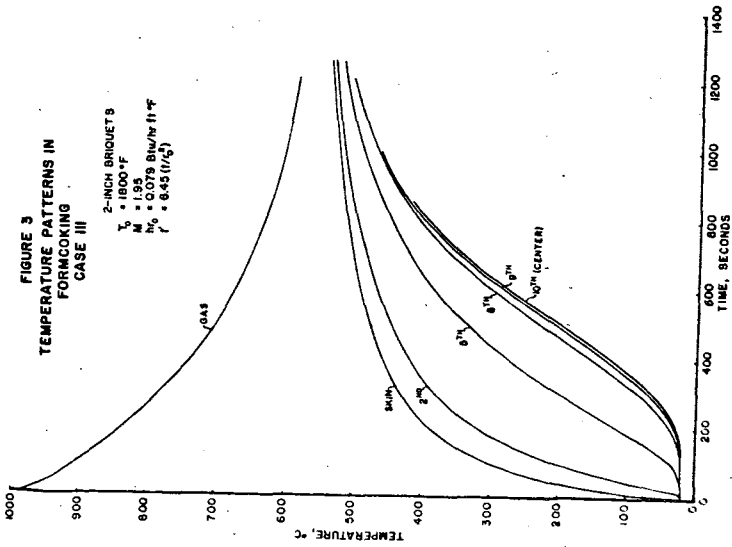
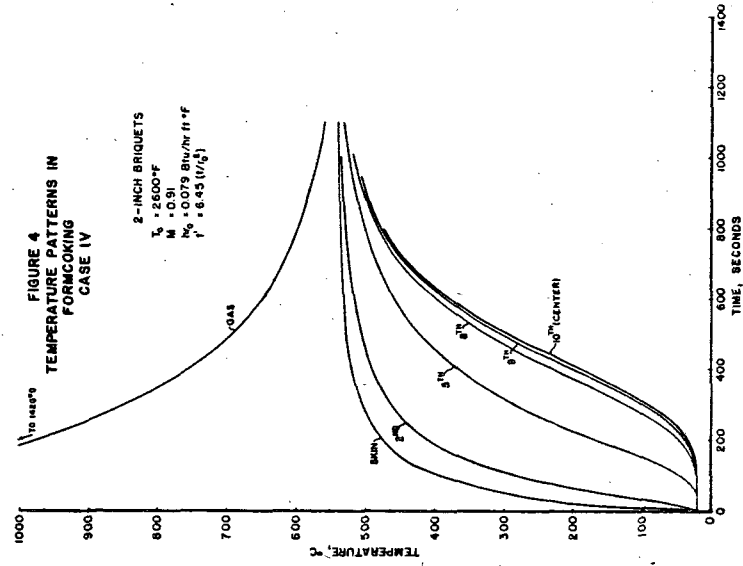


FIGURE 1
TEMPERATURE PATTERNS IN
FORMING
CASE I





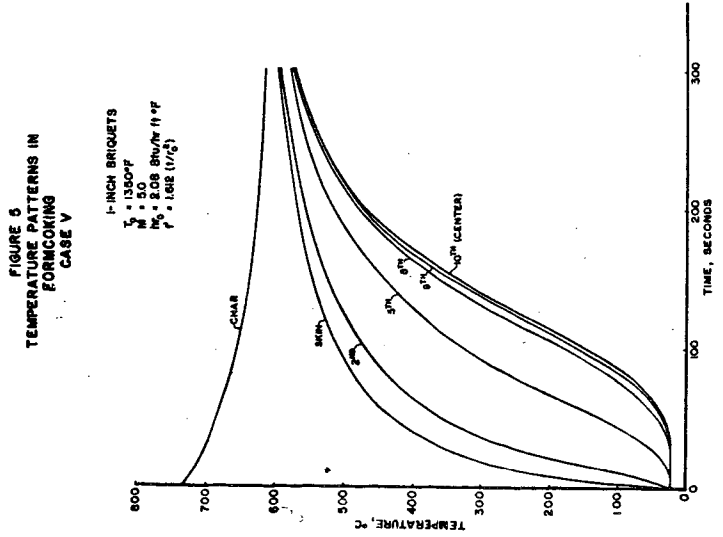
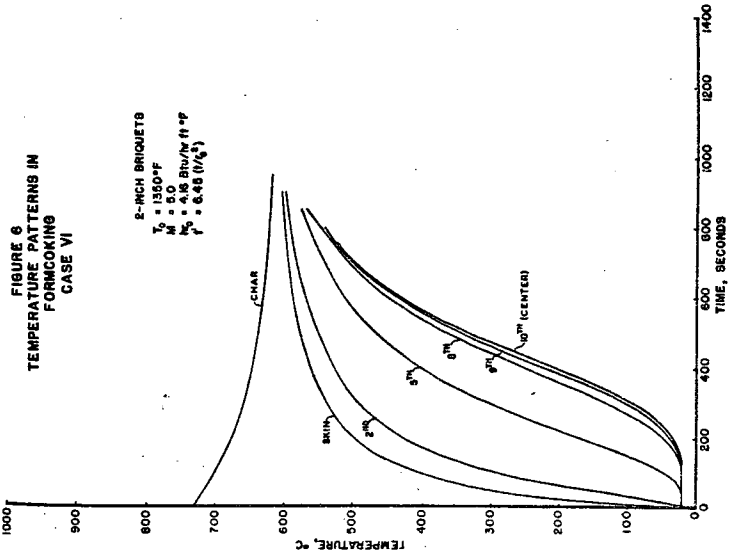


FIGURE 7
TEMPERATURE PATTERNS IN
FORMCOOKING
CASE VII

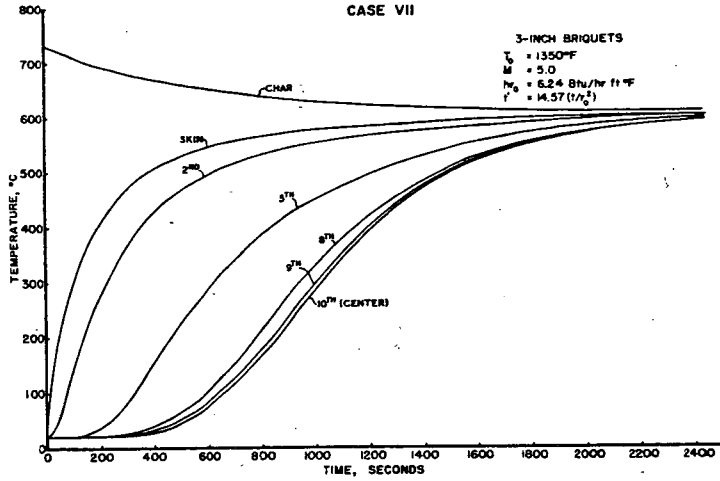


FIGURE 8
TEMPERATURE PATTERNS IN
FORMCOOKING
CASE VIII

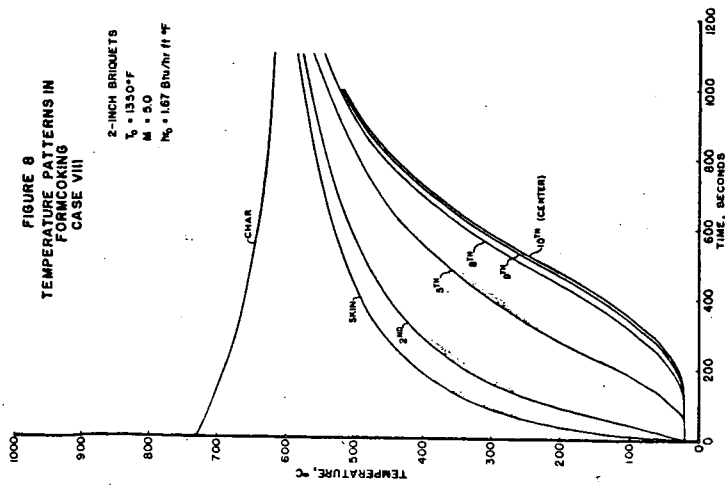


FIGURE 10
 TIME REQUIRED FOR BRIQUET CENTER TO REACH
 A GIVEN TEMPERATURE AS A FUNCTION OF FILM
 COEFFICIENT AND SIZE

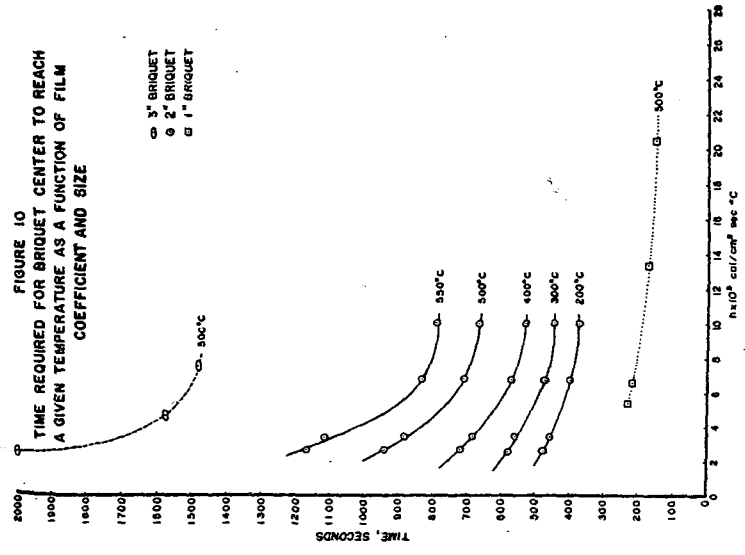


FIGURE 9
 COMPARISON OF CALCULATED TEMPERATURE RISE OF
 BRIQUET CENTER WITH EXPERIMENTAL VALUES
 EFFECT OF SIZE

EXPERIMENTAL POINT	FLUID VELC. $\frac{ft}{min}$
○ 1" BRIQUET	0.28
△ 2" BRIQUET	0.28
◇ 3" BRIQUET	0.45
□ 5" BRIQUET	0.45

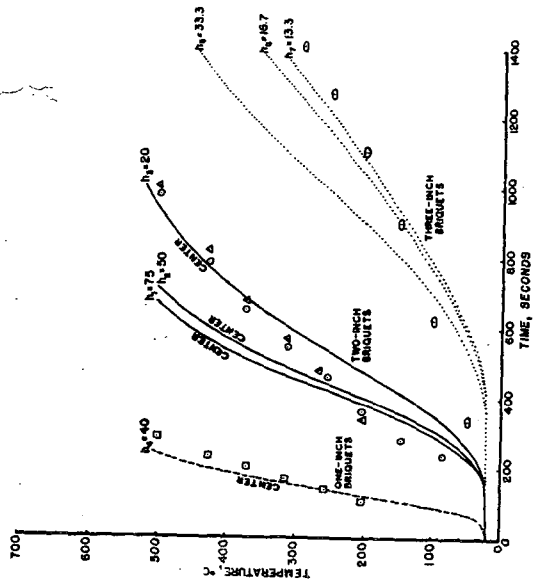


FIGURE 11
CORRELATION OF RATE OF HEATING OF BRIQUETS

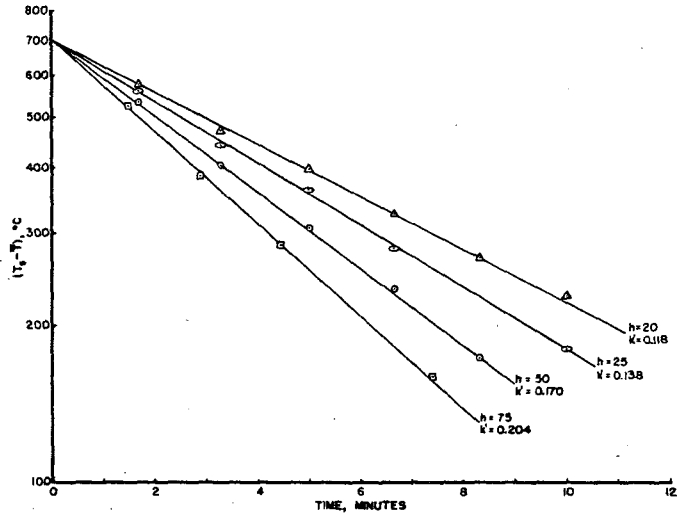


FIGURE 12
THERMAL CONTRACTION OF ARKWRIGHT BRIQUET
AND MIX, SLOW HEATING

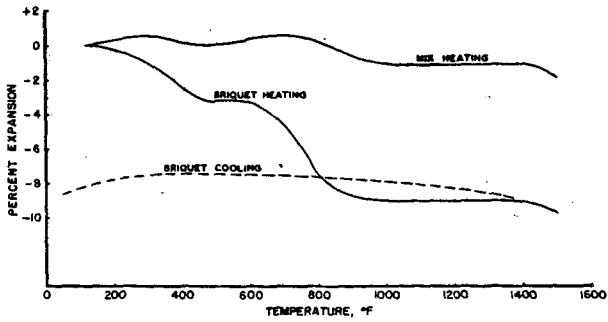


FIGURE 13
THERMAL CONTRACTION OF MOUNDSVILLE BRIQUET.
SLOW HEATING

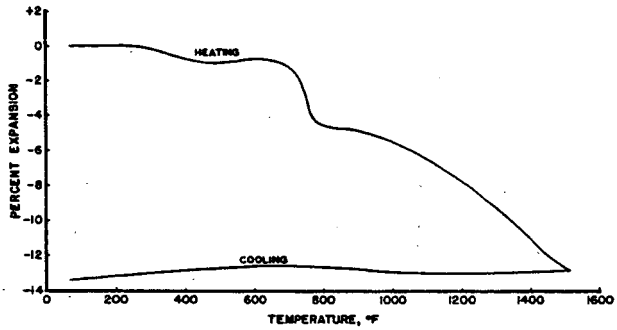


FIGURE 14
THERMAL CONTRACTION OF ARKWRIGHT BRIQUET.
SHOCK HEATING

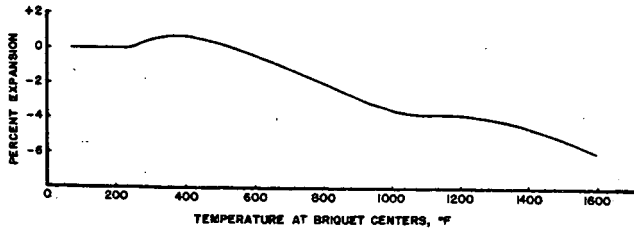


FIGURE 15
RELATIVE THERMAL STRESS IN GAS HEATED
2-INCH BRIQUET AS A FUNCTION OF TIME AND
INITIAL GAS TEMPERATURE

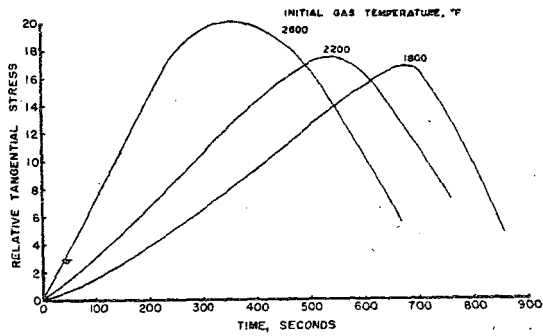
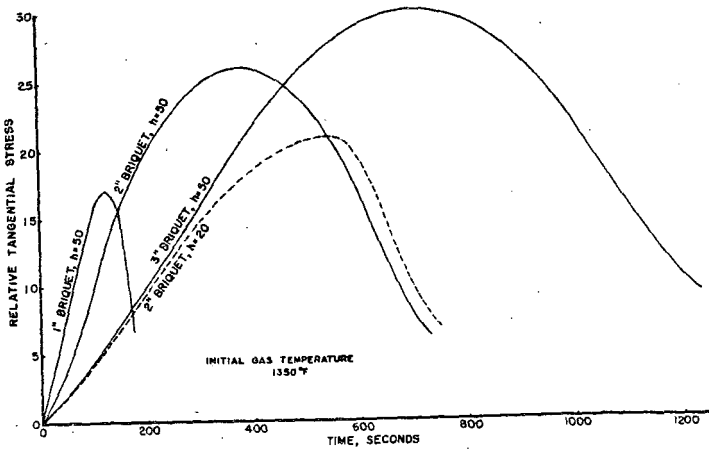


FIGURE 16
RELATIVE THERMAL STRESS IN CHAR HEATED BRIQUETS
AS A FUNCTION OF TIME, BRIQUET SIZE AND h



Chemical, Plastic, and Coking Properties of "Natural Bitumen"

by J. D. Clendenin and J. G. Price
Applied Research Laboratory, United States Steel Corporation
Monroeville, Pennsylvania

Abstract

In the course of evaluating potentially useful blending materials for improving the coking strength of coals, the Applied Research Laboratory of the United States Steel Corporation investigated the potentialities of a coal-like material identified only as "natural bitumen." From this study, the material has been tentatively identified as impsomite, probably resulting from the weathering of grahamite, both of which are asphaltites.

"Natural bitumen," found to be of very low fluidity, possessed coke-improvement properties similar to those of Lower Kittanning low-volatile coking coal and somewhat better than those of Pocahontas low-volatile coking coal. Coked alone, "natural bitumen" produced a carbonization pressure of over 40 psi and a volume expansion of about 32 per cent.

Not for Publication
Presented Before the Division of Gas and Fuel Chemistry
American Chemical Society
Chicago, Illinois, Meeting, Sept. 7 to 12, 1958

Chemical, Plastic, and Coking Properties of "Natural Bitumen"

by J. D. Clendenin and J. G. Price
Applied Research Laboratory, United States Steel Corporation
Monroeville, Pennsylvania

Introduction

In the course of evaluating potentially useful materials for use in blending in coke manufacture and for improving the coking strength of coals, the Applied Research Laboratory of the United States Steel Corporation investigated the potentialities of Impsonite, a coal-like material initially identified only as "natural bitumen." A preliminary examination was completed because of the unique properties possessed by this material.

The efficacy of pitches and asphaltic materials as coke-strengthening agents for the poorer coking coals has been known for many years. Coal-tar pitches have been used with Utah coals in commercial operations^{1,2)} and in tests³⁾ with poorly coking French and Italian coals. A highly fluid asphaltite from Argentina has been blended in carbonization tests with weakly coking Chilean coal.⁴⁾ The effectiveness of these blending materials is usually attributed to their high fluidity, as compared with that of the poor or weakly coking coals with which they are blended.

In this article the chemical and physical properties of "natural bitumen" are described, its tentative identification is presented, and its coking properties when coked alone and in blends with good and poor coking coals are demonstrated.

Experimental

Three different samples of "natural bitumen" were received for study. The first sample, consisting of only a few grams of about 200-mesh by O material, was used in determining Gieseler Fluidity, Free Swelling Index, and Proximate Analysis. The other two samples, on which most of the evaluation was made, were received in 3-inch by O size. In this size, the "natural bitumen" could be easily mistaken for a bright coal, Figure 1.

Chemical and petrographic analyses were performed on representative samples of "natural bitumen." Proximate and ultimate analyses were determined, as were solubilities in selected organic solvents. The "bitumen" was carbonized in blends with several coals and coal blends in the 30-pound Pressure-Test and Sole-Heated Ovens for pressure and volume-change determinations, respectively; the resulting coke from the 30-pound Pressure-Test Oven was tested to provide comparative-strength data. The Laboratory's 30-pound Pressure-Test Oven has been described in several published papers;^{5,6)} the Sole-Heated Oven used is similar to that developed by the U. S. Bureau of Mines⁷⁾ and the first reported in 1938.

Coke strengths were determined by the Laboratory's Modified Tumbler Test, in which 10 pounds of 1-1/2 by 1-inch coke is tumbled for 500 revolutions in the standard ASTM Tumbler Drum. The tumbled coke is screened and the per cent retained on a 3/4-inch screen is designated as the Modified Tumbler Index.⁶⁾

Results and Discussion

Examination of the "natural bitumen" as received showed it to be coal-like and lustrous in appearance; extremely friable, greasy to the touch, and dirty to handle. Macroscopically, banding was not evident, but the presence of cleavage and the checkered appearance suggested some kind of structure. Microscopically, a conchoidal-like fracture was clearly identified, and the surface resembled that found on hard pitches and other similar amorphous organic materials. Smooth, irregular, jet-black, highly reflecting surfaces were prominent, Figure 1.

The physical properties of the "natural bitumen" were similar to those of Lower Kittanning low-volatile coal, Table I. In the 3-inch by 0 size, this material had a bulk density of 49 lb per cu ft, which is only a little lower than that of Lower Kittanning coal, and it floated at a specific gravity as low as 1.23. This "natural bitumen" was slightly soluble in carbon disulfide, but the insoluble residue disintegrated into a fine powder. The behavior in xylene was similar: a lump of "bitumen" disintegrated into an insoluble, fine powder, while the solvent became faintly straw-colored.

In the flame test, a lump of "natural bitumen" decrepitated and burned, and incipient fusion was detectable. Burning ceased when the lump was removed from the flame; this indicated a high-ignition temperature. When the "bitumen" was subjected to the ASTM Free-Swelling Index Test,⁸⁾ in which the sample must be pulverized to 60 mesh, the resulting "button" was strong, coherent, dull black, and non-swollen, and had an index of 1-1/2, see Figure 2. However, when coarse, minus 1/4-inch particles (rather than the standard 60-mesh particles) were used in the ASTM Free-Swelling Index Test, a strong, dense, coherent, shiny black button was formed that had an apparent index of 3 to 4. The outlines of the small lumps were still distinguishable on the outside surfaces of the Free-Swelling Index button, Figure 3.

The proximate analyses in Table II show that the ash content was low, but might be somewhat variable, whereas the sulfur content ranged from 1-1/2 to 2 per cent. Although this material could be designated in the ASTM classification as a medium-volatile coal on the basis of (1) its proximate analysis and (2) the fact that the material was agglomerating, petrographic examination, which revealed no plant structure visible by either transmitted or reflected light, indicated that the material is not of plant origin. None of the structures ordinarily found in coal of the same volatile matter and fixed carbon contents were present. The material appeared homogeneous, with no banding or recognizable cell structure being observed in either the polished or thin section; however, isolated masses and crystals of pyrite were noted.

Because of its poor solubility in carbon disulfide, high percentage of fixed carbon, and high specific gravity, and because no petrographic entities characteristic of coal could be found, this so-called "natural bitumen" has been tentatively identified as impsomite,⁹⁾ one of the asphaltic pyrobitumens, which include elaterite, wurtzillite, and albertite, all characterized by infusibility and insolubility, or poor to slight solubility in carbon disulfide. Impsomite represents the final stage in the metamorphosis of asphaltites and asphaltic pyrobitumens. Outcrops of grahamite,¹⁰⁾ which is an asphaltite, metamorphize readily into impsomite. "Weathered asphaltites ... closely resemble impsomite in their physical and chemical properties and may be classified as such."⁹⁾ The softening and fusion exhibited by the "natural bitumen" upon being heated is the only property not characteristic of impsomite. This may indicate that the material is indeed weathered grahamite, since varieties of this asphaltite exhibit softening, possess good solubility in carbon disulfide, and contain less than 55 per cent fixed carbon.

Deposits of impsomite are reported¹⁰⁾ in Oklahoma, Arkansas, and Nevada, and copper-bearing impsomite has been reported in Michigan. Deposits of grahamite

are reported in West Virginia, Texas, Oklahoma, and Colorado. Dietrich, in a recent publication¹¹) refers to impsonite from the Carboniferous Jackforth sandstone as originally being called "grahamite." Abraham cites¹²) the same deposits (LeFlore County, Oklahoma) and lists it as grahamite, but he notes that grahamite can weather into impsonite. Perhaps Dietrich may have obtained a sample of weathered grahamite.

"Natural bitumen" exhibits plastic properties and very low fluidity similar to those of Lower Kittanning seam low-volatile coking coal, Table II, and possesses good coke-improvement properties comparable with those of Lower Kittanning in blends with high-volatile coking coals, see Table III. This "natural bitumen," like Lower Kittanning coal, exhibits a prohibitively high coking pressure, Table III, when coked alone in the 30-pound Pressure-Test Oven. Also, the "bitumen" showed extremely high expansion; it has an estimated volume change (expansion in the sole-heated oven of approximately 32 per cent, whereas the Lower Kittanning low-volatile coal used for comparison in this evaluation showed expansion of about 14 per cent, at bulk densities of 55 to 58 pounds of dry coal per cubic foot.

A photograph of a lump of coke from "natural bitumen" that was coked alone, is shown in Figure 4. The extremely fine cell structure of the coke, as well as its fingery character, are evident. Chemical analysis and a sulfur balance made on "natural bitumen" and the resultant coke from the 30-pound Pressure-Test Oven indicate sulfur elimination from the "natural bitumen" during carbonization, Tables II and III, is relatively low. Forms of sulfur¹³) are listed in Table II for the raw "natural bitumen."

Carbonization in the 30-pound Pressure-Test Oven of blends containing "natural bitumen" showed that this material was as effective as Lower Kittanning coal in improving the strength of cokes from the highly fluid Pittsburgh Seam high-volatile coal, but somewhat less effective than Lower Kittanning in improving the strength of cokes from the low-fluidity Utah high-volatile coal, see Table III. Replacement of nearly half the Pocahontas low-volatile component by "natural bitumen" in a blend with Kentucky Splint Coal shows that the "bitumen" possesses greater strength-improving power than Pocahontas and that it increases the coking pressure of the blend.

Conclusions

Coking tests reported by Thompson¹) showed that a 15 per cent addition of coal-tar pitch to Utah coal significantly increased the Stability Factor of this coke over that of coke containing no pitch (24 as opposed to 11). As shown in Table III, similar additions of "natural bitumen," and of Lower Kittanning low-volatile coal, both having low fluidity, upgraded the strength of the coke from Utah high-volatile coal to a degree comparable with that found for coal-tar pitch additions in the earlier work cited. Consequently, these results lend no support to the long-held hypothesis that improvement of poorer coking coals is best accomplished by the addition of "fluid" components. It appears, therefore, that coke-strengthening power may be more dependent on some combination of optimum coking pressure and fluidity, rather than on fluidity alone. Also, the high fixed-carbon content of "natural bitumen" (76%) contributes to coke improvement: after the "bitumen" has passed through the fluid state, sufficient carbonaceous residue remains, adding to the strength of the cell walls of the resultant coke, and not much material is lost by devolatilization (which promotes shrinkage).

The following three factors, then, probably explain the success of "natural bitumen" as a coke-improvement additive: (1) coking pressure, that helps consolidate the mass during the coke-formation process, (2) sufficient fluidity, that agglomerates the non-coking entities of the coal in the cell walls of the resultant semi-coke and (3) a comparatively large amount of carbon remaining after decomposition and solidification of the fluid material (compared to that of pitches and asphaltites), that contributes strength to the cell walls of the final, finished coke and thus minimizes the weakening effect of shrinkage.

References

1. Thompson, J. H. "Benefication of Blast Furnace Coke at the Kaiser Steel Company, Fontana, California," Blast Furnace and Steel Plant, Vol. 34, pp. 225 - 230, 350 - 354, 475 - 479, 584 - 586, 624; 1946.
2. Waggoner, C. L., "Observations on Coke Oven and Blast Furnace Practice at the Geneva Coke Plant" -- Blast Furnace and Steel Plant, pp. 325 - 328, 35, 1947.
3. Powell, A. R., "Improving Coking Qualities of Coal by Addition of Various Materials," A Study of the Iron and Steel Industry in Latin America, Vol. II, Proceedings of the Expert Working Group held in Bogota, Published by the United Nations Department of Economic Affairs, New York, 1954, pp. 91 to 96.
4. Powell, A. R., "Argentine Asphaltites as Blending Material for Poorly Coking Coals," op. Cit. pp. 99 - 100.
5. Harris, H. E., Margel, E. W., and Howell, R. B., "A Small Pressure-Test Oven for Measuring Expansion Pressure Developed During the Carbonization of Coal," Proceedings, Blast Furnace, Coke Oven, and Raw Materials Conference, AIME, Volume 13, 1954, pp. 127 - 141.
6. Price, J. G., Shoenberger, R. W., and Perlic, B., "Use of a Thirty-Pound Test Oven for Rapidly Assaying the Coking Strength of Coals," Proceedings, Blast Furnace, Coke Oven, and Raw Materials Conference, AIME, Volume 17, 1958.
7. Anvil, H. S., and Davis, J. D., "Determination of the Swelling Properties of Coal During the Coking Process," U. S. Bureau of Mines, Report of Investigations 3403, 1938.
8. ASTM Procedure D770 - 46 for determining Free-Swelling Index.
9. Abraham, H., "Asphalts and Allied Substances," D. Van Nostrand Co., Inc., Fifth Edition, Vol. I, p. 298.
10. Ibid., p. 270.
11. Dietrich, R. V., Economic Geology, Vol. 51, November, 1956, p. 653.
12. Abraham, H., op. Cit. p. 274.
13. British Standard Method - BS1016 as Revised Under Published date March, 1957. Also A. R. Powell, Ind. and Eng. Chem., Vol. 12 (1920), p. 887.
14. ASTM Procedure D4 - 52 for Determining Carbon Disulfide Insolubles.
15. "Methods of Testing Coal Tar Products," Barrett Division, Allied Chemical and Dye, 1950, Test Method B7 for Benzene Insolubles, pp. 24 - 27.

Erratum: On page 115, paragraph 4, the first 3 words of line 7 should be changed to read ... "Coal-like in fine structure."

Table I

Characteristic Properties of "Natural Bitumen"
 Compared with Lower Kittanning Seam Low-Volatile Coal

	"Natural Bitumen"	Lower Kittanning Seam Low-Volatile Coking Coal
Bulk Density (Modified ASTM)	49 lb per cu ft	52 lb per cu ft
Color in Mass	Black	Black
Fracture	Subconchoidal (conchoidal to hackly)	Cubic
Luster	Bright	Dull to bright
Specific Gravity	Floats at 1.23	Approximately 1.3
Solubility in Carbon Disulfide*	2.3% at 25 C. Lumps disintegrate to a fine powder, which forms a dull black, coherent, non-swollen button in the Free-Swelling Index test similar to that from the original pulverized bitumen.	0.3% at 25 C
Solubility in Xylene	Lumps disintegrate into a fine powder, with pale-straw coloration of solvent	--
Solubility in Benzene **	3.6%	0.6%
Flame Test	Lumps decrepitate violently and burning ceases upon removal of material from flame. Fusion of particles is evident.	Lumps burn slowly, soften, and harden into a semi-coke.
ASTM Free-Swelling Index	1-1/2	2-1/2
Fixed Carbon (from proximate Analysis), %	74 to 78	75
Ash Content, %	1 to 4	7.5
Sulfur Content, %	1 to 2	0.8

* See Reference 14)
 ** See Reference 15)

Table II

Chemical, Plastic, and Free-Swelling Properties of
"Natural Bitumen"

(A) Proximate Analysis, Ultimate Analysis, Sulfur Content, and Heating Value of "Natural Bitumen," all on the dry basis:

Sample No.	<u>1</u>	<u>2</u>	<u>3</u>	Lower Kittanning Low-Volatile Coal
Proximate Analysis, % dry basis:				
Volatile Matter	21.6	21.7	22.0	15.1
Fixed Carbon	77.6	74.3	76.3	76.8
Ash	0.8	4.0	1.7	8.1
Ultimate Analysis, %				
Carbon	-	-	85.7	83.4
Hydrogen	-	-	5.3	4.3
Nitrogen	-	-	1.9	1.2
Oxygen	-	-	3.6	3.0
Ash	-	-	1.7	8.1
Sulfur	1.66	2.05	1.82	1.01
Heating Value, BTU per lb	-	15,120	-	

(B) Gieseler Fluidity and Free-Swelling Index of "Natural Bitumen", and Lower Sunnyside Seam (Utah and Lower-Kittanning Seam Coals):

	Natural Bitumen (Sample No. 1)	Lower Sunnyside High-Volatile Coal	Lower Kittanning Low-Volatile Coal
Plastic Properties:			
Softening Temperature, C	435	377	449
Solidification Temperature, C	480	453	504
Plastic Range*, C	45	76	55
Maximum Fluidity, dial div. per min.	0.6	3	1.1
Temperature of Maximum Fluidity, C	458	413	477
Free-Swelling Index	1-1/2	2-1/2	2-1/2

* Solidification temperature minus softening temperature

(C) Forms of Sulfur in "Natural Bitumen"

Sulfate Sulfur	0.04%	3.0%
Pyritic Sulfur	0.57%	43.5%
"Organic" Sulfur	0.70%	53.5%
Total	1.31%	100.0%

Table III

Coke Strength and Carbonization Pressure from 30-pound Pressure-Test Oven Tests with "Natural Bitumen" and Coking Coals

<u>Blend*</u>	<u>Modified Tumbler Index, cum % plus 3/4 in.</u>	<u>Approximate ASTM Stability Factor</u>	<u>Carbonization Pressure, psi</u>
100% "Natural Bitumen"	---	--	40
100% Lower Kittanning Seam Low-Volatile	--	--	30
45% Kentucky Splint High-Volatile 55% Pocahontas Low-Volatile	55	--	3.5
55% Kentucky Splint High-Volatile 45% "Natural Bitumen"	62	--	6.7
50% Kentucky Splint High-Volatile 30% Pocahontas Low-Volatile 20% "Natural Bitumen"	63	--	4.5
80% Kentucky Splint High-Volatile 20% "Natural Bitumen"	59	--	2.3
100% Pittsburgh Seam High-Volatile	43	--	1
80% Pittsburgh Seam 20% "Natural Bitumen"	63	--	1
80% Pittsburgh Seam 20% Lower Kittanning Seam	61	+	1.5
100% Lower Sunnyside Seam High-Volatile	21	2	1
90% Lower Sunnyside Seam 10% "Natural Bitumen"	31	13	1.4
80% Lower Sunnyside Seam 20% "Natural Bitumen"	43	27	2.2
90% Lower Sunnyside Seam 10% Lower Kittanning Seam	41	25	1.1
80% Lower Sunnyside Seam 20% Lower Kittanning Seam	50	35	1.8

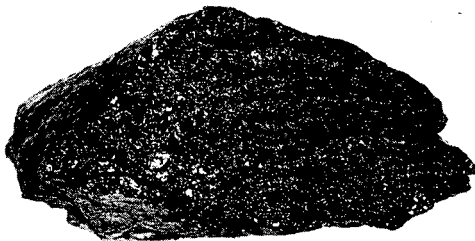
* Bulk Density as charged 50 to 53 lb per cu ft

** Proximate analysis and sulfur content of coke per cent (dry basis):

Volatile Matter	3.0
Fixed Carbon	92.7
Ash	4.3
Sulfur	2.12



SURFACE MAGNIFIED 5x
Negative No. 2-3578B-2

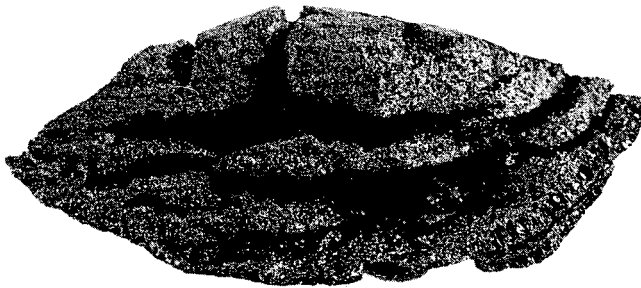


LUMP MAGNIFIED 1x
Negative No. 2-3578B-1

Figure 1. LUMP OF "NATURAL BITUMEN", AS RECEIVED

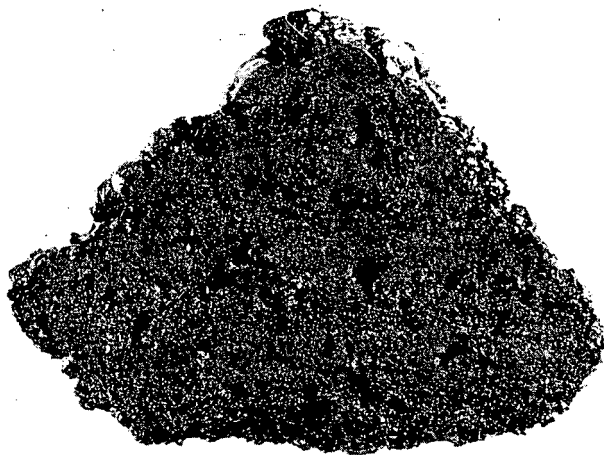


MAGNIFIED 1x
Negative No. 2-3574B-1



CROSS-SECTION, MAGNIFIED 5x
Negative No. 2-3574B-2

Figure 2. FREE-SWELLING INDEX BUTTON - INDEX 1-1/2 - FROM "NATURAL BITUMEN"
PULVERIZED TO MINUS 60 MESH

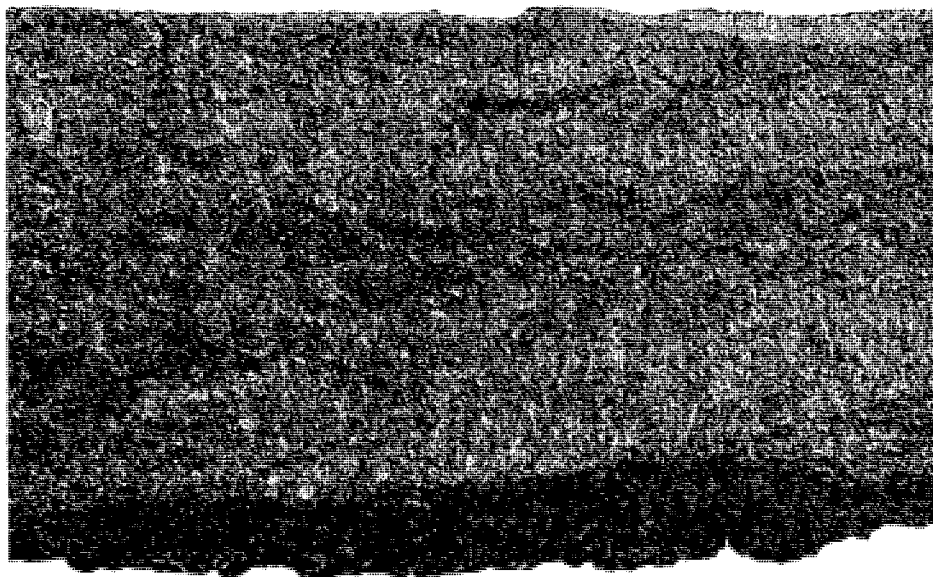


CROSS-SECTION MAGNIFIED 5x
Negative No. 2-3573B-2

Figure 3. FREE-SWELLING INDEX BUTTON - INDEX 4 - FROM MINUS 1/4 INCH
"NATURAL BITUMEN" PARTICLES



FULL LUMP MAGNIFIED 1x
Negative No. 2-3577B-1



SECTION OF LUMP MAGNIFIED 5x
Negative No. 2-3577B-2

Figure 4. LUMP OF COKE FROM "NATURAL BITUMEN" CARBONIZED IN 30-POUND TEST OVEN

The Reaction of Gaseous Acetic Anhydride
With Coal

Paul Fugassi, Ruth Trammell¹ and Philip Masciantonio

Coal Research Laboratory, Department of Chemistry
Carnegie Institute of Technology, Pittsburgh (13) Penna.

A number of coals of the bituminous and sub-bituminous ranks have been acetylated at 45°C. using acetic anhydride vapor at a relative pressure of unity. Acetylation by this procedure gives hydroxyl contents less than that determined by the trimethylsilyl ether method for bituminous coals but higher hydroxyl contents for sub-bituminous coals. It is suggested that acetic anhydride reacts with carboxyl groups to give mixed acid anhydrides and the higher values obtained for sub-bituminous coals is due to the carboxyl group content of such coals. Oxygen gas catalyzes the acetylation of sub-bituminous coals and until the effect of oxygen is investigated in detail, acetylation of lower rank coals with acetic anhydride should be done in the absence of oxygen.

¹Present address, Dept. of Chemistry, Chatham College, Pittsburgh (13) Pa.

Not for Publication

Presented Before the Division of Gas and Fuel Chemistry
American Chemical Society
Chicago, Illinois, Meeting, September 7-12, 1958

The Reaction of Gaseous Acetic Anhydride With Coal

Paul Fugassi, Ruth Trammell¹ and Philip Masciantonio
Coal Research Laboratory, Dept. of Chemistry
Carnegie Institute of Technology, Pittsburgh (13), Pa.

1. Present address, Dept. of Chemistry, Chatham College, Pittsburgh (13), Pa.

Introduction

The hydroxyl contents of coals have been measured by a number of different methods and the results of such work have been summarized by Blom, Edelhausen and Van Krevelen(1). In general methods using different reagents give different hydroxyl contents for coals of the same rank. Even in cases where the same reagent has been employed by different investigators there is not close agreement on the hydroxyl content.

It is the object of this communication to report some experimental work on bituminous and sub-bituminous coals wherein the coals are reacted at 45°C. with gaseous acetic anhydride at a relative pressure close to unity. In comparison to other acetylation work on coal using acetic anhydride, the temperatures employed here are much lower and the reaction times much longer. The extent of the reaction is followed gravimetrically.

Experimental

Apparatus: Measurements were made using McBain-Bakr balances housed in an air thermostat held at 45°C. \pm 0.1°. Because of the corrosive nature of acetic anhydride--acetic acid mixtures, springs made from fine tungsten wire were used. These springs had sensitivities ranging from 3.81 to 4.86 milligrams per millimeter extension. Spring displacements were measured to 0.1 mm using a cathetometer. With sample weights of the order of 500 milligrams the precision is about one part in a thousand.

Chemicals: Acetic anhydride, benzene, and pyridine were freshly distilled before use and stored over Drierite. The following coals of bituminous rank were used: Upper Kittanning, Upper Freeport, Pittsburgh, Bruceton and Bruceton anthraxylon. The coals of sub-bituminous rank were Wyoming (Elkol), Wyoming (Rock Springs), Illinois No. 6 (Clinton), and Illinois No. 6 (Jefferson). The analyses for Wyoming (Rock Springs), Bruceton, Bruceton anthraxylon, and Illinois No. 6 (Jefferson) have been previously published(2). The analyses for the other coals are given in Table I.

Table I
Ultimate Analyses (Moisture Free Basis)

Coal	C	H	N	O	S	Ash
Upper Kittanning	80.6	3.8	1.1	3.7	1.3	9.5
Upper Freeport	78.7	4.3	0.9	4.6	1.7	9.3
Pittsburgh	76.0	5.1	1.5	7.6	1.6	8.2
Wyoming (Elkol)	74.3	5.3	1.2	15.2	0.6	3.4
Illinois No. 6 (Jefferson)	65.2	4.9	1.2	10.4	4.0	14.3

The samples of Upper Kittanning, Upper Freeport, and Pittsburgh coals are standard samples of the Coal Research Board, Commonwealth of Pennsylvania, and were used as received. Samples of Wyoming (Rock Springs), Illinois No. 6 (Jefferson) and Bruceton coals were furnished by the Bruceton Station, U. S. Bureau of Mines and were used as received. Wyoming (Elkol) and Illinois No. 6 (Clinton) were available in bulk. These samples were ground by passage through a hammer mill and used unsieved.

Procedure: The samples of coal, placed in small glass buckets were weighed to 0.1 mg. and allowed to stand overnight in a desiccator. The samples, after being reweighed, were attached to the springs and allowed to stand for one hour, with an atmosphere of air present, to come to thermostat temperature. The extension of the spring was then measured. It is assumed that the weight of the sample had not changed during the hour waiting period. The apparatus was then evacuated and the extension of the springs measured. Usually samples came to constant weight in 8 hours, however evacuation was continued for a minimum of 24 hours.

After the system was closed off from the pumping system, acetic anhydride was admitted at a relative pressure of unity (about 12 mm.) and the system allowed to stand. Readings of the spring extension were taken until the weights of the sample were practically constant. At this point, the system was evacuated for several days and the weight of the sample measured. Gaseous acetic anhydride was then re-admitted and the samples allowed to stand until their weights reached a constant value. Evacuation of the system for several days followed by measurement of the weights of the samples then gave the increase in weight of the sample due to acetylation. In most cases samples of coal were subjected to two consecutive anhydride treatments before the final reading was taken. In a few cases three consecutive anhydride treatments were employed but little or no increase in weight resulted from the third treatment with acetic anhydride.

Discussion

Catalysis: The vapor phase acetylation of coals at 45°C. is a very slow process so a number of qualitative experiments were made with Illinois No. 6 (Clinton) coal to determine if the rate could be accelerated.

Coal is a gel and it is known that for other gels, such as cellulose, acetic anhydride is a poor swelling agent and that for cellulose the rate of acetylation can be increased by the use of suitable swelling agents. The behavior of acetic anhydride with respect to cellulose suggests the use of swelling agents in coal acetylation.

Methanol swells coal so several experiments were made in which the coal before acetylation was exposed to methanol vapor at 45°C. and the methanol

vapor desorbed before acetylation. Methanol is reversibly desorbed and no increase in acetylation rate was noted.

Pyridine swells coal but pyridine is sorbed irreversibly by coal. Coal treated with pyridine vapor, evacuated, and then acetylated showed an increased rate of acetylation. Unfortunately the irreversible sorption of pyridine is large and although the amount of this irreversible sorption on coal can be measured accurately, it is not possible to assume that the amount of pyridine sorbed irreversibly by the coal does not change as the coal is acetylated. For this reason the overall weight change might not be a measure of the extent of acetylation.

Benzene vapor at 45°C. is irreversibly sorbed by coal in amounts ranging from 0.0 to 23.4 milligrams per gram of coal. A coal sample exposed to benzene vapor, evacuated, and then acetylated appears to acetylate faster. However, the increase in rate of acetylation is not striking.

Consequently the experiments made here used acetic anhydride alone. As a consequence of the acetylation reaction acetic acid is present and serves to some extent as a swelling agent. On Illinois No. 6 (Clinton) coal it has been shown that acetic acid vapor is reversibly desorbed on coal previously acetylated with acetic anhydride.

Effect of Oxygen: In carrying out the acetylations it was noted that while the coals of bituminous rank gave reproducible increases in weight within $\pm 5\%$, the coals of sub-bituminous rank would sometimes give high values and in other experiments low values. Although all samples were evacuated for at least 24 hours using a two stage mercury vapor pump, the system could not be baked out and small but variable amounts of oxygen might be present in individual sets of experiments. Whenever a small amount of oxygen, 5 mm., was added to the system the results became more reproducible and it appears, for sub-bituminous coals, oxygen has a catalytic effect. However the presence of oxygen introduces the possibility of an oxidation of the coal. To check this point five coal samples after the usual evacuation were exposed to 5 mm. of oxygen, with no anhydride present, for a period of 21 days. The experimental results are tabulated in Table II and are the increases in weight after evacuation.

Table II
Oxidation of Coals; 5 mm. O₂, 21 days at 45°C.

Coal	Upper Kittanning	Upper Freeport	Pittsburgh	Illinois (Clinton)	Wyoming (Elkol)
Wt. Increase mg/gram	4.1	1.8	2.0	11.2	13.5

It will be noted that the first three coals of bituminous rank show little or no change in weight. The two sub-bituminous coals, Illinois (Clinton) and Wyoming (Elkol) show relatively greater changes in weight. Pressure changes during these experiments were negligible and it was concluded that oxidation under the experimental conditions used was a very slow process relative to the slow acetylation reaction.

Acetylation: Most of the acetylation experiments were made with 5 mm of oxygen present but sufficient data with no added oxygen are available to indicate that the presence of oxygen has little or no effect on the weight increase for

bituminous coals. The acetylation data are tabulated in Table III. These data are all for experiments at 45°C., with a relative pressure of acetic anhydride of unity and include, in the average weight increase, experiments with and without added oxygen. All samples were given at least two consecutive treatments with acetic anhydride and in some cases three consecutive treatments. The spread of the individual values from the average is within $\pm 5\%$. Reaction times ranged from 23 to 37 days.

Table III
Acetylation Data (45°C.)

Coal	Average Wt. Increase ($\frac{\text{milligrams}}{\text{gram}}$)
Upper Kittanning	32
Upper Freeport	30
Pittsburgh	24
Bruceton Anthraxylon	13
Bruceton	78
Illinois No. 6 (Clinton)	140
Illinois No. 6 (Jefferson)	158
Wyoming (Rock Springs)	143
Wyoming (Elkol)	175

Calculation of Hydroxyl Content: If it is assumed that the increase in weight of the coal sample is caused mainly by replacement of a hydrogen atom from an hydroxyl group by the acetyl radical then the weight increase divided by 42 will give millimoles of hydroxyl groups per gram of coal (m.f. basis). The implications of such an assumption will be discussed. Processes leading to a weight increase other than replacement of hydrogen by the acetyl group might be 1. Irreversible sorption of acetic anhydride, 2. Irreversible sorption of acetic acid resulting from the acetylation process and 3. Reaction of acetic acid with salts of weak acids, such as pyrites, present in the coal. There is no independent evidence which indicates the magnitude of irreversibility of acetic anhydride sorption on coal. However the hydroxyl content as calculated assuming no trapped acetic anhydride is already low relative to the values obtained by other methods for coals of the bituminous rank. The effect of trapped acetic anhydride would be to make these values lower still. With regard to acetic acid it has been shown that acetic acid sorption is reversible on acetylated Illinois coal. This fact suggests that the amount of acetic acid trapped must be small. The reaction of acetic acid with pyrites can be assumed to give sulfur, iron acetate, and hydrogen sulfide. Assuming a 500 milligram sample containing 1% of iron sulfide, the weight increase would be around 2.9 milligrams per gram of coal if hydrogen sulfide is lost on evacuation. From other experiments it is known that the evaporation of elemental sulfur at 45°C. is very slow.

For four of the coals used data on the hydroxyl content are available as determined by the trimethylsilyl ether method(2). A comparison of these data with the data obtained by acetylation is given in Table IV.

Table IV
Hydroxyl Content of Coals (millimoles per gram)

Coal	Acetylation (Vapor)	Trimethylsilyl Ether
Bruceton Anthraxylon	0.3	2.3
Bruceton	1.9	2.3
Wyoming (Rock Springs)	3.4	2.8
Illinois No. 6 (Jefferson)	3.8	3.4

For the bituminous coal the hydroxyl content as determined by acetylation is lower than that obtained by the trimethylsilyl ether method. One presumes that certain sterically hindered hydroxyl groups react very slowly with acetic anhydride. On the other hand the hydroxyl content as determined by acetylation is higher for two sub-bituminous coals. Although it is known(3) that certain polycyclic structures photo-oxidize readily in the presence of acetic anhydride and oxygen such a reaction is excluded here because 1. Acetylation experiments with light excluded gave about the same weight increases as with light present and 2. No decrease in pressure caused by oxygen consumption was observed. However it is known that sub-bituminous coals contain carboxylic acid groups and the possibility exists that with sub-bituminous coals acetic anhydride reacts with acidic groups to form mixed anhydrides in addition to reacting with hydroxyl groups to form esters. The mixed anhydride would be expected to react with water more rapidly at a given temperature than the ester. Accordingly a series of five coals were acetylated and then exposed to water vapor at 20 mm pressure at 45°C. The results of these hydrolysis experiments are shown in Table V.

Table V
Hydrolysis of Acetylated Coals (45°C.)

Coal	Exposure Time H ₂ O (20 mm.)	Relative Weight
Upper Kittanning	0 hours	1.00
	1	1.00
	3	1.06
	22	1.00
	70	0.90
	70	0.89
Upper Freeport	0	1.00
	1	1.10
	3	1.15
	22	1.15
	70	0.89
	70	0.89
Pittsburgh	0	1.00
	1	1.08
	3	1.08
	22	1.08
	70	1.00
	70	1.00
Illinois No. 6 (Clinton)	0	1.00
	1	0.95
	3	0.95
	22	0.91
	70	0.86
	70	0.86
Wyoming (Elkol)	0	1.00
	1	0.94
	3	0.92
	22	0.90
	70	0.81
	70	0.81

Comparison of these data indicate that the three bituminous coals show small changes in weight on treatment with water even for periods as long as 70 hours. This indicates that the ester group present is relatively stable to the action of water vapor. On the other hand the two sub-bituminous coals show greater decreases in weight under the same conditions. It appears probable that acetylated sub-bituminous coals contain groups which differ in their behavior with respect to water stability and as has been mentioned the mixed anhydride group from its known properties would fulfill this requirement. Acetylated sub-bituminous coals would contain acetate esters and mixed anhydrides.

Summary

A number of coals of the bituminous and sub-bituminous ranks have been acetylated at 45°C. using acetic anhydride vapor at a relative pressure of unity. Acetylation by this procedure gives hydroxyl contents less than that determined by the trimethylsilyl ether method for bituminous coals but higher hydroxyl contents for sub-bituminous coals. It is suggested that acetic anhydride reacts with carboxyl groups to give mixed acid anhydrides and the higher values obtained for sub-bituminous coal is due to the carboxyl group content of such coals. Oxygen gas catalyzes the acetylation of sub-bituminous coals and until the effect of oxygen is investigated in detail, acetylation of lower rank coals with acetic anhydride should be done in the absence of oxygen.

Acknowledgment

The authors wish to thank BCR, Inc. and the Coal Research Board, Commonwealth of Pennsylvania, for furnishing coal samples and analyses. They also wish to thank Dr. S. Friedman and Dr. Irving Wender, Bruceton Station, U. S. Bureau of Mines, for furnishing coal samples.

References

1. Blom, L., Edelhausen, L., and Van Krevelen, D. W., Fuel (London) 36, 135 (1957).
2. Friedman, S., Steiner, W. A., Raymond, R., and Wender, I., Preprint, Gas and Fuel Division, New York Meeting, September, 1957.
3. Fugassi, P., Masciantonio, F., Trammell, R., Preprint in this volume.

Not for Publication
Presented Before the Division of Gas and Fuel Chemistry
American Chemical Society
Chicago, Illinois, Meeting, September 7-12, 1958

The Photo-Oxidation of Polycyclic Hydrocarbons

Paul Fugassi, Philip Masciantonio, and Ruth Trammell
Coal Research Laboratory, Dept. of Chemistry
Carnegie Institute of Technology, Pittsburgh (13), Pa.

Summary

Solutions of anthracene and tetracene in acetic anhydride and other solvents in the presence of air and ultra-violet light at room temperature photo-oxidize to the 9,10 and 5,12 quinones respectively. Other polycyclic hydrocarbons such as chrysene, pyrene and triphenylene do not photo-oxidize under these conditions. With naphthalene and phenanthrene oxidation takes place but the reaction appears to continue past the quinone stage. The photo-oxidation reaction is catalyzed by bases and is not inhibited by sodium hydrogen sulfite indicating that the mechanism is probably not a free radical chain reaction.

Discussion

In an investigation now underway in the Coal Research Laboratory involving the vapor phase acetylation of various coals with acetic anhydride it was noted that with certain coals a very slow reaction (weeks) was superimposed on the main reaction (days) so that after a relatively rapid weight change, the weight of the coal sample increased gradually over a period of many weeks. As the main reaction can be assumed to be the acetylation of the hydroxyl and traces of amino groups present in the coal it became necessary to consider the possibility that gaseous acetic anhydride was reacting directly with hydrocarbon structures present in the coal.

The acetylation of coal is being carried out using an adsorption type apparatus. The course of the acetylation is followed directly by use of McBain-Baker spring balances. All experiments are being made at 45°C. with the relative pressure of acetic anhydride being fixed at unity. The very slow reaction is particularly noticeable when small amounts of oxygen are present so that most experiments have been made with 5 mm of oxygen gas present in the system. Under these conditions the coal sample is present in large excess relative to the acetic anhydride. Acetic acid resulting from the acetylation process is also present. In an attempt to determine the type or types of hydrocarbon structures which would react with mixtures of acetic anhydride and acetic acid a series of experiments using various polycyclic hydrocarbons have been made in which the experimental conditions approximate those utilized in the work on coal.

If a saturated solution of anthracene in acetic anhydride is allowed to stand in a Pyrex flask, loosely stoppered so that air has access to the flask, and exposed to light there appears a light tan, crystalline precipitate which on isolation proved to be anthracene-9,10-quinone. No other product in appreciable amounts could be isolated from the reaction mixture except starting material. As the reaction involving anthracene progresses the solution becomes light yellow in color. With other hydrocarbons the solution becomes deeply colored. The coloring material is present in such small amounts that it can not be isolated

and might well be due to traces of impurities present in the starting material. A systematic investigation of this reaction was undertaken to determine the conditions under which it takes place.

Effect of oxygen: Saturated solutions of anthracene in acetic anhydride are placed in small Pyrex tubes, evacuated, and sealed. The tubes are then exposed to sunlight and to the radiation from a 3605L fluorescent lamp. After several months exposure at room temperature to the ultra-violet radiation the solutions remained colorless. A white crystalline product which precipitated from the solution proved to be the photo-dimer of anthracene. These experiments indicate that oxygen from the air is the oxidizing agent for anthraquinone formation.

Effect of light: Solutions of anthracene in acetic anhydride saturated with air and kept in the dark at room temperature for several months remain colorless and no quinone (negative vat test) is present. A solution of anthracene in acetic anhydride was refluxed three weeks under conditions where little light reached the system. The solution becomes red in color but no quinone is present. After cooling the mixture was exposed to the radiation from a 3603L lamp. After several weeks anthracene-9,10-quinone precipitated and the red color gradually disappeared. These experiments indicate that the dark reaction is very slow. The cause of the color is not known.

Effect of temperature and light intensity: From qualitative experiments samples kept at room temperature appeared to react slower than samples exposed to sunlight and kept outdoors during the winter months. The temperature coefficient of the photo-oxidation, as one would expect, must be small. Since sunlight represents much higher intensities than the radiation from lamps it seems likely that the rate of the reaction increases with increasing intensity of incident light.

Catalysts: It has been found that the rate of anthracene-9,10-quinone formation is increased by the addition of bases to the acetic anhydride solution. Suitable catalysts are the sodium or potassium salts of organic acids such as formic, acetic, phthalic, and benzoic acids and pyridine bases such as pyridine, quinoline, and acridine.

Inhibitors: Most of the common organic inhibitors would be expected to react with acetic anhydride. Small amounts of sodium hydrogen sulfite added to the acetic anhydride solutions appear to have little or no effect upon the rate of quinone formation. It is therefore unlikely that the photo-oxidation reaction is a chain reaction.

Types of hydrocarbons: The following polycyclic hydrocarbons have been employed: naphthalene, anthracene, phenanthrene, tetracene, pyrene, chrysene, and triphenylene. With anthracene and tetracene the only products are anthracene-9,10-quinone and tetracene-5,12-quinone. It has been previously reported (1) that

L. C. Dufraisse and R. Horclois, Bull. Soc. Chim. France (5) 3, 1880 (1936)

tetracene in xylene solution photo-oxidizes to the 5,12 quinone. Pyrene, chrysene and triphenylene gave no appreciable amount of any reaction product although the solutions became colored. Naphthalene and phenanthrene gave a mixture of reaction products which have not been completely characterized. Solutions in acetic anhydride of phenanthrene-9,10-quinone are not stable in the presence of oxygen and ultra-violet light but apparently undergo further oxidation. On the other hand saturated solutions of anthracene-9,10-quinone in acetic anhydride have been exposed to the radiation from the 3608L lamp for several months and no reaction has been noticed. The ultraviolet absorption spectra of naphthalene and phenanthrene begins rather far in the ultra-violet region (2) where the

2. E. Clar, *Aromatische Kohlenwasserstoffe*, Springer, Berlin 1952, pages 134 and 142

absorption by Pyrex is appreciable and where the intensity of such radiation from the 360BL lamp is low. The photo-oxidation reactions for the two hydrocarbons will need to be investigated in quartz flasks with lower wave length radiation.

Solvents: The photo-oxidation of anthracene proceeds in the following solvents: acetic anhydride, acetic acid, mixtures of acetic acid and anhydride, carbon disulfide, methanol, pyridine, quinoline, and dimethylformamide. The formation of anthracene-9,10-quinone was proven by its isolation in all cases except dimethylformamide. For this solvent a positive vat test for quinone was obtained using sodium hydrosulfite as the reducing agent. The formation of anthracene-9,10-quinone is very slow in benzene and cyclohexane as indicated by the vat test. It has been shown (3) that the photo-oxidation of anthracene in carbon disulfide

3. C. Dufraisse and M. Gerard. *Bull. Soc. Chim. France* 4, 2052 (1937)

solution leads to the formation of a photo-oxide. Carbon disulfide is one of the few solvents which inhibits the formation of the photo-dimer of anthracene. According to H. E. Ocampo (4), the photo-oxidation of anthracene in nitrobenzene

4. H. E. Ocampo, *C. A.* 40, 6458 (1946)

solution gives anthracene-9,10-quinone.

Mechanism: The most recent investigation of the photo-oxidation of anthracene has been made by E. J. Bowen and his collaborators (5). Their work was done

5. E. J. Bowen et al., *Trans. Faraday Soc., Discussions* 14, 143, 146 (1953); *Trans. Faraday Soc.*, 51, 475 (1955)

primarily in benzene solution although solvent mixtures were also used. According to Bowen the irradiation of benzene solutions of anthracene saturated with oxygen gives the following reactions: 1. Formation of the photo-dimer, 2. Formation of the photo-oxide, and 3. Reaction with certain added solvents such as CCl_4 . Our work indicates that with long exposure times there is a fourth possibility, the formation of the quinone. The experimental conditions for the two sets of experiments are quite different. Bowen used benzene as his primary solvent which as has been indicated inhibits quinone formation, used high light intensities, used shorter times of radiation (hours relative to days), used higher oxygen pressures, and used dilute solutions of anthracene. Bowen postulated that the formation of the photo-oxide of anthracene is a non-chain process. From the results with sodium hydrogen sulfite it is believed that quinone formation is a non-chain process. In the work described here the photo-dimer was not detected in the photo-oxidation reaction. The photo-dimer is known to show a photo-stationary state indicating that the reverse reaction, dissociation of the dimer into anthracene, has a finite velocity constant at room temperature. During the long exposure times used in this work any photo-dimer could be eventually converted completely into the quinone.

Experimental

Apparatus: The experiments described here were made in Pyrex flasks using the radiation from a 360BL fluorescent lamp. A few experiments used sunlight. The transmission characteristics of Pyrex glass and the distribution of radiation from the 360BL lamp have been published by L. R. Koller (6). The radiation of this

6. L. R. Koller, *Ultraviolet Radiation*, John Wiley and Sons, Inc., New York, 1952, pages 68 and 147.

lamp is in the region 3200-4400 Å and peaks at 3600 Å. Pyrex glass cuts off around 3000 Å. It is probable that the effective radiation is in the region 3000-4000 Å although with the long periods of exposure used appreciable amounts of shorter wavelength radiation might have passed through the solutions.

Chemicals: The hydrocarbons used were in stock at the Coal Research Laboratory and were originally from American and foreign manufacturers. Anthracene (blue-white fluorescence) was an Eastman product and was used without further purification. All other hydrocarbons were recrystallized at least once and in some cases two or three times. Recrystallizations were continued until the melting point of a given hydrocarbon was less than one degree from the melting point cited by E. Clar (2) for this hydrocarbon. All solvents were freshly distilled before use.

Procedure: The general procedure was to make a saturated solution of the hydrocarbon in the desired solvent and place it in a Pyrex flask, loosely stoppered with an aluminum foil covered cork so that air had access to the solution. The flask was then placed one foot from the 360EL lamp. The contents of the flask were at room temperature. At times small portions of the solution were withdrawn and added to an alkaline aqueous solution of sodium hydrosulfite. The mixture was then heated and the color changes observed. After exposure to the radiation for usually a period of a week or more, the flask was placed in a water bath and the solvent evaporated under vacuum with a water aspirator. With solvents of lower volatility the water bath was warmed to about 50°C. The solid residue was washed with water to remove catalyst, if the salt of an organic acid was used, and then dissolved in methanol or some other suitable solvent such as benzene. The product was recrystallized at least twice in all cases. Yields of product were as high as 70% of theoretical and depended mainly on the time of exposure and the intensity of the light source. Sunlight always gave the higher yields for equal exposure times.

The product from the anthracene oxidation melted at 287-289°C. which was identical with the melting point of an authentic sample of anthracene-9,10-quinone. A mixture of authentic sample and reaction product gave the same melting point, 287-289°. Using the reaction product from the photo-oxidation of anthracene, benzanthrone (1,9-10) was prepared by reacting the product with glycerol in 92-93% sulfuric acid-water solution using iron powder as the reducing agent and a reaction temperature of 113 to 120°C. After one hour heating the reaction mixture was poured in water, precipitated solid recovered and recrystallized from methanol. The purified benzanthrone was bright yellow, melted at 167-169°, gave an orange colored solution in sulfuric acid which shows a bright red-orange fluorescence. These properties agree with the properties of benzanthrone cited by J. Houben (7), who lists 170° as being the melting point of this compound.

7. J. Houben, *Das Anthracen und Die Anthrachinone*, G. Thime, Leipzig, 1920, page 575.

For tetracene the reaction product from acetic anhydride solution was compared with the reaction product using xylene solution. The reaction product from the photo-oxidation of tetracene in xylene has been identified as tetracene-5,12-quinone (1). The reaction product from acetic anhydride had a melting point of 293-295° and that from xylene had a melting point of 296-297°. The melting point for a mixture of the two products was found to be 295-296°.

The reaction product which precipitated by radiation of an anthracene solution in acetic anhydride which had been placed in an evacuated and sealed tube gave a melting point of 245-250°C. J. Houben (8) lists for the photo-dimer

8. J. Houben, loc. cit., page 135

of anthracene the melting points, 242-244°, 244°, 272-274°, and 270-280°. The wide variation is attributed to the fact that on heating, the photo-dimer dissociates slowly into anthracene and the melting point obtained depends on the rate of heating. The sample on being allowed to cool and reheated gave a melting point of 208°. This behavior together with the white color and the lack of fluorescence by the solid, can be considered as evidence that the reaction product obtained in the absence of O₂ is the photo-dimer of anthracene.

Not for Publication

Presented Before the Division of Gas and Fuel Chemistry
American Chemical Society
Chicago, Illinois, Meeting, September 7-12, 1958

The Kinetics of the Sorption and Desorption of
Methanol on Coals of Various Ranks

George Ostapchenko and Paul Fugassi
Coal Research Laboratory, Dept. of Chemistry
Carnegie Institute of Technology, Pittsburgh (13), Pa.

SUMMARY

The kinetics of the sorption and desorption of methanol were measured on eight American coals varying in rank from lignite to bituminous and were found to obey a second order rate equation. A mechanism for the sorption process is proposed which explains the variation of the experimental velocity constants with pressure and with the rank of the coal. An equilibrium sorption isotherm derived from the sorption mechanism permits the calculation of the moles of sorption sites per gram of coal, A . The value of A for the eight coals is found to be related to the oxygen content, O , in moles per gram of coal by the relationship, $A = 0.667(O)$. This relationship is consistent with the hypothesis that sorption occurs on hydroxyl groups, either unassociated or associated with carbonyl groups. From the evidence gathered from this relationship, it is concluded that sorption occurs on specific sites, probably hydroxyl groups, throughout the coal substance.

INTRODUCTION

There has been much discussion in the literature concerning the measurement of the surface area of coal and the interaction of polar molecules with the coal substance. A great deal of this discussion has been summarized recently(1) and it was concluded that the sorption of polar molecules is apparently complicated by swelling and imbibition, involving weak bonds between the sorbate and polar groups in the coal.

A kinetic study of the sorption of methanol on coal was made(2) and it was found to obey a second order rate equation. This rate equation was also found to be descriptive in cases of water and methanol sorption on such things as cellulose and proteins(3). In the case of methanol sorption on cellulose a mechanism was proposed which led to a new sorption isotherm equation that contains as one of the parameters, the moles of sorption sites per gram of sorbing material. This paper is concerned with the kinetics of the sorption of methanol on coals of various rank in order to obtain quantitative data concerning the interaction of methanol with coals as the rank changes from lignite to bituminous.

APPARATUS AND PROCEDURE

The apparatus and the procedures used in this kinetic study were the same as previously described(2) with the exception that three adsorption tubes connected in series were used instead of one. The spring constants were 1.92, 1.54 and 1.56 milligrams per millimeter extension.

ABSORBENTS AND ABSORBATES

The coal samples used in the sorption experiments are listed along with their ultimate analyses in Table I.

Table I
Ultimate Analyses of the Coal Samples

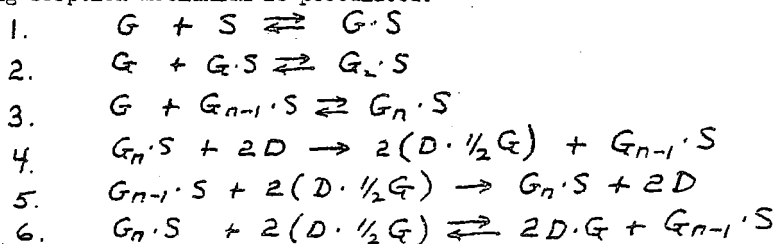
Coal Sample	Ultimate Analysis*					Ash
	C	H	N	O	S	
Upper Kittanning	80.6	3.8	1.1	3.7	1.3	9.5
Lower Kittanning	77.9	4.7	0.9	4.1	2.3	10.1
Upper Freeport	78.7	4.8	0.9	4.6	1.7	9.3
Wyoming	74.3	5.3	1.2	15.2	0.6	3.4
Kincaid Lignite	67.2	4.6	1.0	20.4	0.6	6.2
Illinois No. 6	65.2	4.9	1.2	10.4	4.0	14.3
Hendrix	81.8	5.5	1.7	6.8	1.1	3.1
Moundsville	74.5	5.2	1.4	5.7	4.2	9.0

*Moisture Free

All the coal samples were used in an unsieved, powdered form. The adsorbate, absolute methyl alcohol, analytical reagent, was obtained from the Fisher Scientific Company and was used without purification.

THE SORPTION MECHANISM

In setting up the mechanism for methanol sorption on coal, the mechanism has been made to conform to three requirements: (1) explanation of the second order rate equation, (2) explanation of the variance of the experimental velocity constant with pressure and (3) explanation of having one molecule on one site at equilibrium conditions. This third requirement is necessary since the equation for the equilibrium isotherm is a function of the pressure to the first power. The following sorption mechanism is postulated:



Reactions 1, 2 and 3 represent the adsorption of methanol vapor, G, on the surface sites, S, of the coal. All reactions involving surface adsorption of the physical type are known to be rapid both on theoretical and experimental grounds. The double arrow is used to indicate that these reactions are in equilibrium. Reaction 4 is the slow rate-determining step for the sorption process. A molecule from a site of the $G_n \cdot S$ type migrates into the interior and is held on two internal, D, sites, where n may be 1, 2, 3, or combinations of 1, 2, 3, The exact value of n, or combination of n's, depends on the nature of the coal's surface and interior sites. The fraction of surface sites covered with n molecules is a function of the pressure and since these sites precede internal sorption, their concentration will enter into the experimental rate equation. Reaction 5 is the reverse of reaction 4 and is necessary to account for the reversibility of the reaction. Reaction 6 is a rapid equilibrium type reaction which accounts for the fact that one molecule is held on one site when equilibrium is reached.

THE RATE EQUATION

The rate equation derived from the above sequence of reactions is

$$k_4 \theta_n W_c t = \frac{f}{1-f}$$

In this equation k_4 is the true velocity constant, θ_n is the fraction of surface sites covered by n molecules, W_c is the moles of adsorbate per gram of sorbent at equilibrium, t is the time, and f is the fraction of the reaction completed at time t .

THE EQUILIBRIUM SORPTION EQUATION

The equilibrium sorption equation derived in a previous paper(3) is

$$W_c = \frac{AKK_1 p_0 c}{(1 + (K_1 - K_2) p_0 c)(1 - K_2 p_0 c) + K_1 K_1 p_0 c}$$

In this equation, A is the moles of sorption sites per gram of sorbent, K is the equilibrium constant for the distribution of methanol between the surface sites and the interior sites, K_1 is the equilibrium constant for the interaction of gas molecules and the surface sites containing one molecule, K_2 is the equilibrium constant for the interaction of gas molecules and the surface sites containing two molecules, p_0 is the vapor pressure of the adsorbate at the temperature of the experiment and c is the relative pressure.

RESULTS AND DISCUSSIONS

The experimental velocity constants, k_x , are derived from the experimental data by using equation 1. $f/(1-f)$ is plotted against t and a straight line is obtained whose slope is $k_x W_c$. Since W_c is known experimentally, the value of k_x is readily obtained. A typical plot of $f/(1-f)$ is shown in Figure 1 for methanol sorption at 45°C. on Wyoming coal at a relative pressure of 0.485. The kinetic data plotted in this way for the eight coal samples fell reasonably well on straight lines which covered 90% of the reaction.

The experimental velocity constant is given by the expression $k_x = k_4 \theta_n$. Since the k_4 is a constant k_x should vary with the relative pressure, c , in the same manner as θ_n . In the derivation of the equilibrium sorption equation θ_n is given by the following relationships:

$$\theta_n = (K_2 p_0 c)^{n-1} \theta_1$$

$$\theta_1 = \frac{K_1 p_0 c (1 - K_2 p_0 c)}{1 + (K_1 - K_2) p_0 c}$$

where

In Figure 2, θ_1 , θ_2 and θ_3 are plotted against c , using values of 1, 5 and 10 for $K_1 p_0$ and assuming $K_2 p_0 = 1$. In the region $K_1 p_0 = 5$ to $K_1 p_0 = 10$, the curve for θ_1 has a maximum at about $c = 0.3$, the curve for θ_2 has a maximum at about $c = 0.5$ and the curve for θ_3 has a maximum at about $c = 0.7$. The experimental curves of k_x versus c for Wyoming coal, Kincaid lignite and Illinois coal show a maximum at about 0.3, indicating that θ_1 contributes most in the kinetic mechanism. The curves for Hendrix and Moundsville coals show a maximum at about $c = 0.5$, indicating that θ_2 contributes most to the kinetic mechanism. The curves for Upper and Lower Kittanning coals show a maximum at about $c = 0.7$,

indicating that Θ_3 contributes most to the kinetic mechanism. The curve for Upper Freeport coal appears to be a straight line indicating that neither Θ_1 , Θ_2 , nor Θ_3 predominate but perhaps all three contribute in such a way as to give a straight line.

In Figures 3 to 6 are plotted the values of Θ_n for each of the coal samples studied. These curves were drawn using the experimental values for K_1 derived from the equilibrium sorption equation. Also plotted in these figures are the values of k_x/k_4 which should equal Θ_n at corresponding values of c . The agreement of these values is quite good. The values of k_4 used in the calculations are listed in Table 2.

Table 2
Values of the True Velocity Constants

Coal Sample	t, °C.	gms. coal
		k_4 , mole CH_3OH - hr
Upper Kittanning	45	100,000
	40	96,000
	35	92,000
Lower Kittanning	45	88,000
	40	72,000
	35	56,000
Wyoming	45	14,500
	35	12,600
	30	9,700
Kincaid Lignite	45	13,400
	35	11,100
	30	9,100
Illinois No. 6	45	21,500
	35	17,200
	30	14,000
Hendrix	45	78,000
	35	54,000
	30	50,000
Moundsville	45	65,000
	35	50,000
	30	45,000

In comparing this phenomena with the rank of the coal, it is seen that as the rank of the coal goes from lignite to bituminous the controlling factor in the sorption mechanism goes from Θ_1 through Θ_2 to Θ_3 . It can be postulated that this change is controlled by the relative attractive power of the surface sites and the interior sites for the methanol molecule. The surface of coal can be imagined as having many adsorption sites, each having a different affinity for the methanol molecule. The sites could be the same atom or group of atoms but having different affinities due to steric factors or interactions with other sites.

The sites having the lowest affinity would be capable of holding only one methanol molecule, Θ_1 , and those having a slightly greater affinity would be capable of holding two methanol molecules Θ_2 , etc. The internal sites would then attract the weakest held methanol molecule on the surface in greatest concentration. It is postulated that the methanol molecule most weakly held on the surface is the third molecule going on a site holding three molecules, the next would be the second molecule going on a site holding two molecules, the next would be the molecule going on a site capable of holding only one molecule. When the attractive power of the internal sites is high, the internal site will attract the methanol molecules on sites of most abundance. As the attractive power of the internal sites decreases the surface sites with one methanol molecule become stable and the interior sites attract the next most abundant and less weakly held methanol molecule or Θ_2 . This argument can be applied again for Θ_3 controlling the reaction mechanism. A measure of this attractive power would be the difference in free energy change for the methanol vapor going on the surface and the free energy change for the methanol vapor going into the interior. This information is available from the equilibrium sorption equation which will be discussed later and is shown in Table 3.

Table 3
Average Standard Free Energy Differences at 30°-45°C.

<u>Coal Sample</u>	<u>Free Energy Differences, cal./mole</u>
Lower Kittanning	+23
Upper Kittanning	- 6
Upper Freeport	-407
Moundsville	-708
Wyoming	-814
Hendrix	-918
Kincaid Lignite	-1117
Illinois No. 6	-1282

It can be seen from this Table and from Figures 3 to 6 that as the free energy difference goes from a high to a low negative value, the type of site controlling the kinetic mechanism changes from Θ_1 through Θ_2 to Θ_3 . The sites for methanol sorption on coal are probably the same type in the high rank coals as in the low rank coals. If it were assumed that all the properties of the coals were the same, except for the number of sites, then free energy changes would all be equal. However, there is evidence(4) that as the rank of the substance increases, the degree of compactness of the coal micelles increases. It is probable then, as the coal micelles become more compact the free energy change of the methanol molecule due to sorption will decrease.

The energies of activation, E_a , for the sorption process were calculated from the values in Table 2 by plotting $\ln k_s$ versus $1/T$ and measuring the slope. The values of E_a for the coal samples are shown in Table 4.

Table 4
Activation Energies for the Sorption Process

<u>Coal Sample</u>	<u>E_a, cal./mole</u>	<u>E_d, cal./mole</u>	<u>E_a - E_d, cal./mole</u>
Upper Kittanning	1625	7035	--5409
Lower Kittanning	8798	7191	1607
Upper Freeport	6614	4947	1640
Wyoming	5513	4795	358
Kincaid Lignite	5395	4850	545
Illinois No. 6	5826	2991	2835
Hendrix	5235	2162	3073
Moundsville	5501	2514	2987

The case of methanol sorption on Upper Freeport coal is similar to that reported earlier(2) for Pittsburgh Edenborn coal. The velocity constant for sorption did not vary with pressure, making it difficult to determine the degree of contribution of θ_1 , θ_2 , and θ_3 for the rate determining step. In this case the average value of k_x was used in determining the activation energy for sorption. These values are reported in Table 5.

Table 5
Experimental Velocity Constants for Upper Freeport Coal

<u>Coal Sample</u>	<u>t, °C.</u>	<u>k_x (av.)</u>	<u>$\frac{\text{gms. coal}}{\text{mole CH}_3\text{OH} - \text{hr.}}$</u>
Upper Freeport	45		2717
	40		2265
	35		2010

DESORPTION

The velocity constants for the desorption of methanol from coal were all independent of the pressure indicating that the experimental velocity constant is the true velocity constant. The velocity constants for the desorption of methanol for the eight coal samples are listed in Table 6.

Table 6
Velocity Constants for Desorption

<u>Coal Sample</u>	<u>t °C.</u>	<u>k_x, $\frac{\text{mas. coal}}{\text{mole CH}_3\text{OH} - \text{hr.}}$</u>
Upper Kittanning	45	4,000
	40	3,130
	35	2,790
Lower Kittanning	45	4,090
	40	3,270
	35	2,830
Upper Freeport	45	1,640
	40	1,470
	35	1,270
Wyoming	45	2,200
	35	1,780
	30	1,530
Kincaid Lignite	45	1,640
	35	1,370
	30	1,150
Illinois	45	3,360
	35	3,010
	30	2,710
Moundsville	45	3,930
	35	3,610
	30	3,110
Hendrix	45	3,870
	35	3,470
	30	3,270

The energies of activation of desorption calculated from these values are listed in Table 4, along with the differences in the activation energies. This difference is the heat of reaction for the rate-determining step (equation 4 of the sorption mechanism).

Considering the assumptions made and the experimental errors involved, it is difficult to draw any conclusions concerning the differences in energies for the different coal samples. However, it can be noted that the magnitude of the energies involved excludes compound formation of methanol with coal and indicates that the type of bonding is probably hydrogen bonding.

THE EQUILIBRIUM DATA

Equation 2, the equilibrium sorption equation contains 3 parameters A, K and K_1 which can be evaluated by solving a series of simultaneous equations. The values for A, K and K_1 for the eight coal samples are listed in Table 7.

Table 7
 Constants for the Equilibrium Sorption Equation

Coal Sample	t, °C.	moles of sites x 10 ⁴		K	K ₁
		A, gm. coal			
Upper Kittanning	45	16.4		2.66	6.82
	40	16.7		2.31	9.06
	35	16.4		2.41	10.33
Lower Kittanning	45	15.7		2.43	5.73
	40	15.6		2.09	8.11
	35	15.2		2.33	9.43
Upper Freeport	45	22.9		1.90	8.46
	40	23.2		1.62	11.69
	35	22.9		1.52	14.10
Wyoming	45	61.4		1.15	9.19
	35	66.0		1.06	15.71
	30	67.7		1.04	20.49
Kincaid Lignite	45	73.7		1.04	14.30
	35	82.7		0.84	25.34
	30	83.2		0.90	28.29
Illinois No. 6	45	53.0		0.79	14.48
	35	57.6		0.80	21.12
	30	61.0		0.69	32.29
Hendrix	45	25.9		1.60	14.48
	35	25.2		1.39	21.12
	30	23.9		1.21	32.29
Moundsville	45	22.8		1.64	12.00
	35	21.7		1.68	17.16
	30	20.4		1.35	26.10

It can be seen from Table 7 that the values for A, the moles of sites per gram of coal are independent of temperature and that the values decrease as the rank of the coal increases. It has been suggested(3) that the atom which forms the site for methanol sorption on coal is probably oxygen. In Figure 7 is plotted the moles of sites per gram of coal versus the moles of oxygen per gram of coal. The relationship obtained is linear with a slope of 2/3 which indicates 2/3 of the oxygen in coals from high rank to low rank, form sites for methanol sorption. Several workers(5)(6) have analyzed coals of varying rank in terms of OH, COOH, OCH₃, C=O, and non-reactive O groups in an effort to follow the changes occurring during the coalification process. Using the data of Blom et al.(6) and assuming various combinations of oxygen groups, it was found that the sum of OH and COOH groups gave the best agreement with the number of sorption sites in the coal. These data are plotted in Figure 7 and the agreement is quite good considering the experimental difficulties in determining the oxygen groups in coals. The fact that the sites responsible for sorption remain at a constant ratio with respect to the total oxygen during the coalification process indicates that the oxygen is lost in a very specific manner as coal ages. The exact manner in which the oxygen is lost is difficult to determine since little is known about the manner of the changes of the carbon and hydrogen during coalification.

Since the equilibrium constants K and K₁ are known at three temperatures, the values of ΔH, ΔF°, and ΔS could be determined. These values in cal/mole for ΔH and ΔF° and cal/degree for ΔS are shown in Table 8.

Table 8
Values of ΔH , ΔF° and ΔS for Equilibrium Sorption

Coal Sample	ΔH	$\frac{K}{\Delta F^\circ}$	ΔS	ΔH	$\frac{K_1}{\Delta F^\circ}$	ΔS
Upper Kittanning	1951	-620	8.1	-8111	-1215	-21.7
		-522	7.9		-1372	-21.5
		-540	8.1		-1430	-21.7
Lower Kittanning	843	-560	4.4	-9751	-1104	-27.2
		-459	4.2		-1303	-27.0
		-518	4.4		-1375	-27.2
Upper Freeport	4429	-408	12.6	-9980	-1351	-27.1
		-302	13.2		-1531	-27.0
		-256	13.5		-1621	-27.0
Wyoming	1131	- 67	3.8	-10,204	-1402	-27.7
		- 37	3.8		-1637	-27.7
		- 25	3.8		-1820	-27.7
Kincaid Lignite	1191	- 27	3.8	-7928	-1683	-19.6
		11	3.8		-1930	-19.3
		6	3.9		-2012	-19.5
Illinois No. 6	2331	151	6.9	-11,129	-1690	-29.7
		136	7.1		-1869	-30.0
		224	7.0		-2094	-29.8
Hendrix	3843	-297	13.0	-9508	-1628	-24.8
		-200	13.1		-2006	-24.4
		-113	13.1		-2045	-24.6
Moundsville	3440	-312	11.8	-10,827	-1572	-29.1
		-318	12.2		-1741	-29.5
		-179	11.9		-1966	-29.1

These values show that the energy associated with the sorption of methanol on coals is small compared to energies due to chemical reactions and, as pointed out in the discussion of the rate equation, are probably due to hydrogen bonding. There seems to be no correlation of these values with the rank of the coal.

CONCLUSIONS

The sorption of methanol on coal takes place in two steps. (1) The adsorption of methanol molecules on to the surface of the coal in a multilayer manner. (2) Migration of the molecules from the surface into the interior of the coal substance. The first step is rapid and the number of sites involved is small compared to the total number of sites responsible for sorption since the second order rate equation is obeyed during the entire sorption process.

The migration of the methanol molecules into the interior occurs primarily from only one type of surface site. This site may be holding either one, two or three methanol molecules, depending on the rank of the coal sample. As the rank of the coal increases from lignite to bituminous, the type of site determining changes from a surface site holding one methanol molecule to a surface site holding three methanol molecules. This change is related to the free energy changes for methanol sorption caused by the coalification process.

The moles of sites per gram of coal, A, responsible for methanol sorption can be calculated from the equilibrium sorption isotherm. The value of A

decreases as the rank of the coal increases and it was found that A varies directly with the oxygen content of the coal, O, in moles per gram according to the relationship $A = 0.667 (O)$. Since the oxygen content of coal cannot be obtained directly by analytical means, and is obtained by difference, the sorption of methanol on coal might be used as a means of determining oxygen directly.

The variation of the value of A with the rank of the coal is consistent with the hypothesis that the sites responsible for sorption are hydroxyl groups either isolated or in conjunction with a carbonyl group. This is corroborated by the energies derived from the sorption data which show that the type of bonding which occurs during methanol sorption is probably hydrogen bonding. The loss of oxygen in coal during the coalification process occurs in such a manner that for every two hydroxyl groups lost one other type of oxygen group is also lost. The loss of oxygen in this manner is quite specific and further investigations along these lines might provide quantitative data concerning the coalification process.

This communication has been abstracted from the thesis of George Ostapchenko submitted to the Graduate School, Carnegie Institute of Technology, in partial fulfillment of the requirements for the degree, Doctor of Philosophy. The authors wish to acknowledge and thank BCR, Inc. and the Coal Research Board, Commonwealth of Pennsylvania, for furnishing samples and analytical data for the Kittanning and Freeport coals. They also wish to thank Dr. Martin Neuworth, Pittsburgh-Consolidation Coal Co., for samples of Hendrix and Moundsville coals.

REFERENCES

1. Anderson, R. B., Hall, W. K., Lecky, J. A., and Stein, K. C., J. of Phys. Chem. 60, 1548 (1956)
2. Fugassi, J. P., Ostapchenko, G. and Trammell, R., Fuel, 37, 36 (1958)
3. Fugassi, J. P. and Ostapchenko, G., unpublished material
4. Bangham, D. H., Franklin, R. E., Hirst, W. and Maggs, F. A. P., Fuel, 28, 231 (1949)
5. Ihnatowicz, M., Prace Glownego Inst., Gornictwa (Katowice), Komm., 125 (1952)
6. Blom, L., Edelhausen, L. and van Krevelen, D. W., Fuel, 36 (1957)

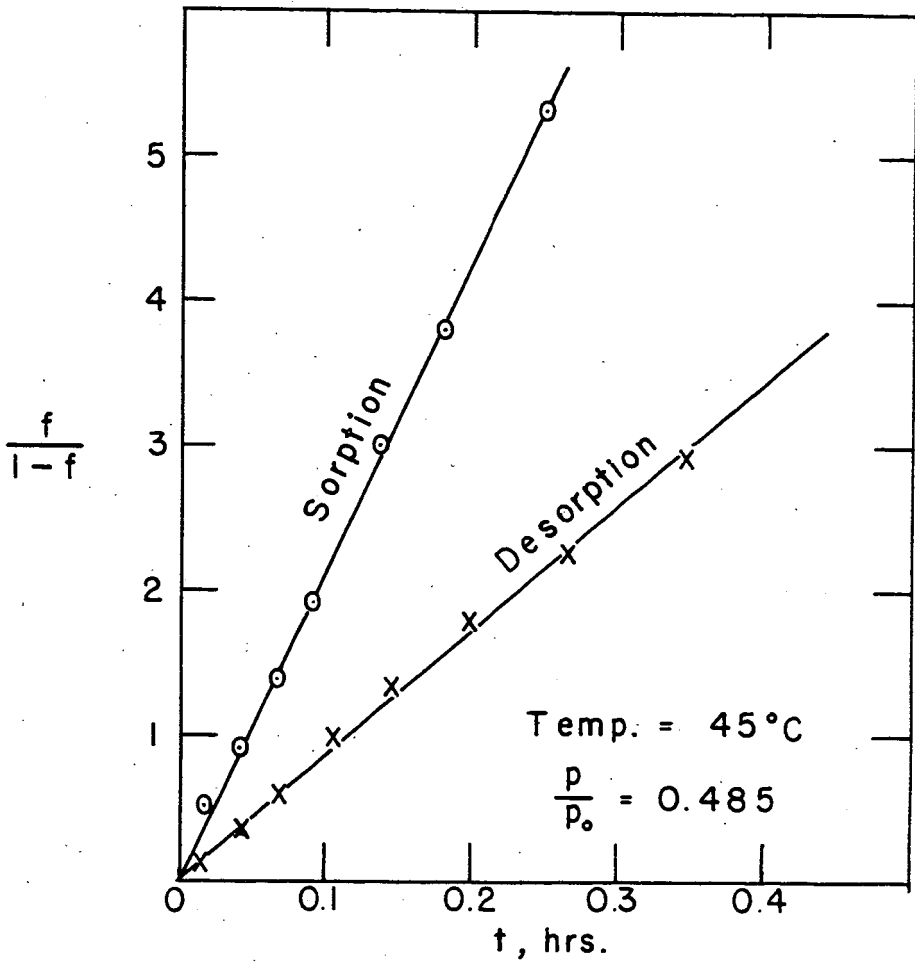


FIGURE 1 - RATE PLOTS

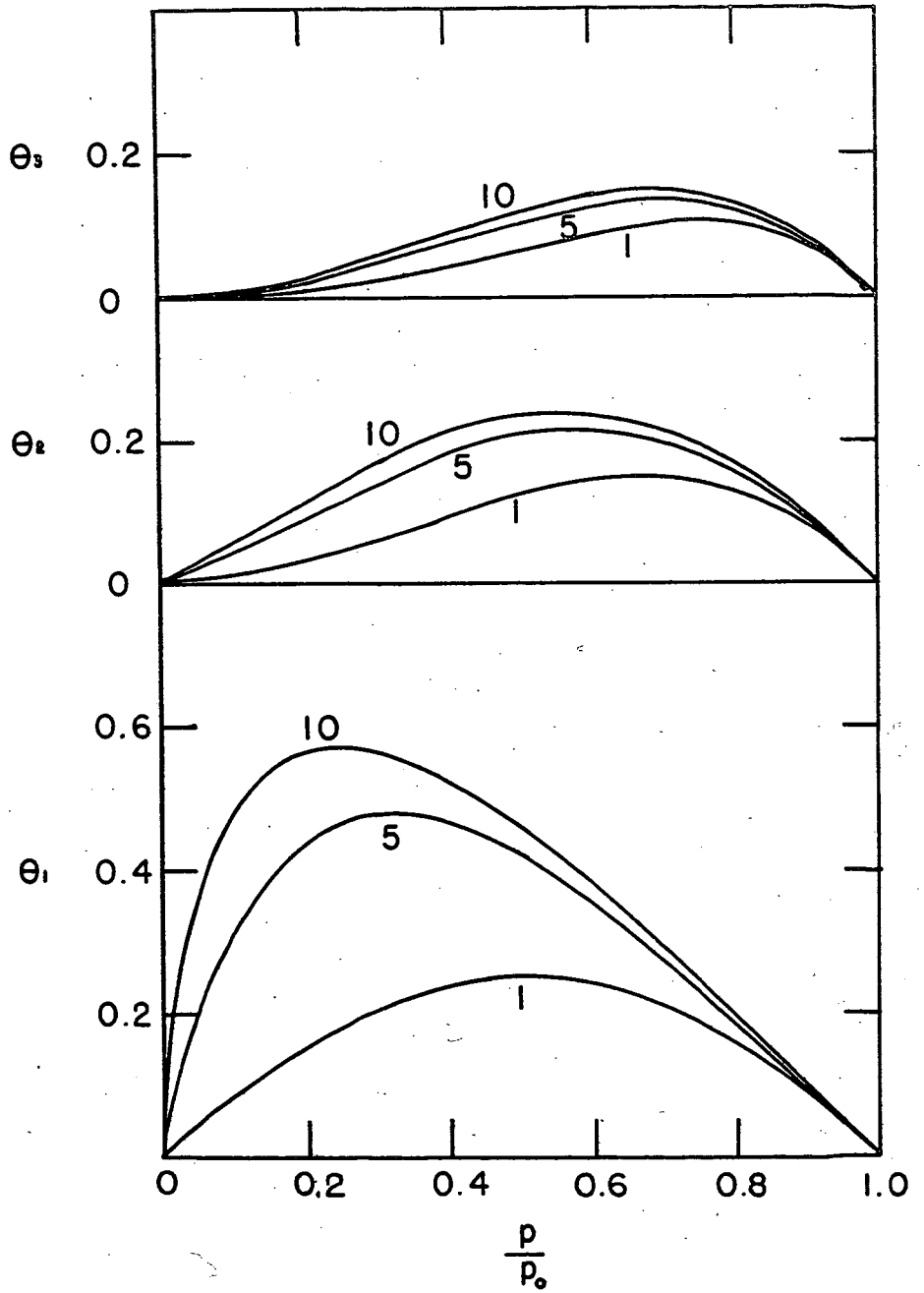


FIGURE 2 - θ AS A FUNCTION OF c

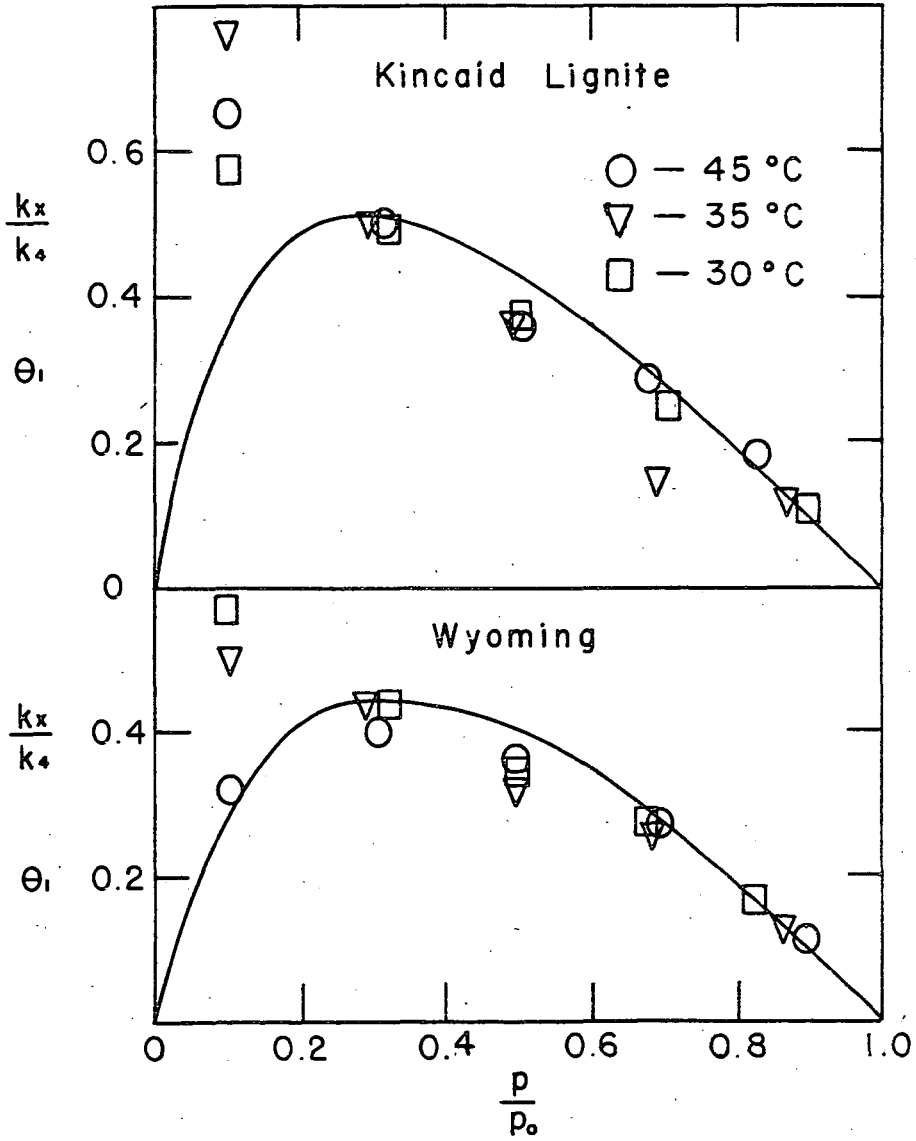


FIGURE 3 - θ_1 AS A FUNCTION OF c

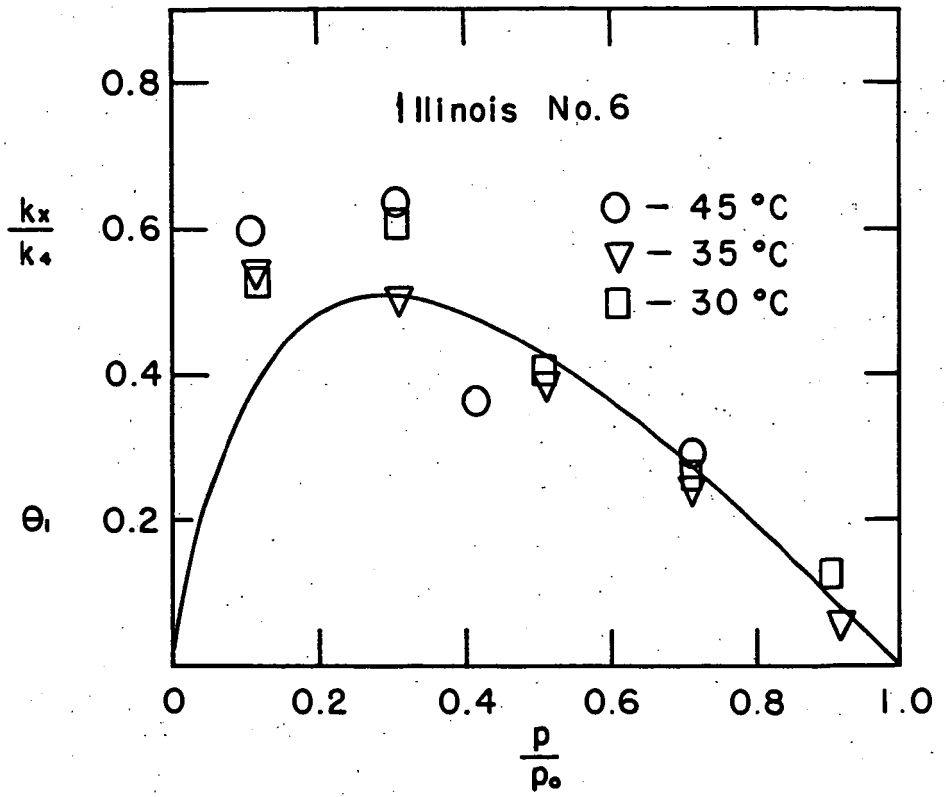


FIGURE 4 - θ_1 AS A FUNCTION OF c

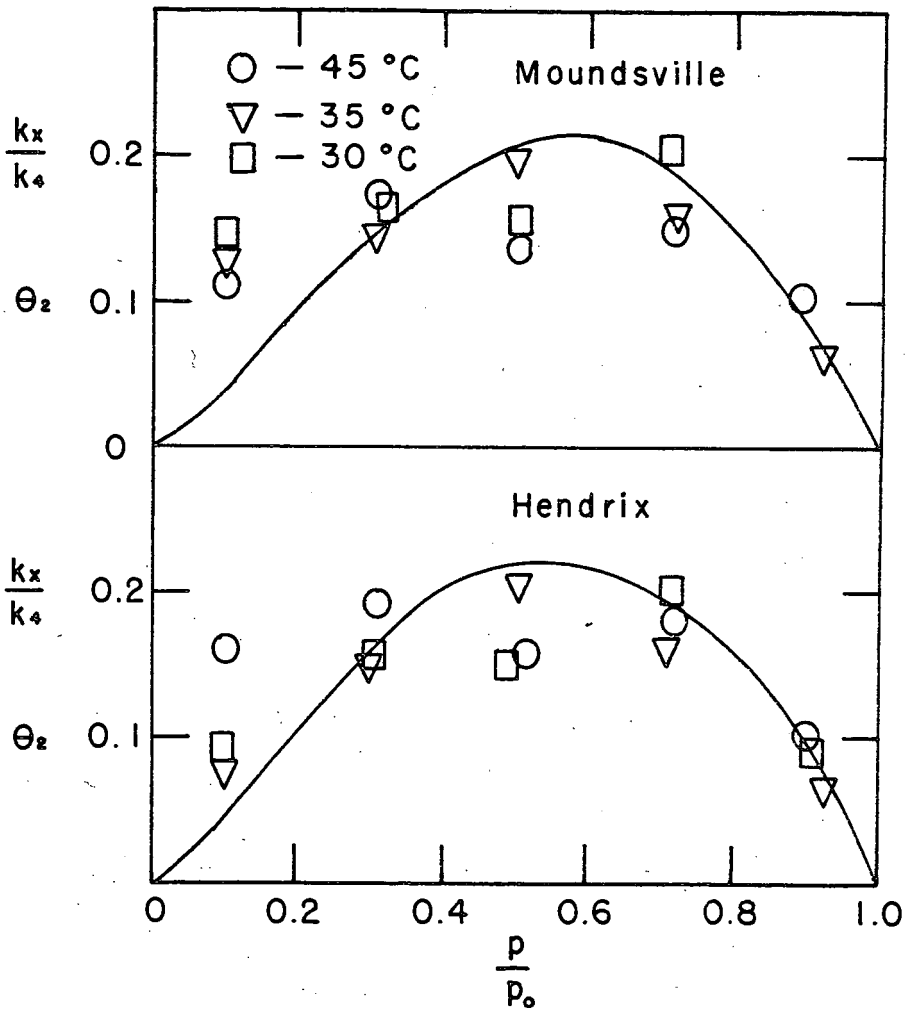


FIGURE 5 - θ_2 AS A FUNCTION OF c

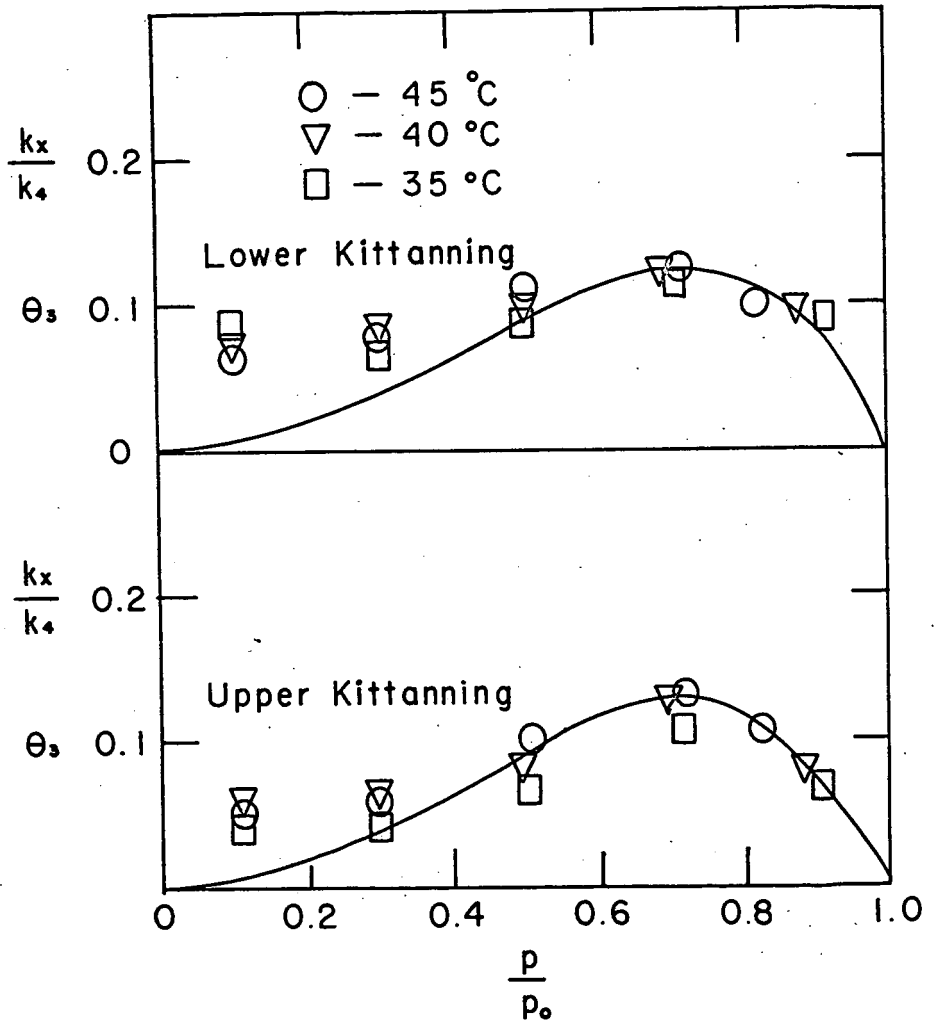


FIGURE 6 - θ_3 AS A FUNCTION OF c

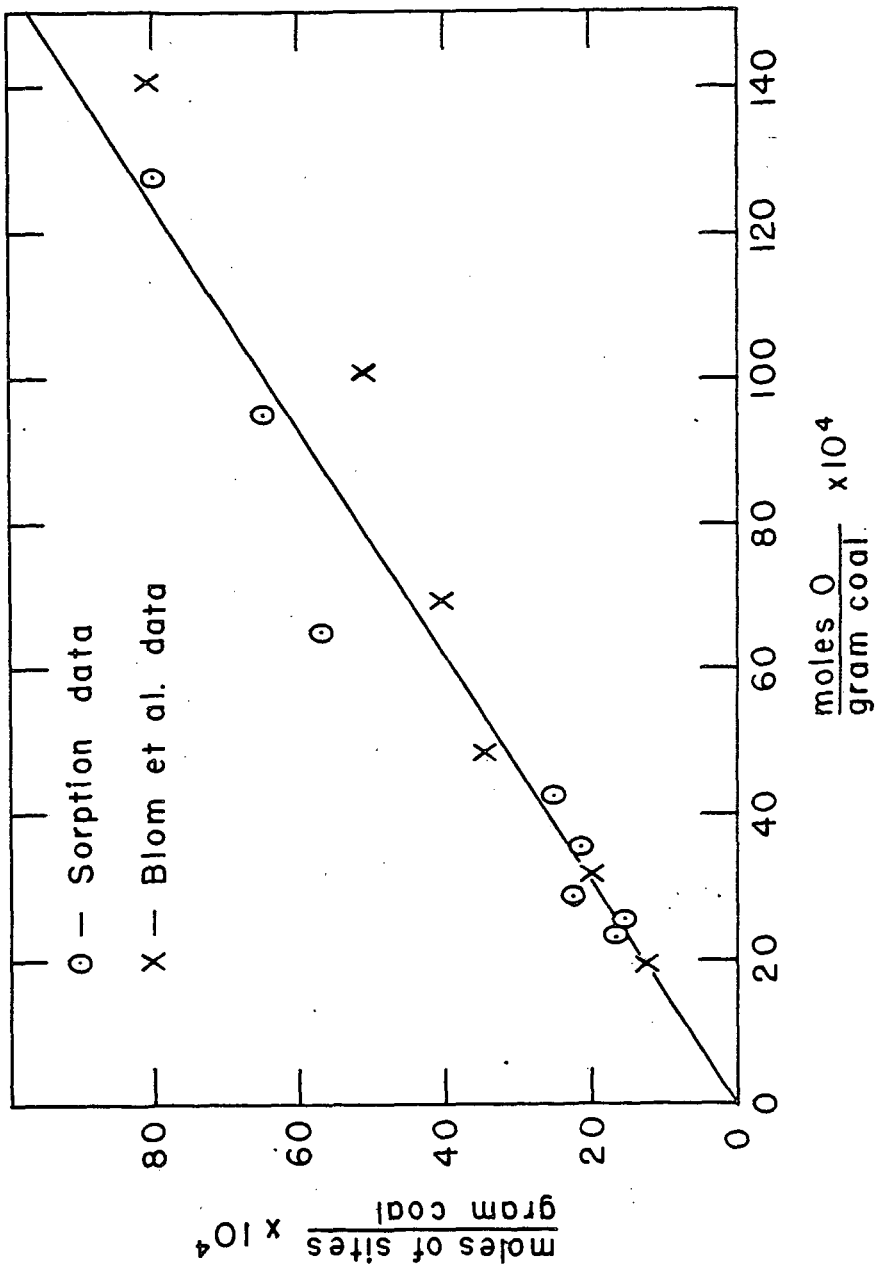


FIGURE 7 - RELATIONSHIP BETWEEN A AND TOTAL OXYGEN CONTENT